



HAL
open science

Properties of Photosystem II lacking the PsbJ subunit

Alain Boussac, Julien Sellés, Marion Hamon, Miwa Sugiura

► **To cite this version:**

Alain Boussac, Julien Sellés, Marion Hamon, Miwa Sugiura. Properties of Photosystem II lacking the PsbJ subunit. *Photosynthesis Research*, In press, 10.1101/2021.09.04.458961 . hal-03365514v1

HAL Id: hal-03365514

<https://hal.science/hal-03365514v1>

Submitted on 4 Oct 2022 (v1), last revised 5 Oct 2022 (v2)

HAL is a multi-disciplinary open access archive for the deposit and dissemination of scientific research documents, whether they are published or not. The documents may come from teaching and research institutions in France or abroad, or from public or private research centers.

L'archive ouverte pluridisciplinaire **HAL**, est destinée au dépôt et à la diffusion de documents scientifiques de niveau recherche, publiés ou non, émanant des établissements d'enseignement et de recherche français ou étrangers, des laboratoires publics ou privés.

Photosynthesis Research

Properties of Photosystem II lacking the PsbJ subunit.

--Manuscript Draft--

Manuscript Number:	PRES-D-21-00074R2	
Full Title:	Properties of Photosystem II lacking the PsbJ subunit.	
Article Type:	Original article	
Keywords:	Photosystem II; PsbJ, plastoquinone; assembly; photoinhibition	
Corresponding Author:	alain boussac, PhD I2BC SB2SM: Service de Bioenergetique Biologie Structurale et Mecanismes Gif sur Yvette, FRANCE	
Corresponding Author Secondary Information:		
Corresponding Author's Institution:	I2BC SB2SM: Service de Bioenergetique Biologie Structurale et Mecanismes	
Corresponding Author's Secondary Institution:		
First Author:	alain boussac, PhD	
First Author Secondary Information:		
Order of Authors:	alain boussac, PhD	
	Julien Sellés, PhD	
	Marion Hamon, PhD	
	Miwa Sugiura, PhD	
Order of Authors Secondary Information:		
Author Comments:	submitted to the special issue "Photosystem II: assembly, repair and regulation"	
Funding Information:	anr-10-inbs-05	Dr. alain boussac
	anr-11-labx-0011-01	Dr. Julien Sellés
	cacsice anr-11-eqpx-0008	Dr. Marion Hamon
	jsps-kakenhi (JP17H06435)	Prof. Miwa Sugiura
	jsps-kakenhi (21H02447)	Prof. Miwa Sugiura
Abstract:	<p>Photosystem II (PSII), the oxygen-evolving enzyme, consists of 17 trans-membrane and 3 extrinsic membrane proteins. Other subunits bind to PSII during assembly, like Psb27, Psb28, Tsl0063. The presence of Psb27 has been proposed (Zabret et al. 2021; Huang et al. 2021; Xiao et al. 2021) to prevent the binding of PsbJ, a single transmembrane α-helix close to the quinone Q_B binding site. Consequently, a PSII rid of Psb27, Psb28 and Tsl0034 prior to the binding of PsbJ would logically correspond to an assembly intermediate. The present work describes experiments aiming at further characterizing such a DPsbJ-PSII, purified from the thermophilic <i>Thermosynechococcus elongatus</i>, by means of MALDI-TOF spectroscopy, Thermoluminescence, EPR spectroscopy and UV-visible time-resolved spectroscopy. In the purified DPsbJ-PSII, an active Mn₄CaO₅ cluster is present in 60-70 % of the centers. In these centers, although the forward electron transfer seems not affected, the E_m of the Q_B/Q_B⁻ couple increases by ≥ 120 mV thus disfavoring the electron coming back on Q_A. The increase of the energy gap between Q_A/Q_A⁻ and Q_B/Q_B⁻ could contribute in a protection against the charge recombination between the donor side and Q_B⁻, identified at the origin of photoinhibition under low light (Keren et al. 1997), and possibly during the slow photoactivation process.</p>	
Response to Reviewers:	Referee #2 : 1) References in the abstract should be removed (or given in full) so that the abstract	

	<p>can stand alone. -Done</p> <p>2) On page 9 "Before to study" change to Before studying... -Corrected</p> <p>3) Page 11, line 17. Change to something like: As will be shown later, this is not the case in the ΔPsbJ-43H/PSII studied and so another explanation is needed -Corrected</p> <p>4) Page 11, line 27. Change, Before to go to Before going... -Corrected</p> <p>5) Page 15, line 12. Fix typo sate to state -Done</p> <p>6) Page 15, line 16. Change to: ...these kinetic are similar... -Corrected</p> <p>7) Page 17. First sentence. Do you mean: Nevertheless, despite the lack of strong... -Yes. The word "despite" has been added.</p> <p>8) Page 18, line 7 need to needs -Corrected</p> <p>9) Page 18. The last sentence needs rewording to something like: ...as the origin of the damage by about 2 orders of magnitude higher than induced by the... -Corrected</p>
Additional Information:	
Question	Response

Saclay, September 28th 2021

Dear Dr. Vinyard,

Please find attached a new revised version of the manuscript entitled "Properties of Photosystem II lacking the PsbJ subunit" by Julien Sellés, Marion Hamon, Miwa Sugiura and myself and originally referenced PRES-D-21-00074.

The minor corrections requested by Referee 2 have been done and the changes requested by the editor have been addressed. All these changes can be easily viewed in the file "changes indicated".

We hope that this manuscript is now acceptable for publication in the special issue of Photosynthesis Research.

Sincerely yours

Alain Boussac

Guest Editor:

I understand that multiple papers that use the same tools will use similar language and I appreciate the edits you already made in the revision. However, the publisher's system is still flagging some sections of this current work as being too similar to your *Physiologia Plantarum* 2020 paper. I think this issue can be fixed if you revise the second paragraph of the introduction (page 4, lines 19-45) and parts of materials and methods (page 7 line 33 to page 8 line 40). For the latter sections, you may want to shorten the descriptions and simply cite the other work. Thank you for dealing with these technicalities. I agree with your earlier assessment that this is an imperfect system.

-As requested, parts of the text in the materials and methods have been deleted and replaced by citations to previous papers (although we do not like it....). The second paragraph of the introductions has been modified as much as possible.

Referee #2 :

1) References in the abstract should be removed (or given in full) so that the abstract can stand alone.

-Done

2) On page 9 "Before to study" change to Before studying...

-Corrected

3) Page 11, line 17. Change to something like: As will be shown later, this is not the case in the Δ PsbJ-43H/PSII studied and so another explanation is needed

-Corrected

4) Page 11, line 27. Change, Before to go to Before going...

-Corrected

5) Page 15, line 12. Fix typo sate to state

-Done

6) Page 15, line 16. Change to: ...these kinetic are similar...

-Corrected

7) Page 17. First sentence. Do you mean: Nevertheless, despite the lack of strong...

-Yes. The word "despite" has been added.

8) Page 18, line 7 need to needs

-Corrected

9) Page 18. The last sentence needs rewording to something like: ...as the origin of the damage by about 2 orders of magnitude higher than induced by the...

-Corrected

Properties of Photosystem II lacking the PsbJ subunit.

Alain Boussac¹, Julien Sellés², Marion Hamon³, Miwa Sugiura⁴

¹ I²BC, UMR CNRS 9198, CEA Saclay, 91191 Gif-sur-Yvette, France.

² Institut de Biologie Physico-Chimique, UMR CNRS 7141 and Sorbonne Université, 13 rue Pierre et Marie Curie, 75005 Paris, France.

³ Institut de Biologie Physico-Chimique, UMR8226/FRC550 CNRS and Sorbonne-Université, 13 rue Pierre et Marie Curie, 75005 Paris, France.

⁴ Proteo-Science Research Center, and Department of Chemistry, Graduate School of Science and Technology, Ehime University, Bunkyo-cho, Matsuyama, Ehime 790-8577, Japan.

*Corresponding authors: alain.boussac@cea.fr, miwa.sugiura@ehime-u.ac.jp

The authors declare that they have no conflict of interest.

ORCID numbers:

Alain Boussac, 0000-0002-3441-3861

Julien Sellés, 0000-0001-9262-8257

Keywords: Photosystem II, PsbJ, plastoquinone, assembly, photoinhibition.

Acknowledgments

This work has been in part supported by i) the French Infrastructure for Integrated Structural Biology (FRISBI) ANR-10-INBS-05, ii) the Labex Dynamo (ANR-11-LABX-0011-01), iii) EQUIPEX (CACSICE ANR-11-EQPX-0008), notably through funding of the Proteomic Platform of IBPC (PPI). MS was supported by the JSPS-KAKENHI grant in Scientific Research on Innovative Areas JP17H06435 and a JSPS-KAKENHI grant 21H02447.

Abbreviations:

1
2
3 Chl, chlorophyll; Chl_{D1}/Chl_{D2}, accessory Chl's on the D1 or D2 side, respectively; DCMU, 3-
4 (3,4-dichlorophenyl)-1,1-dimethylurea; PSII, Photosystem II; MES, 2-(*N*-morpholino)
5 ethanesulfonic acid; P₆₈₀, primary electron donor; P_{D1} and P_{D2}; Chl monomer of P₆₈₀ on the
6 D1 or D2 side, respectively, Phe_{D1} and Phe_{D2}, pheophytin on the D1 or D2 side, respectively;
7
8 Q_A, primary quinone acceptor; Q_B, secondary quinone acceptor; Tyr_D, redox active tyrosine
9 160 of D2; Tyr_Z, redox active tyrosine 161 of D1; TL, thermoluminescence; WT*3, *T.*
10 *elongatus* mutant strain containing only the *psbA₃* gene and a His₆-tag on the C-terminus of
11 CP43. EPR, Electron Paramagnetic Resonance spectroscopy; MALDI-TOF, Matrix Assisted
12 Laser Desorption Ionization - Time of Flight.
13
14
15
16
17
18
19
20
21
22
23
24
25
26
27
28
29
30
31
32
33
34
35
36
37
38
39
40
41
42
43
44
45
46
47
48
49
50
51
52
53
54
55
56
57
58
59
60
61
62
63
64
65

Abstract

1
2
3
4
5 Photosystem II (PSII), the oxygen-evolving enzyme, consists of 17 trans-membrane and 3
6 extrinsic membrane proteins. Other subunits bind to PSII during assembly, like Psb27, Psb28,
7 Tsl0063. The presence of Psb27 has been proposed (Zabret et al. 2021 Nature Plants 7: 524–
8 538; Huang et al. 2021 Proc Natl Acad Sci USA 118: e2018053118; Xiao et al. 2021 7: 1132–
9 1142) to prevent the binding of PsbJ, a single transmembrane α -helix close to the quinone Q_B
10 binding site. Consequently, a PSII rid of Psb27, Psb28 and Tsl0034 prior to the binding of
11 PsbJ would logically correspond to an assembly intermediate. The present work describes
12 experiments aiming at further characterizing such a Δ PsbJ-PSII, purified from the
13 thermophilic *Thermosynechococcus elongatus*, by means of MALDI-TOF spectroscopy,
14 Thermoluminescence, EPR spectroscopy and UV-visible time-resolved spectroscopy. In the
15 purified Δ PsbJ-PSII, an active Mn_4CaO_5 cluster is present in 60-70 % of the centers. In these
16 centers, although the forward electron transfer seems not affected, the Em of the Q_B/Q_B^-
17 couple increases by ≥ 120 mV thus disfavoring the electron coming back on Q_A . The increase
18 of the energy gap between Q_A/Q_A^- and Q_B/Q_B^- could contribute in a protection against the
19 charge recombination between the donor side and Q_B^- , identified at the origin of
20 photoinhibition under low light (Keren et al. 1997 Proc Natl Acad Sci USA 94: 1579–1584),
21 and possibly during the slow photoactivation process.
22
23
24
25
26
27
28
29
30
31
32
33
34
35
36
37
38
39
40
41
42
43
44
45
46
47
48
49
50
51
52
53
54
55
56
57
58
59
60
61
62
63
64
65

Introduction

Photosystem II (PSII), the water-splitting enzyme in cyanobacteria, algae and higher plants, is responsible for the production of the atmospheric O₂ that is essential for aerobic organisms and it is the first step in the production of food, fibers and fossil fuels. The mature Photosystem II, in cyanobacteria, consists of 20 subunits (Umena et al. 2011; Suga et al. 2015) with 17 trans-membrane and 3 extrinsic membrane proteins (Roose et al. 2016). The PSII also binds 35 chlorophylls, 2 pheophytins, 2 hemes, 1 non-heme iron, 2 plastoquinones (Q_A and Q_B), the Mn₄CaO₅ cluster, 2 Cl⁻, 12 carotenoids and 25 lipids (Umena et al. 2011; Suga et al. 2015). Most of the cofactors involved in the water oxidation and electron transfer bind to the reaction center subunits, PsbA (also called D1) and PsbD (also called D2).

After the absorption of a photon by one of the antenna chlorophylls, the excitation is transferred from chlorophyll to chlorophyll to the photochemical trap formed by the four chlorophylls P_{D1}, P_{D2}, Chl_{D1} and Chl_{D2}. A few picoseconds later, a charge separation occurs forming the Chl_{D1}⁺Phe_{D1}⁻ and then the P_{D1}⁺Phe_{D1}⁻ radical pairs (Holzwarth et al. 2006; Romero et al. 2017). In the ns time range, P_{D1}⁺ oxidizes Tyr_Z, the Tyr161 of the D1 polypeptide. In the μs to ms time range, the radical Tyr_Z[•] oxidizes the Mn₄CaO₅ cluster, see (Shen 2015, Cox et al. 2020) for reviews. On the electron acceptor side, Phe_{D1}⁻ reduces the primary quinone electron acceptor Q_A. The electron on Q_A⁻ is in turn transferred to the second quinone electron acceptor Q_B. Whereas Q_A is only singly reduced under normal conditions, Q_B can be doubly reduced and can bind two protons before to leave its binding site, reviewed in (de Causmaecker et al. 2019). The Mn₄CaO₅ complex is oxidised sequentially in four successive charge separations. In doing so, it passes through five redox states denoted by S_n, where n represents the number of stored oxidative equivalents (Kok et al. 1970; Joliot and Kok 1975). When the S₄-state is formed, *i.e.* after the 3rd flash of light given on dark-adapted PSII that is in the S₁-state, the two water molecules bound to the cluster are oxidized, the O₂ is released and the S₀-state is reformed. In cyanobacteria, in addition to the subunits involved in the cofactors binding (PsbA, PsbD, CP43, CP47, PsbE, PsbF), there are several small subunits consisting in only a transmembrane α-helix as PsbT, PsbM, PsbJ, PsbK, PsbL, PsbI, PsbX, PsbY, Psb30 (formerly Ycf12), *e.g.* (Kashino et al. 2002, 2007; Nowaczyk et al. 2012; Sugiura et al. 2012). Some roles have been attributed to these low molecular weight subunits either upon site directed mutagenesis, mainly for PsbT, or upon the deletion of the protein as for PsbM, PsbJ, Psb30, PsbK, PsbX, PsbZ.

1 It has been proposed that the interaction between Phe239 of PsbA and the PsbT subunit
2 is required to restrict the movement of the DE loop of PsbA. In turn, the disruption of this
3 interaction may perturb the binding of bicarbonate to the non-heme iron that could contribute
4 to the signal for PSII to undergo a repair following photodamages (Forsman and Eaton-Rye
5 2021). Deletion of PsbM has been reported to mainly affect the Q_B environment (Uto et al.
6 2017). PSII depleted of Psb30 exhibited a lower efficiency under high light conditions and
7 Psb30 favors the stabilization of the PSII complex (Sugiura et al. 2010a; Inoue-Kashino et al.
8 2011). Deletion of PsbK has been proposed to destabilize the association of PsbZ and Psb30
9 (Ycf12) with PSII complex and to alter the Q_B function (Iwai et al. 2010). PsbZ has been
10 proposed to stabilize the binding of Psb30 (Takasaka et al. 2010). Deletion of PsbX has been
11 shown to affect the PSII integrity in both *Arabidopsis thaliana* (Garcia-Cerdan et al. 2009)
12 and *Synechocystis sp.* PCC 6803 (Funk 2000). In plant PSII, the PsbL subunit seems to
13 prevent the back electron flow from the reduced plastoquinol pool thus protecting the PSII
14 from photoinactivation (Ohad et al. 2004). In *Synechocystis sp.* PCC 6803, PsbL also
15 influences forward electron transfer from Q_A⁻ to Q_B (Luo et al. 2014).

16
17
18
19
20
21
22
23
24
25
26
27 The *psbJ* gene belongs to the *psbEFLJ* operon coding for the PsbE and PsbF subunits
28 bearing the two histidine residues His23 and His24, respectively, which are the heme iron
29 axial ligands of the Cytb₅₅₉ (Umena et al. 2011). The PsbJ subunit is close to PsbK and its
30 possible involvement in the exchange of the plastoquinone has been discussed (Kaminskaya
31 et al. 2007; Müh et al. 2012; van Eerden et al. 2017) with a role in the efficiency of forward
32 electron flow following the charge separation process by affecting the Q_A and Q_B properties
33 (Ohad et al. 2004; Regel et al. 2001). In *Synechocystis sp.* PCC 6803, double mutants lacking
34 PsbJ and either PsbV or PsbO are unable to grow photoautotrophically (Choo et al. 2021).

35
36
37
38
39
40
41
42 In most of the deletion mutants, the observed phenotype is an alteration of the acceptor
43 side. However, it is difficult to attribute these changes more to a specific role of the deleted
44 subunits, rather than to perturbations in the overall structure of PSII. Cyanobacteria have
45 several PsbA isoforms (Mulo et al. 2009; Sugiura and Boussac, 2014; Sheridan et al. 2020). In
46 *Thermosynechococcus elongatus*, the deletion of the *psbJ* gene has different consequences
47 with either PsbA1 or PsbA3 as the D1 protein. In PsbA3-PSII, the effects are minor whereas
48 in the purified ΔPsbJ-PsbA1/PSII several other subunits including PsbY, PsbU, and PsbV are
49 lacking (Sugiura et al. 2010b). In contrast, Psb27, Psb28 and Tsl0063, have been found to be
50 associated to a proportion of the ΔPsbJ-PsbA1/PSII (Nowaczyk et al. 2012). These three
51 proteins are known to be PSII assembly factors (Nowaczyk et al. 2006; Roose and Pakrasi
52 2008; Komenda et al. 2012; Liu et al. 2013; Huang et al. 2021; Zabret et al. 2021). It should
53
54
55
56
57
58
59
60
61
62
63
64
65

1 be noted that Tsl0063 is named either Psb34 in (Zabret et al. 2021) or Psb36 in (Xiao et al.
2 2021). Structures of PSII corresponding to assembly intermediates have been recently solved
3 by using cryo-EM by using different strategies (Zabret et al. 2021; Huang et al. 2021; Xiao et
4 al. 2021). Upon deletion of the *psbJ* gene it became possible to isolate a “PSII-I” intermediate
5 with Psb27, Psb28 and Tsl0063 bound and in which the major conformational change was a
6 distortion of the Q_B binding site and the replacement of bicarbonate with glutamate as a ligand
7 of the non-heme iron (Zabret et al. 2021). From a *psbV* deletion mutant a dimeric Psb27-PSII
8 (Huang et al. 2021) and Psb28-PSII (Xiao et al. 201) have also been purified in which the
9 dissociation of PsbJ occurs. Such changes are proposed to protect the PSII from damage
10 during biogenesis until an active Mn₄CaO₅ cluster is assembled (Zabret et al. 2021; Xial et al.
11 2021).

12 Since the presence of Psb27 prevents the binding of PsbU and induces the dissociation
13 of PsbJ and PsbY (Huang et al. 2021) and since PsbJ also seems to trigger the release of
14 Psb28 (Zabret et al. 2021), the binding of PsbJ during the PSII assembly process very likely
15 occurs *after* the release of Psb27 and Psb28. Consequently, a PSII without Psb27, Psb28,
16 Tsl0063, and without PsbJ would logically also correspond to an assembly intermediate. In
17 the present work, we describe the results of experiments aiming at further characterizing the
18 Δ PsbJ-PsbA1/PSII purified from *Thermosynechococcus elongatus* by means of MALDI-TOF
19 spectroscopy, Thermoluminescence, EPR spectroscopy and UV-visible time-resolved
20 spectroscopy.

21 **Materials and Methods**

22 *Samples used*

23 The *Thermosynechococcus elongatus* strains used were; *i*) the Δ *psbA*₂, Δ *psbA*₃ deletion
24 mutant, referred to as either WT*1-PSII or PsbA1-PSII, *ii*) the Δ *psbA*₁, Δ *psbA*₂ deletion
25 mutant, referred to as either WT*3-PSII or PsbA3-PSII (Sugiura et al. 2010b), and *iii*) the
26 Δ PsbJ-43H deletion mutant (Sugiura et al. 2010b) which has the three *psbA* genes but in
27 which only the PsbA1-PSII is produced under the culture conditions used in this work, see
28 thereafter. These strains were constructed from the *T. elongatus* 43-H strain that had a His₆-
29 tag on the carboxy terminus of CP43 (Sugiura and Inoue 1999). PSII purification was
30 achieved as previously described (Sugiura et al. 2014). The final resuspending medium
31
32
33
34
35
36
37
38
39
40
41
42
43
44
45
46
47
48
49
50
51
52
53
54
55
56
57
58
59
60
61
62
63
64
65

1 contained 1 M betaine, 15 mM CaCl₂, 15 mM MgCl₂, 40 mM Mes, pH 6.5 adjusted with
2 NaOH.
3

4 5 *MALDI-TOF measurements* 6

7 All reagents and solvents were purchased from Sigma-Aldrich (Saint Quentin-
8 Fallavier, France) with the highest purity available. Peptides and protein used for calibration
9 were purchased from LaserBio Labs (TOF Mix) and Sigma (equine apomyoglobin),
10 respectively. For intact mass analysis, 1 μ L of PSII complex prepared at a concentration of
11 \sim 100 μ g Chl /mL in the medium mentioned above was mixed with 2 μ L of a saturated
12 solution of sinapinic acid in 60/0.1 acetonitrile/trifluoroacetic acid. Two microliters of this
13 premix were spotted onto the sample plate and allowed to dry under a gentle air stream.
14 Spectra were acquired in positive reflectron and linear mode on an Axima Performance
15 MALDI-TOF/TOF mass spectrometer (Shimadzu, Manchester, UK) with a pulse extraction
16 fixed at 4000 for 3000-10000 m/z range and at 10000 for 6000-20000 m/z range acquisitions.
17 All spectra were externally calibrated using a homemade calibrant mixture prepared by
18 mixing 1 μ L of 50 μ M apomyoglobine in water with 2 μ L of TOF Mix solution containing
19 ACTH [7-38] peptide at a concentration of 6 μ M.
20
21
22
23
24
25
26
27
28
29
30

31 32 *UV-visible time-resolved absorption change spectroscopy* 33

34 Absorption changes measurements have been performed with a lab-built spectro-
35 photometer (Béal et al. 1999) slightly modified as previously described (Sugiura et al. 2020)
36

37 The samples were diluted in 1 M betaine, 15 mM CaCl₂, 15 mM MgCl₂, and 40 mM
38 Mes (pH 6.5). PSII samples were dark-adapted for \sim 1 h at room temperature (20–22°C)
39 before, when indicated, the addition of 0.1 mM phenyl *p*-benzoquinone (PPBQ) dissolved in
40 dimethyl sulfoxide. The chlorophyll concentration of all the samples was \sim 25 μ g of Chl/mL.
41 After the $\Delta I/I$ measurements, the absorption of each diluted batch of samples was precisely
42 controlled to avoid errors due to the dilution of concentrated samples and the $\Delta I/I$ values were
43 normalized to $A_{673} = 1.75$, with $\epsilon \sim 70 \text{ mM}^{-1} \cdot \text{cm}^{-1}$ at 674 nm for dimeric PSII (Müh and Zouni
44 2005).
45
46
47
48
49
50
51
52

53 54 *EPR spectroscopy* 55

56 X-band cw-EPR spectra were recorded with a Bruker Elexsys 500 spectrometer
57 previously described (Sugiura et al. 2020) Flash illumination at room temperature was provided
58
59
60
61
62
63
64
65

1
2
3
4
5
6
7
8
9
10
11
12
13
14
15
16
17
18
19
20
21
22
23
24
25
26
27
28
29
30
31
32
33
34
35
36
37
38
39
40
41
42
43
44
45
46
47
48
49
50
51
52
53
54
55
56
57
58
59
60
61
62
63
64
65

by a neodymium:yttrium–aluminum garnet (Nd:YAG) laser (532 nm, 550 mJ, 8 ns Spectra Physics GCR-230-10). Illumination at 198 K with visible light was done in a non-silvered Dewar filled with ethanol cooled with dry ice for approximately 5-10 seconds with a 800 W tungsten lamp filtered by water and infrared cut-off filters. Illumination at 4.2 K was done in the EPR cavity using a low-voltage halogen lamp (24V, 250W, Philips Type 13163) filtered by water and infrared cut-off filters. After a 1 h dark-adaptation at room temperature the samples were frozen in the dark to 198 K in a dry ice ethanol bath and then transferred to 77 K in liquid N₂. Prior to the recording of the spectra the samples were degassed at 198 K.

Thermoluminescence measurements

Thermoluminescence (TL) curves were measured with a lab–built apparatus (Ducruet 2003; Ducruet and Vass 2009). PSII samples were diluted in 1 M betaine, 40 mM MES, 15 mM MgCl₂, 15 mM CaCl₂, pH 6.5 and then dark-adapted for at least 1 h at room temperature. When used, DCMU (100 μM, final concentration), dissolved in ethanol, was added after the dark-adaptation. Flash illumination was given at -10°C by using a saturating xenon flash. Two reasons justifies the choice of this temperature. Firstly, with the resuspending medium used, the freezing/melting of the samples occurs at ~ -15°C. Since the frozen samples are strongly diffusing, the flash illumination was done at a temperature slightly above -15°C. Secondly, an artefact occurs in the melting region which makes difficult the detection of small signals. It has been checked after the dilutions that the PSII samples had the same OD at 673 nm equal to 0.70 *i.e.* ~ 10 μg Chl/mL.

The measurements have been done on two different ΔPsbJ-PSII preparations with at least two measurements on each PSII samples except for the period 4 oscillation experiment at 291 nm done on only one PSII preparation. In addition to MALDI-TOF analysis, the protein content of the ΔPsbJ-PSII has been previously monitored with SDS-page and the oligomeric state of PSII was also analyzed by gel permeation (Sugiura et al. 2010b). Most of the ΔPsbJ-PSII, although not all, was in monomeric form and there was no evidence for the presence of any of the 3 proteins Psb28, Psb27 and Tsl0063 in significant amounts. For the spectroscopic measurements all samples were dark-adapted for one hour at room temperature before the measurements for allowing a full decay of S₂ and S₃ into S₁ (Sugiura et al. 2004).

Results

1 Before studying the effects of the PsbJ deletion some control experiments were
 2 performed. Indeed, it has been reported (Nowaczyk et al. 2012) that in *T. elongatus* cells
 3 having all the *psbA1*, *psbA2* and *psbA3* genes, and the *psbJ* gene inactivated by insertion of a
 4 cassette, PsbA1 was replaced by PsbA3 in the Δ PsbJ-PSII. Although this substitution was not
 5 observed in the most recent work done by the same group (Zabret et al. 2021) it seemed
 6 important to us to verify that the D1 subunit was indeed PsbA1 in our Δ PsbJ-43H/PSII which
 7 also contains the 3 genes, *psbA1*, *psbA2* and *psbA3*. For that, we have recorded the
 8 electrochromic blue shift undergone by Phe_{D1} in the Q_X spectral region upon the formation of
 9 Q_A⁻. This electrochromic C-550 band shift is well known to be red shifted by ~ 3.0 nm from
 10 544 nm in PsbA1-PSII to 547 nm in PsbA3-PSII. This shift reflects a hydrogen bond from the
 11 13¹-keto C=O group of Phe_{D1} stronger with the carboxylate group of E130 in PsbA3-PSII
 12 than with the amine group of Q130 in PsbA1-PSII (Merry et al. 1998; Cuni et al. 2004;
 13 Hughes et al. 2010; Shibuya et al. 2010).

14 Figure 1 shows the C-550 bandshift with PsbA1-PSII (black spectrum), in PsbA3-PSII
 15 (blue spectrum) and in Δ PsbJ-43H/PSII (red spectrum). For these measurements, the samples
 16 were first dark-adapted for one hour at room temperature. Then, the absorption changes were
 17 measured 15 μ s after each actinic flash in a series in the presence of PPBQ. The data points
 18 are the average of the individual absorption changes induced by the 2nd to 7th flashes. In the
 19 Δ PsbJ-43H/PSII the electrochromic band shift was similar to that in the PsbA1/PSII sample,
 20 showing unambiguously that the D1 protein is PsbA1 in the Δ PsbJ-43H/PSII.

21 Secondly, the polypeptide content was analysed in WT*1-PSII and Δ PsbJ-43H/PSII
 22 with MALDI-TOF spectroscopy. Panel A in Figure 2 shows the *m/z* region from 3500 to
 23 6500. The inset in Panel A shows the *m/z* region corresponding to PsbM (4009 Da calc.) and
 24 PsbJ (4002 Da calc.) by a using the reflection mode. The different peaks for one protein
 25 correspond to the different proportions of ¹³C in the proteins starting from no ¹³C (100% ¹²C)
 26 to 1, 2, 3, and so on, ¹³C per protein. The two peaks for PsbJ spaced by ~16 *m/z* likely
 27 correspond to an oxygen adduct for the larger *m/z* value, also seen in earlier reports as in
 28 (Sugiura et al. 2010b; Nowaczyk et al. 2012). Panel B in Figure 2 shows the *m/z* region from
 29 6500 to 16000. The PsbJ subunit, as expected, is missing in the Δ PsbJ-43H/PSII (Sugiura et
 30 al. 2010b; Nowaczyk et al. 2012). In Δ PsbJ-43H/PSII, other subunits are missing as PsbY,
 31 PsbU, PsbV (the Cyt_{c550}) as previously observed. However, PsbM and PsbF are now detected
 32 in 43H/ Δ PsbJ-PSII exhibiting a peak with an amplitude comparable to that in WT*1-PSII and
 33 with a single peak for PsbM while two peaks (native and formylated) were previously
 34

1 observed in (Sugiura et al. 2010b). The reasons for such a difference between the two
 2 observations is at present unclear. A reexamination of the raw data in (Sugiura et al. 2010b)
 3 indicates that at that time we did not pay attention to the possible presence of Psb28 in a very
 4 small proportion of our Δ PsbJ-43H/PSII. Indeed, a very small peak at $m/z \sim 12787$ was
 5 present (Sugiura et al. 2010b). Panel B in Figure 2 also shows a very small peak at 12787 that
 6 could well correspond to Psb28. However, the amplitude of this peak is close to the limit of
 7 the detection. A small peak detected at $m/z=13424$ in some traces could correspond to Psb27
 8 (not shown). A peak at $m/z=5936$, not attributed in (Sugiura et al. 2010b) could originate from
 9 Tsl0063 recently detected in Δ PsbJ-PsbA1/PSII (Zabret et al. 2021). This protein is however
 10 not detected in Figure 2. The MALDI-TOF data described above in comparison with those in
 11 literature show that upon the deletion of PsbJ in PsbA1-PSII, the PSII composition may
 12 slightly vary from prep to prep. If present, the 3 proteins Psb27, Psb28 and Tsl0063 are in a so
 13 minor proportion of the Δ PsbJ-43H/PSII studied here that this proportion will not contribute
 14 significantly to the results described thereafter. We cannot eliminate the possibility that these
 15 3 proteins are removed during the PSII purification. This, however, does not modify the fact
 16 that the studied Δ PsbJ-43H/PSII does not bind Psb27, Psb28 and Tsl0063.

17
 18 In *Synechocystis* 6803, the deletion of PsbJ has been proposed to alter both the
 19 forward electron flow from Q_A^- to the plastoquinone pool and the back reaction between Q_A^-
 20 and the oxidized Mn_4CaO_5 cluster (Regel et al. 2001). These conclusions were done in part
 21 from thermoluminescence experiments (Rutherford et al. 1982) in whole cells. Here, similar
 22 measurements have been done but in purified WT*1-PSII and Δ PsbJ-43H/PSII. Figure 3
 23 shows the TL curves after 1 flash given at -10°C in WT*1-PSII, black traces, and Δ PsbJ-
 24 43H/PSII, red traces. In Panel A, the TL measurements were done without any addition
 25 whereas in Panel B they were done in the presence of DCMU. The TL curves in WT*1-PSII
 26 arising from the $S_2Q_B^-$ charge recombination in Panel A with a peak temperature at $\sim 43^\circ\text{C}$
 27 and from the $S_2Q_A^-$ /DCMU charge recombination in Panel B with a peak temperature at
 28 $\sim 13^\circ\text{C}$ are those expected in *T. elongatus* with an heating rate of 0.4°C/s . In Δ PsbJ-43H/PSII,
 29 no signal was detected both in Panels A and B. The very small signal around 0°C in Panels A
 30 and B is very similar in the absence and the presence of DCMU and therefore cannot arise
 31 from the $S_2Q_B^-$ and $S_2Q_A^-$ /DCMU charges recombinations studied here. The TL results in
 32 Figure 3 differ significantly from those in *Synechocystis* whole cells where in the Δ PsbJ
 33 mutant a small TL signal was detected at a slightly lower temperature for the $S_2Q_B^-$ charge
 34 recombination and at a slightly higher temperature for the $S_2Q_A^-$ /DCMU charge
 35 recombination.

1 recombination (Regel et al. 2001). However, the amplitude of a TL signal depends on the
 2 proportion of centers with Q_B^- in the dark-adapted state, something that is difficult to control
 3 in whole cells. The lack of a TL signal in Δ PsbJ-43H/PSII both with and without DCMU may
 4 be explained if 100% of the centers are in the Q_B^- state upon the dark adaptation. As will be
 5 shown later, this is not the case in the Δ PsbJ-43H/PSII studied and so another explanation is
 6 needed.
 7
 8
 9

10 The first simple explanation is that the radiative charge recombination in the Δ PsbJ-
 11 43H/PSII occurs either *i*) at a temperature much above a bearable temperature for PSII (*i.e.*
 12 $\gg 60^\circ\text{C}$) or *ii*) at a temperature much lower than 0°C . In the first case, the *Em* of the Q_A/Q_A^-
 13 couple, upon the deletion of PsbJ, would be strongly increased and, in the second case,
 14 strongly decreased. The second possibility could be a situation in which the Mn_4CaO_5 cluster
 15 in the Δ PsbJ-43H/PSII is inactive or lost because we know that under continuous illumination
 16 the activity is significantly decreased (Sugiura et al. 2010b).
 17
 18
 19
 20
 21
 22
 23

24 Before going further in the interpretation of the TL experiments, we have performed
 25 some EPR measurements for clarifying the situation.
 26

27 Figure 4 shows the EPR spectra recorded at 8.6 K in dark-adapted samples (black
 28 spectra) and after a continuous illumination at 198 K (red spectra). The blue spectra are the
 29 light-*minus*-dark spectra. At 198 K, the electron transfers from Q_A^- to Q_B and from Q_A^- to Q_B^-
 30 are blocked so that only one charge separation may occur (Fufezan et al. 2005). In WT*1-
 31 PSII, the black spectrum is very similar to the spectrum recorded in PsbA3-PSII under the
 32 same conditions, see (Boussac et al. 2011) for a detailed description of the spectra. The signal
 33 between 3600 and 5000 gauss originates from $\text{Fe}^{2+}Q_B^-$ (Fufezan et al. 2005; Boussac et al.
 34 2011; Sedoud et al. 2011). After illumination at 198 K for ~ 5 -10 s, the S_2 multiline signal
 35 was formed together with a signal at $g = 1.6$ (~ 4100 gauss). The $g = 1.6$ signal originates
 36 from the $Q_A^- \text{Fe}^{2+} Q_B^-$ state. The $Q_A^- \text{Fe}^{2+}$ signal formed in centers with Q_B oxidized prior to the
 37 illumination is difficult to detect in the presence of the multiline signal. A careful examination
 38 of the blue spectrum in the $g = 6$ to $g = 8$ region indicates that the non-heme iron was oxidized
 39 in a very small fraction of the dark-adapted centers and was reduced upon the 198 K
 40 illumination (Boussac et al. 2011). The spectrum in the dark-adapted Δ PsbJ-43H/PSII also
 41 exhibits a $\text{Fe}^{2+}Q_B^-$ signal with a somewhat smaller amplitude (see also Figure 7) than in
 42 WT*1-PSII. This observation rules out the hypothesis that the lack of a TL signal is due to
 43 centers with 100% Q_B^- in the dark-adapted state. In agreement with the MALDI-TOF data
 44 above, and as previously reported (Sugiura et al. 2010b), the EPR also shows that the Cyt_{c550}
 45
 46
 47
 48
 49
 50
 51
 52
 53
 54
 55
 56
 57
 58
 59
 60
 61
 62
 63
 64
 65

(PsbV) is missing in the purified PSII as evidenced by the much smaller signals at $g \sim 3$ and $g \sim 2.2$ (3000 gauss) corresponding to the g_z and g_y resonances of cytochrome signals, respectively (the g_x feature is difficult to detect under the conditions used for the recording of these spectra). We have nevertheless previously shown that PsbV was detectable in the Δ PsbJ-43H/thylakoids (Sugiura et al. 2010b). Cyt b_{559} is detected because it is in the low potential oxidized form in Δ PsbJ-43H/PSII (Sugiura et al. 2010). The detection of a signal at $g = 6$ (~ 1100 gauss) indicates that a proportion of Cyt b_{559} is also present in an oxidized high spin ($S = 5/2$) configuration. Importantly, the S_2 multiline signal is detectable upon the 198 K illumination with an amplitude close to 60-70 % of that in WT*1-PSII. Therefore, the total absence of a TL signal in this sample is also not due to an inactive or missing Mn_4CaO_5 cluster. The proportion of Δ PsbJ-43H/PSII in which the Mn_4CaO_5 is able to progress to the S_2 state upon an illumination at 198 K is higher than the O_2 evolution activity found in this PSII that is about 30% (Sugiura et al. 2010b). However, it is well known that the O_2 activity under continuous illumination does not necessarily correlate with the proportion of active centers. For example, upon the substitution of Ca^{2+} for Sr^{2+} the O_2 activity under continuous illumination is decreased by a least of factor of 2 whereas all the centers are fully active (Ishida et al. 2008). In an additional control experiment (not shown) aiming at following the period four oscillation measured at 291 nm and 100 ms after each flash of a series (Lavergne 1991; Ishida et al. 2008) it has been found that in the Δ PsbJ-43H/PSII the miss parameter is close to 20% instead of $\sim 8\%$ in the PsbA1-PSII.

The remaining possible explanations for the lack of a TL signal in Δ PsbJ-43H/PSII are either *i*) an inefficient charge separation after one flash illumination in contrast to the continuous illumination at 198 K, and/or *ii*) a too fast, even at $-10^\circ C$, or too slow charge recombination in the temperature range probed by the TL thus preventing the detection of the signal. These possibilities have been tested in the EPR experiments reported in Figure 5 and Figure 6.

Panel A in Figure 5 shows the magnetic field range in which most of the EPR signals are detectable except Tyr D^\bullet . The Tyr D^\bullet signal is shown in Panel B. The black spectra were recorded in dark-adapted PSII and they are, of course, similar to those described in Figure 4. The green spectra have been recorded after one saturating flash given at room temperature ($\sim 20-22^\circ C$) followed by an as-fast-as possible freezing of the sample (~ 2 s) in a dry ice bath at 198 K. Then, the red spectra were recorded after a further continuous illumination at 198 K following the one flash illumination. In WT*1-PSII, the difference in the amplitude of the S_2

1 multiline between the green and red spectra is mainly due to the proportion of centers in
 2 which the $S_0\text{Tyr}_D^\bullet$ to $S_1\text{Tyr}_D^\bullet$ transition occurs with the one flash illumination. As the Tyr_D^\bullet
 3 signal (Panel B) does not vary significantly, this suggests that the proportion of centers in
 4 which the $S_1\text{Tyr}_D$ to $S_1\text{Tyr}_D^\bullet$ transition occurs is negligible (Styring and Rutherford 1987).
 5

6
 7 In contrast, in $\Delta\text{PsbJ-43H/PSII}$, upon the illumination at 198 K, the increase of the S_2
 8 multiline and Tyr_D^\bullet signals was much more pronounced than in WT*1-PSII . This results
 9 shows that in dark-adapted $\Delta\text{PsbJ-43H/PSII}$ there is a proportion of centers in the $S_1\text{Tyr}_D$ state
 10 and a larger proportion of centers in the $S_0\text{Tyr}_D^\bullet$ state than in WT*1-PSII . Since the
 11 proportion of centers in the $\text{Q}_A\text{Fe}^{2+}\text{Q}_B^-$ state is smaller in the $\Delta\text{PsbJ-43H/PSII}$ than in WT*1-
 12 PSII after the dark adaptation, this ratio is inversed after the one flash illumination.
 13 Consequently, the illumination at 198 K is expected to induce a larger $\text{Q}_A^-\text{Fe}^{2+}\text{Q}_B^-$ in $\Delta\text{PsbJ-}$
 14 43H/PSII than in WT*1-PSII and that is indeed what is observed here. It should be mentioned
 15 that, normally, an illumination at 198 K is unable to oxidize Tyr_D in active centers. The
 16 increase seen in Panel B therefore likely occurs in the proportion of inactive $\Delta\text{PsbJ-43H/PSII}$.
 17 The important result in this experiment is that the one-flash illumination is able to induce the
 18 S_2 state in the $\Delta\text{PsbJ-43H/PSII}$ although to a slightly less extent than in WT*1-PSII due to a
 19 higher proportion of centers in the $S_1\text{Tyr}_D$ and $S_0\text{Tyr}_D^\bullet$ states and also to a higher miss
 20 parameter. The stability of the S_2 state has then been monitored in an experiment
 21 corresponding to the TL experiment in the presence of DCMU.
 22
 23
 24
 25
 26
 27
 28
 29
 30
 31
 32
 33
 34
 35

36 In Figure 6, the black spectra were recorded in dark-adapted PSII without any addition
 37 and the red spectra after the addition of DCMU. Two observations can be made here. Firstly,
 38 in both WT*1-PSII and $\Delta\text{PsbJ-43H/PSII}$, the addition of DCMU resulted in the formation of
 39 $\text{Q}_A^-\text{Fe}^{2+}/\text{DCMU}$ to the detriment of $\text{Fe}^{2+}\text{Q}_B^-$ (Velthuys 1981). In both samples, Q_A^-
 40 $\text{Fe}^{2+}/\text{DCMU}$ exhibited either the $g = 1.9$ signal or the $g = 1.82$ signal (Rutherford et al. 1983,
 41 Rutherford and Zimmermann 1984), see below for a better description of the signals in Figure
 42 6. Secondly, in WT*1-PSII , the addition of DCMU also modified the non-heme iron signal as
 43 previously observed (Diner and Petrouleas 1987). The blue spectra were then recorded after a
 44 continuous illumination at 198 K. The S_2 multiline signal was formed in the open centers, *i.e.*
 45 in those with no Q_B^- prior to the addition of DCMU. The larger $\text{Q}_A^-\text{Fe}^{2+}$ signal at $g = 1.9$ in
 46 $\Delta\text{PsbJ-43H/PSII}$ than in WT*1-PSII have two possible explanations: *i*) a lower amount of Q_B^-
 47 before the addition of DCMU and *ii*) a smaller proportion of oxidized non-heme iron. Indeed,
 48 the oxidation of Q_A^- by the oxidized non-heme iron results in the disappearance of the non-
 49
 50
 51
 52
 53
 54
 55
 56
 57
 58
 59
 60
 61
 62
 63
 64
 65

1 heme iron signal is WT*1-PSII. Unfortunately, in Δ PsbJ-43H/PSII, the presence of the high
 2 spin Cyt_{b559} signal does not allow the detection of the non-heme iron signal.

3
 4 After the illumination at 198 K, the samples were immersed for 1 to 2 seconds, in total
 5 darkness, in an ethanol bath at 0°C and immediately refrozen in a dry ice bath at 198 K and
 6 the green spectra were recorded. In WT*1-PSII, the brief passage at 0°C induced almost no
 7 change in the amplitude of the S₂ multiline signal. In contrast, in Δ PsbJ-43H/PSII, almost all
 8 the S₂ multiline signal and the $g = 1.9$ quinone signal disappeared thus showing that the
 9 recombination in the S₂Q_A⁻/DCMU state is very fast at 0°C in this sample. This very likely
 10 explains the lack of a TL signal in Figure 3B. The proportion of the $g = 1.9$ signal which
 11 decayed during the warming at 0°C appears larger than the proportion the $g = 1.82$ signal
 12 which decayed. This suggests that the recombination was more efficient with the quinone in
 13 the $g = 1.9$ state than in the $g = 1.82$ state (Demeter al. 1993; Rutherford, personal
 14 communication). Finally, the samples were immersed, in the dark, in an ethanol bath at 20°C
 15 and immediately refrozen in a dry ice bath at 198 K and the spectra in magenta were recorded.
 16 In WT*1-PSII, the S₂ multiline now decreased significantly as expected from the peak
 17 temperature observed in this sample. In Δ PsbJ-43H/PSII, the spectrum was not significantly
 18 different from that one after the thawing at 0°C. The recording of the Tyr_D[•] spectra as in Panel
 19 B of Figure 5 showed again that Tyr_D[•] could be induced at 198 K and that a decay occurs
 20 upon the short incubation at 0°C (not shown). The experiments described above focused on
 21 the charge recombinations. In the following, we will address the forward electron transfer.
 22
 23
 24
 25
 26
 27
 28
 29
 30
 31
 32
 33
 34
 35
 36

37 Figure 7 shows the flash-induced $\Delta I/I$ and its decay at 320 nm after the 2nd flash given
 38 on dark-adapted WT*3-PSII (blue), WT*1-PSII (black) and Δ PsbJ-43H/PSII (red). The Q_A⁻-
 39 *minus*-Q_A and Q_B⁻-*minus*-Q_B difference spectra are similar and have their maximum
 40 amplitude at around 320 nm (Schatz and van Gorkom 1985). After the 1st flash and the 3rd
 41 flash, the S₁ to S₂ and S₃ to S₀ transitions also contribute significantly to the flash induced
 42 absorption changes at 320 nm (Lavergne 1991). In addition, the first flash is also complicated
 43 by the Q_A⁻ to Fe²⁺ electron transfer (Boussac et al. 2011) with possible contribution in this
 44 spectral range of the Fe³⁺/Fe²⁺ couple (Sellés and Boussac, unpublished) and with the
 45 formation of the Tyr_Z[•] radical in inactive centers (with a flash spacing of 300 ms, the dead
 46 centers contribute mainly on the first flash due to the slow decay of Tyr_Z[•]). For all these
 47 reasons, Figure 7 only shows the data after the second flash which is the easiest kinetics to
 48 analyze. In centers with Q_B oxidized in the dark-adapted state the flash illumination forms the
 49 Q_A⁻Q_B state and then the Q_AQ_B⁻ state. In these centers, the flash-induced $\Delta I/I$ does not decay
 50
 51
 52
 53
 54
 55
 56
 57
 58
 59
 60
 61
 62
 63
 64
 65

and it is responsible for the remaining stable $\Delta I/I$ at the longest times. In dark-adapted centers with Q_B^- present, the flash illumination forms the $Q_A^-Q_B^-$ state and then the $Q_AQ_BH_2$ state. This reaction is at the origin of the decay in Figure 7 and these kinetics are similar in the 3 samples with a $t_{1/2}$ of 2-3 ms. The similar apparent lag phase with a duration of ~ 1 ms likely corresponds to the electron transfer between Q_A^- and either Q_B or Q_B^- . This experiment shows that the forward electron transfer is not affected by the deletion of PsbJ.

Finally, Figure 8 shows EPR spectra in WT*1-PSII (black spectra) and Δ PsbJ-43H/PSII (red spectra) recorded with a magnetic field scale allowing a better observation of the quinone signals. Panel A shows the $Fe^{2+}Q_B^-$ signal recorded in the dark-adapted samples. The signal is smaller in the Δ PsbJ-43H/PSII as mentioned previously and very slightly shifted. Panel B shows the spectra after a further illumination at 4.2 K. In centers with Q_B^- present in the dark this 4.2 K illumination resulted in the formation of the $Q_A^-Fe^{2+}Q_B^-$ signal that is larger in the WT*1-PSII. In the Δ PsbJ-43H/PSII, consequently to the larger proportion of centers with Q_B in the dark-adapted state, the 4.2 K illumination resulted in a larger proportion of $Q_A^-Fe^{2+}Q_B$ giving rise to the $g = 1.9$ signal between 3500 and 3700 gauss. Panel C shows the spectra recorded after an illumination at 4.2 K of samples in which a low amount of ferricyanide has been added (less than 100 μ M) upon the dark adaptation to have the highest proportion of Q_B without the risk to oxidize the non-heme iron. Although there was still a low amount of $Q_A^-Fe^{2+}Q_B^-$ signal in Δ PsbJ-43H/PSII, in both samples such a procedure resulted in the formation of a similar $Q_A^-Fe^{2+}Q_B$ characterized by the $g = 1.9$ signal. Finally, in Panel D the spectra were recorded after the addition of DCMU which resulted in the formation of $Q_A^-Fe^{2+}/DCMU$ in centers with Q_B^- present in the dark. Two signals are observed in the two samples, the signal at $g = 1.9$ and a much broader ~ 300 gauss-width signal reminiscent of a signal previously observed (Sedoud et al. 2011). The larger amplitude of these two signals in WT*1-PSII resulted of the higher concentration of Q_B^- in the dark in this PSII.

Discussion

In PSII lacking the PsbJ subunit it is possible to observe a proportion of the enzyme associated to polypeptides known to be assembly cofactors such as Psb27, Psb28 and Tsl0063, and which are not detected in the mature PSII, *e.g.* (Nowaczyk et al. 2006; Roose and Pakrasi 2008; Komenda et al. 2012; Liu et al. 2013; Huang et al. 2021; Zabret et al.

2021). The cryo-EM structure of an intermediate state was resolved (Zabret et al. 2021) with the interesting observation that the bicarbonate ligand of non-heme iron is replaced with a glutamate (glu241 of PsbD), a structural motif found in purple bacteria. Such a motif was further proposed to protect PSII from damage during biogenesis. Although the 3 proteins Psb27, Psb28 and Tsl0063 are possibility detected in the Δ PsbJ-43H/PSII studied here, the MALDI-TOF signals are so weak that we can reasonably consider that the purified PSII studied here is devoid of these assembly cofactors, see also (Sugiura et al. 2010b). The main peptides which are missing in this Δ PsbJ-43H/PSII are PsbY, PsbU and PsbV. Although PsbV is present in the Δ PsbJ-thylakoids (Sugiura et al. 2010b), the g_z value is lower than in intact PSII. This indicates (Roncel et al. 2003) that PsbV is not properly bound to PSII in thylakoids in the absence of PsbJ. Therefore, PsbJ very likely stabilizes the binding of the extrinsic peptides PsbU and PsbV and possibly of the trans-membrane α -helix PsbY as previously suggested (Zabret et al. 2021; Huang et al. 2021; Xiao et al. 2021). The Δ PsbJ-43H/PSII is essentially monomeric (Sugiura et al. 2010b) and in agreement with such a destabilization for PsbY, it was observed that although present, no electron density corresponding to PsbY was found in a crystal of monomeric PSII (Broser et al. 2010).

Despite the close proximity of PsbJ with the Q_B binding pocket, from the data in Figure 8, the lack of this subunit does not dramatically perturb, from an EPR point of view, any of the four states $Q_AFe^{2+}Q_B^-$, $Q_A^-Fe^{2+}Q_B$, $Q_A^-Fe^{2+}Q_B^-$ and $Q_A^-Fe^{2+}/DCMU$. The quinone Q_B is present and DCMU binds in the Q_B pocket, with the same consequences, as in the wild type PSII. Nevertheless, despite the lack of strong structural changes, the energetics is strongly modified. Since a great proportion of Δ PsbJ-43H/PSII has an intact Mn_4CaO_5 cluster, this allowed us to probe these changes by using thermoluminescence (Rutherford 1982; Johnson et al. 1995; Cser and Vass 2007; Rappaport and Lavergne 2009).

In WT*1-PSII, the TL peak corresponding to the $S_2Q_A^-/DCMU$ recombination is downshifted by $\sim 32^\circ C$, from $45^\circ C$ to $13^\circ C$, when compared to the $S_2Q_B^-$ recombination. According to a correspondence of $0.3-0.4^\circ C/mV$ estimated by Rappaport and Lavergne (2009), see also (Cser and Vass 2007), this locates the energy level of the $S_2Q_A^-/DCMU$ state at least 80 mV ($= 32/0.4$) above the energy level of the $S_2Q_B^-$ state in WT*1-PSII. If we assume that the Em of the Q_A/Q_A^- couple is increased by about 50 mV with DCMU bound as in plant PSII (Krieger et al. 1995), this would locate the energy level of the $S_2Q_A^-$ state at least $80 + 50 = 130\text{ mV}$ above that of the $S_2Q_B^-$ state in WT*1-PSII.

1 In Δ PsbJ-43H/PSII neither the $S_2Q_A^-$ /DCMU nor the $S_2Q_B^-$ charge recombinations are
 2 detectable in the temperature range from -10°C to 70°C . The same reasoning done above for
 3 the WT*1-PSII would locate the energy level of the $S_2Q_A^-$ /DCMU state at least 200 mV (= $80/0.4$)
 4 above the $S_2Q_B^-$ state in Δ PsbJ-43H/PSII, 80°C being the lower limit for the difference
 5 in the TL peaks corresponding to the $S_2Q_A^-$ /DCMU and $S_2Q_B^-$ charge recombinations in this
 6 sample.
 7
 8
 9

10 We cannot totally discard the possibility that the release of PsbV affects the stability of
 11 S_2 in the Δ PsbJ-43H/PSII. However, *Synechocystis* mutants lacking PsbV exhibit TL peaks at
 12 a slightly higher temperature than in the wild type (Shen et al. 1998) suggesting an increase of
 13 the S_2 stability that is the opposite of what is seen here.
 14
 15
 16
 17

18 For analyzing the TL data, two extreme cases will be considered assuming that the
 19 effect of the deletion occurs mainly on the acceptor side. In the first one, the deletion of PsbJ
 20 would only affect the Em of the Q_A/Q_A^- couple whereas in the second case, only the Em of the
 21 Q_B/Q_B^- couple would be affected. We cannot discard a possible effect on both Q_A and Q_B . In
 22 this case, the changes will apply on Q_A and Q_B but to a less extent on each of them.
 23
 24
 25
 26
 27

28 In the first case, we will assume that in Δ PsbJ-43H/PSII the binding of DCMU also
 29 increases the Em of the Q_A/Q_A^- couple by ~ 50 mV as supposed above for WT*1/PSII.
 30 Therefore, with an energy level of the $S_2Q_A^-$ /DCMU state at least 200 mV above that of the
 31 $S_2Q_B^-$ state this would locate the energy level of the $S_2Q_A^-$ state (without DCMU) at least
 32 $200+50=250$ mV above the $S_2Q_B^-$ state in Δ PsbJ-43H/PSII instead of 130 mV in WT*1-PSII.
 33 Although the value of 250 mV could be overestimated, this high value explains the lack of the
 34 $S_2Q_B^-$ charge recombination experimentally observed in the TL experiment and the very fast
 35 $S_2Q_A^-$ /DCMU charge recombination. The decrease in the Em of the Q_A/Q_A^- couple could also
 36 explain the faster charge recombination observed in *Synechocystis* 6803 (Regel et al. 2001) in
 37 the absence of PsbJ if we are in conditions with a large proportion of the quinone pool fully
 38 reduced as often observed with whole cells.
 39
 40
 41
 42
 43
 44
 45
 46
 47

48 In the second case, the Em of the Q_B/Q_B^- couple would reach a value disfavoring the
 49 electron coming back on Q_A . However, the energy level of the $S_2Q_A^-$ /DCMU also needs to be
 50 much higher in Δ PsbJ-43H/PSII than in WT*1-PSII to explain the lack of a TL signal in the
 51 presence of DCMU above -10°C . Since the peak in WT*1-PSII is observed at 13°C , a peak at
 52 a temperature below -10°C correspond to a decrease by at least ~ -58 mV ($-23/0.4$) for the Em
 53 of the Q_A/Q_A^- couple in the presence of DCMU when compared to WT*1-PSII. Since PsbJ is
 54 close to the Q_B pocket and therefore close to the DCMU binding site, a DCMU effect on the
 55
 56
 57
 58
 59
 60
 61
 62
 63
 64
 65

1 *Em* of the Q_A/Q_A^- couple different in Δ PsbJ-43H/PSII than in plant PSII would not be
2 unlikely. If we further push the reasoning assuming no change in the *Em* Q_A/Q_A^- couple in the
3 Δ PsbJ-43H/PSII, the effect of the DCMU binding could be negligible. Indeed, the *Em* of the
4 Q_A/Q_A^- couple with DCMU bound in the Δ PsbJ-43H/PSII would be the same than for the
5 Q_A/Q_A^- couple in the absence of DCMU in WT*1/PSII. A higher *Em* of the Q_B/Q_B^- couple
6 may also explain the lower O_2 evolution under continuous illumination by the Δ PsbJ-
7 43H/PSII (Sugiura et al. 2010b) by decreasing the efficiency of the electron transfer between
8 Q_B^- and the added quinone.
9

10
11
12
13
14
15
16
17
18
19
20
21
22
23
24
25
26
27
28
29
30
31
32
33
34
35
36
37
38
39
40
41
42
43
44
45
46
47
48
49
50
51
52
53
54
55
56
57
58
59
60
61
62
63
64
65
Alone, a low *Em* of the Q_A/Q_A^- couple in Δ PsbJ-43H/PSII is expected to increase the
damages due to the repopulation of triplet states in the functional enzyme. For that reason we
would favor the model in which only the *Em* of the Q_B/Q_B^- couple is affected (increased) in
 Δ PsbJ-43H/PSII. The increase of the ΔE_m between Q_A/Q_A^- and Q_B/Q_B^- , and without affecting
the forward electron transfer, could contribute in a protection against the charge
recombinations between the donor side and Q_B^- . Such a charge recombination was identified
as the origin of the damage by about 2 orders of magnitude higher than induced by the same
amount of energy delivered by continuous light (Keren et al. 1997) and a protection against it
would favor the photoactivation process, see (Bao and Burnap 2016) for a recent review on
photoactivation.

Legends of the figures

1
2
3
4 Figure 1: Light-induced difference spectra around 545 nm. The flash-induced absorption
5 changes were measured in PsbA1/PSII (black spectrum), Δ PsbJ-43H/PSII (red spectrum) and
6 PsbA3-PSII (blue spectrum). The data points are the average of the $\Delta I/I$ values detected 15 μ s
7 after the 2nd to 7th actinic flashes given to dark-adapted PSII. After dark adaptation for 1 h at
8 room temperature, 100 μ M PPBQ (dissolved in dimethyl sulfoxide) was added to the samples.
9 The amplitude of the spectra were normalized to a Chl concentration corresponding to
10 $OD_{673nm}=1.75$.
11
12
13
14
15
16
17

18 Figure 2: MALDI-TOF MS profiling of PSII subunits. (A) Linear mode MALDI-TOF spectra
19 of subunits from Δ PsbJ-43H/PSII (upper panel) and WT*1-PSII (lower panel) strains. For
20 presentation, both spectra were internally recalibrated on known peaks of PSII subunits using
21 their theoretical average masses (formylated PsbT, $m/z = 3902.67$ Da; PsbK, $m/z = 4099.88$
22 Da; PsbL, $m/z = 4297.02$ Da; acetylated PsbF, $m/z = 4975.66$ Da; formylated PsbZ, $m/z =$
23 6792.18 Da; PsbE, $m/z = 9441.53$ Da) according to (Sugiura et al. 2010a 2010b, Boussac et al.
24 2013, Nowaczyk et al. 2012). In the inset, zoom of the 3090-4025 m/z range of high-
25 resolution MALDI-TOF spectra from Δ PsbJ-43H/PSII mutant (upper panel) and WT*1-PSII
26 wild-type (lower panel) strains acquired in reflection mode. Both spectra were internally
27 recalibrated on known mono-isotopic peaks of PSII subunits using their theoretical mono-
28 isotopic masses (formylated PsbT, $m/z = 3900.09$ Da; PsbK, $m/z = 4097.32$ Da; PsbL, $m/z =$
29 4294.32 Da; acetylated PsbF, $m/z = 4972.61$ Da. (B) Linear mode MALDI-TOF spectra of
30 Δ PsbJ-43H/PSII mutant (upper panel) and WT*1/PSII (lower panel) strains. In the upper
31 panel which shows the 11000-15000 m/z range for the Δ PsbJ-43H/PSII mutant spectrum, the
32 amplitude was magnified 10 times. (*) this 206 Da mass shift could correspond to farnesyl
33 adduct find in mono-charged and discharged PsbV. There is no peak at 16472 m/z which
34 suggests that the peak at 8236 m/z does not correspond to a double charged ion. Instead, it
35 could correspond to a contamination by the subunit c of the ATP synthase (Suhai et al. 2008).
36
37
38
39
40
41
42
43
44
45
46
47
48
49
50
51
52

53 Figure 3: Thermoluminescence curves after one flash given at -10°C either without any
54 addition (Panel A) or in the presence of DCMU (Panel B). Black curve, WT*1/PSII; red
55 curve, Δ PsbJ-43H/PSII. The concentration of the samples was adjusted exactly to
56 $OD_{673nm}=0.7$ (~ 10 μg Chl/mL) before to be dark-adapted at room temperature for at least 1 h.
57
58
59
60
61
62
63
64
65

1
2
3
4
5
6
7
8
9
10
11
12
13
14
15
16
17
18
19
20
21
22
23
24
25
26
27
28
29
30
31
32
33
34
35
36
37
38
39
40
41
42
43
44
45
46
47
48
49
50
51
52
53
54
55
56
57
58
59
60
61
62
63
64
65

In Panel B, the final concentration of DCMU, dissolved in ethanol, was 100 μM . After the addition of DCMU, the samples were immediately loaded into the cuvette in total darkness. The heating rate was 0.4°C/s.

Figure 4: EPR spectra recorded in WT*1-PSII and $\Delta\text{PsbJ-43H/PSII}$. The spectra were recorded after dark-adaptation for 1 hour at room temperature (black spectra) and after a continuous illumination at 198 K (red spectra). The blue spectra are the light-*minus*-dark spectra. The concentration was 1.1 mg Chl/mL. Instrument settings: temperature, 8.6 K; modulation amplitude, 25 G; microwave power, 20 mW; microwave frequency, 9.4 GHz; modulation frequency, 100 kHz.

Figure 5: EPR spectra recorded in WT*1/PSII and $\Delta\text{PsbJ-43H/PSII}$. The spectra were recorded after dark-adaptation for 1 hour at room temperature (black spectra), after illumination by one flash at room temperature (green spectra) and after a further continuous illumination at 198 K (red spectra). The concentration was 1.1 mg Chl/mL. Instrument settings: temperature, 8.6 K; microwave frequency, 9.4 GHz; modulation frequency, 100 kHz. Modulation amplitude, 25 G and microwave power, 20 mW in Panel A and modulation amplitude, 2.8 G and microwave power, 2 μW in Panel B. In the conditions used for the recording of the Tyr_D[•] spectra, the microwave power is still slightly saturating so that an increase in the relaxation properties upon the formation of S₂ induces an increase of the signal amplitude (Styring and Rutherford 1988). This effect is larger in the negative part of the signal and is less when using a smaller modulation frequency (not shown) which is indicative of a rapid-passage effect (Styring and Rutherford 1988).

Figure 6: EPR spectra recorded in WT*1-PSII (Panel A) and $\Delta\text{PsbJ-43H/PSII}$ (Panel B). The spectra were recorded after dark-adaptation for 1 hour at room temperature (black spectra) and after the addition (100 μM) dissolved in ethanol (red spectra). Then, the blue spectra were recorded after an illumination at 198 K. The green spectra were recorded after a brief (1-2 s) warming of the samples at 0°C and the spectra in magenta were recorded after a second brief warming at 20°C. The concentration was 1.1 mg Chl/mL. Instrument settings: temperature, 8.6 K; microwave frequency, 9.4 GHz; modulation frequency, 100 kHz; modulation amplitude, 25 G; microwave power, 20 mW.

1
2
3
4
5
6
7
8
9
10
11
12
13
14
15
16
17
18
19
20
21
22
23
24
25
26
27
28
29
30
31
32
33
34
35
36
37
38
39
40
41
42
43
44
45
46
47
48
49
50
51
52
53
54
55
56
57
58
59
60
61
62
63
64
65

Figure 7: Time-courses of the $\Delta I/I$ changes at 320 nm after the 2nd flash given on dark-adapted WT*1-PSII (black points), Δ PsbJ-43H/PSII (red points) and WT*3-PSII (blue data points). Flashes spaced 300 ms apart. Chl concentration adjusted to $OD_{673nm}=1.75$.

Figure 8: EPR spectra recorded in WT*1-PSII (black spectra) and Δ PsbJ-43H/PSII (red spectra). Panel A, the spectra were recorded after dark-adaptation for 1 hour at room temperature. Panel B, the spectra were recorded after a further illumination at 4.2 K. Panel C, the spectra were recorded after the addition of 100 μ M of ferricyanide on dark-adapted samples followed by an illumination at 4.2 K. Panel D, the spectra were recorded after the addition of DCMU (100 μ M) dissolved in ethanol to dark-adapted samples. The concentration was 1.1 mg Chl/mL. Instrument settings: temperature, 4.2 K except for Panel A in which T = 8.6 K; microwave frequency, 9.4 GHz; modulation frequency, 100 kHz; modulation amplitude, 25 G; microwave power, 20 mW.

References

- 1
2
3 Bao H, Burnap RL (2016) Photoactivation: The light-driven assembly of the water oxidation
4 complex of Photosystem II. *Front Plant Sci* 7:article 578.
5
6 <https://doi.org/10.3389/fpls.2016.00578>
7
8
9 Beal D, Rappaport F, Joliot P (1999) A new high-sensitivity 10-ns time-resolution
10 spectrophotometric technique adapted to in vivo analysis of the photosynthetic apparatus. *Rev*
11 *Sci Instrum* 70: 202–207. <https://doi.org/10.1063/1.1149566>
12
13
14
15 Boussac A, Sugiura M, Rappaport F (2011) Probing the quinone binding site of photosystem
16 II from *Thermosynechococcus elongatus* containing either PsbA1 or PsbA3 as the D1 protein
17 through the binding characteristics of herbicides. *Biochim Biophys Acta* 1807:119–129.
18
19 <https://doi.org/10.1016/j.bbabi.2010.10.004>
20
21
22
23 Broser M, Gabdulkhakov A, Kern J, Guskov A, Muh F, Saenger W, Zouni A (2010) Crystal
24 structure of monomeric Photosystem II from *Thermosynechococcus elongatus* at 3.6-Å^o
25 resolution. *J Biol Chem* 285: 26255–26262. <https://doi.org/10.1074/jbc.M110.127589>.
26
27
28
29 Choo P, Forsman JA, Hui LL, Khaing EP, Summerfield TC, Eaton-Rye JJ (2021) The PsbJ
30 protein is required for photosystem II activity in centers lacking the PsbO and PsbV luminal
31 subunits. *Photosynth Res*, early access. <https://doi.org/10.1007/s11120-021-00862-y>
32
33
34
35
36 Cox N, Pantazis DA, Lubitz W (2020) Current understanding of the mechanism of water
37 oxidation in Photosystem II and its relation to XFEL data. *Annu. Rev. Biochem.* 89:795–820.
38
39 <https://doi.org/10.1146/annurev-biochem-011520-104801>
40
41
42
43 Cser K, Vass I (2007) Radiative and non-radiative charge recombination pathways in
44 Photosystem II studied by thermoluminescence and chlorophyll fluorescence in the
45 cyanobacterium *Synechocystis* 6803. *Biochim Biophys Acta* 1767: 233–243.
46
47 <https://doi.org/10.1016/j.bbabi.2007.01.022>
48
49
50
51 Cuni A, Xiong L, Sayre R, Rappaport F, Lavergne J (2004) Modification of the pheophytin
52 midpoint potential in Photosystem II: modulation of the quantum yield of charge separation
53 and of charge recombination pathways. *Phys Chem Chem Phys* 6: 4825–4831
54
55
56 <https://doi.org/10.1039/B407511K>
57
58
59
60
61
62
63
64
65

1 de Causmaecker S, Douglass JS, Fantuzzi A, Nitschke W, Rutherford AW (2019) Energetics
2 of the exchangeable quinone, Q_B, in Photosystem II. Proc Natl Acad Sci USA 116: 19458–
3 19463. www.pnas.org/cgi/doi/10.1073/pnas.1910675116
4

5
6 Demeter S, Goussias C, Bern G, Kovács L, Petrouleas V (1993) Participation of the g = 1.9
7 and g = 1.82 EPR forms of the semiquinone-iron complex, Q_A⁻Fe²⁺ of photosystem II in the
8 generation of the Q and C thermoluminescence bands, respectively. FEBS 336: 352–356.
9
10 [https://doi.org/10.1016/0014-5793\(93\)80836-J](https://doi.org/10.1016/0014-5793(93)80836-J)
11

12
13
14 Diner BA, Petrouleas V (1987) Light-induced oxidation of the acceptor-side Fe(II) of
15 Photosystem II by exogenous quinones acting through the Q_B binding site. II. Blockage by
16 inhibitors and their effects on the Fe(III) EPR spectra. Biochim Biophys Acta 893: 138–148.
17
18 [https://doi.org/10.1016/0005-2728\(87\)90033-8](https://doi.org/10.1016/0005-2728(87)90033-8)
19

20
21
22 Ducruet JM (2003) Chlorophyll thermoluminescence of leaf discs: simple instruments and
23 progress in signal interpretation open the way to new ecophysiological indicators. J Exp Bot
24 54: 2419–2430. <https://doi.org/10.1093/jxb/erg268>
25

26
27
28 Ducruet JM, Vass I (2009) Thermoluminescence: experimental. Photosynth Res 201: 195–
29 204. <https://doi.org/10.1007/s11120-009-9436-0>
30

31
32
33 Forsman JA, Eaton-Rye JJ (2021) The interaction between PsbT and the DE loop of D1 in
34 Photosystem II stabilizes the quinone-iron electron acceptor complex. Biochemistry 60: 53–
35 63. <https://doi.org/10.1021/acs.biochem.0c00668>.
36

37
38
39 Fufezan C, Zhang CX, Krieger-Liszkay A, Rutherford AW (2005) Secondary quinone in
40 photosystem II of *Thermosynechococcus elongatus*: semiquinone-iron EPR signals and
41 temperature dependence of electron transfer. Biochemistry 44: 12780–12789.
42
43 <https://doi.org/10.1021/bi051000k>
44

45
46
47 Funk C (2000) Functional analysis of the PsbX protein by deletion of the corresponding gene
48 in *Synechocystis sp.* PCC 6803. Plant Mol Biol 44: 815–827.
49
50 <https://doi.org/10.1023/A:1026764728846>
51

52
53
54 Garcia-Cerdan JG, Sveshnikov D, Dewez D, Jansson S, Funk C, Schroder WP (2009)
55 Antisense inhibition of the PsbX protein affects PSII integrity in the higher plant *Arabidopsis*
56 *thaliana*. Plant Cell Physiol 50: 191–202. <https://doi.org/10.1093/pcp/pcn188>
57
58
59
60
61
62
63
64
65

1 Holzwarth AR, Müller MG, Reus M, Nowaczyk M, Sander J, Rögner M (2006) Kinetics and
2 mechanism of electron transfer in intact photosystem II and in the isolated reaction center:
3 pheophytin is the primary electron acceptor. Proc Natl Acad Sci USA 103: 6895–6900.

4 <https://doi.org/10.1073/pnas.0505371103>
5
6

7
8 Huang G, Xiao Y, Pi X, Zhao L, Zhu Q, Wang W, Kuang T, Han G, Sui S-F, Shen J-R
9 (2021) Structural insights into a dimeric Psb27-photosystem II complex from a
10 cyanobacterium *Thermosynechococcus vulcanus*. Proc Natl Acad Sci USA 118:
11 e2018053118. <https://doi.org/10.1073/pnas.2018053118>
12
13
14

15
16 Hughes JL, Cox N, Rutherford AW, Krausz E, Lai T-L, Boussac A, Sugiura M (2010) D1
17 protein variants in Photosystem II from *Thermosynechococcus elongatus* studied by low
18 temperature optical spectroscopy. Biochim Biophys Acta 1797: 11–19.

19 <https://doi.org/10.1016/j.bbabi.2009.07.007>
20
21
22

23
24 Inoue-Kashino N, Kashino Y, Takahashi Y (2011) Psb30 is a photosystem II reaction center
25 subunit and is required for optimal growth in high light in *Chlamydomonas reinhardtii*. J
26 Photochem Photobiol 104: 220–228. <https://doi.org/10.1016/j.jphotobiol.2011.01.024>
27
28
29

30
31 Ishida N, Sugiura M, Rappaport F, Lai T-L, Rutherford AW, Boussac A (2008) Biosynthetic
32 exchange of bromide for chloride and strontium for calcium in the photosystem II oxygen-
33 evolving enzyme. J Biol Chem 283: 13330–13340. <https://doi.org/10.1074/jbc.M710583200>
34
35
36

37
38 Iwai M, Suzuki T, Kamiyama A, Sakurai I, Dohmae N, Inoue Y, Ikeuchi M (2010) The PsbK
39 subunit is required for the stable assembly and stability of other small subunits in the PSII
40 complex in the thermophilic cyanobacterium *Thermosynechococcus elongatus* BP-1. Plant
41 Cell Physiol 51: 554–560. <https://doi.org/10.1093/pcp/pcq020>
42
43
44

45
46 Johnson GN, Rutherford AW, Krieger A (1995) A change in the midpoint potential of the
47 quinone QA in Photosystem II associated with photoactivation of oxygen evolution. Biochim
48 Biophys Acta 1229: 202–207. [https://doi.org/10.1016/0005-2728\(95\)00003-2](https://doi.org/10.1016/0005-2728(95)00003-2)
49
50

51
52 Joliot P, Kok B (1975) Oxygen evolution in photosynthesis, in: Govindjee (Ed.),
53 Bioenergetics of Photosynthesis, Academic Press, New York, pp. 387–412.
54
55

56
57 Kaminskaya O, Shuvalov VA, Renger G (2007) Evidence for a novel quinone-binding site in
58 the photosystem II (PS II) complex that regulates the redox potential of cytochrome b559.
59 Biochemistry 46: 1091–1105. <https://doi.org/10.1134/S1607672907010048>
60
61
62
63
64
65

1 Kashino Y, Lauber WM, Carroll JA, Wang Q, Whitmarsh J, Satoh K, Pakrasi HB (2002)
2 Proteomic analysis of a highly active photosystem II preparation from the cyanobacterium
3 *Synechocystis* sp. PCC 6803 reveals the presence of novel polypeptides. *Biochemistry* 41:
4 8004-8012. <https://10.1021/bi026012>
5
6

7 Kashino Y, Takahashi T, Inoue-Kashino N, Ban A, Ikeda Y, Satoh K, Sugiura M (2007)
8 Ycf12 is a core subunit in the photosystem II complex. *Biochim Biophys Acta* 1767: 1269–
9 1275. <https://doi.org/10.1016/j.bbabi.2007.08.008>
10
11
12

13 Keren N, Berg A, VanKan PJM, Levanon H, Ohad I (1997) Mechanism of photosystem II
14 photoinactivation and D1 protein degradation at low light: The role of back electron flow.
15 *Proc Natl Acad Sci USA* 94: 1579–1584. <https://doi.org/10.1073/pnas.94.4.1579>.
16
17
18
19

20 Kok B, Forbush B, McGloin M (1970) Cooperation of charges in photosynthetic O₂
21 evolution–I. A linear four step mechanism. *Photochem Photobiol* 11: 457–475.
22
23 <https://doi.org/10.1111/j.1751-1097.1970.tb06017.x>
24
25
26

27 Komenda J, Sobotka R, Nixon PJ (2012) Assembling and maintaining the Photosystem II
28 complex in chloroplasts and cyanobacteria. *Curr Opin Plant Biol* 15: 245-251;
29
30 <https://doi.org/10.1016/j.pbi.2012.01.017>
31
32

33 Krieger A, Rutherford AW, Johnson GN (1995) On the determination of redox midpoint
34 potential of the primary quinone electron acceptor, Q_A, in photosystem II. *Biochim Biophys*
35 *Acta* 1229:193–201. [https://doi.org/10.1016/0005-2728\(95\)00002-Z](https://doi.org/10.1016/0005-2728(95)00002-Z)
36
37
38
39

40 Lavergne J (1991) Improved UV-visible spectra of the S-transitions in the photosynthetic
41 oxygen-evolving system. *Biochim Biophys Acta* 1060: 175–188.
42
43 [https://doi.org/10.1016/S0005-2728\(09\)91005-2](https://doi.org/10.1016/S0005-2728(09)91005-2)
44
45

46 Liu HJ, Chen JW, Huang RYC, Weisz D, Gross ML, Pakrasi HB (2013) Mass Spectrometry-
47 based Footprinting Reveals Structural Dynamics of Loop E of the Chlorophyll-binding
48 Protein CP43 during Photosystem II Assembly in the Cyanobacterium *Synechocystis* 6803. *J*
49 *Biol Chem* 288: 14212–14220. <https://doi.org/10.1074/jbc.M113.467613>
50
51
52
53

54 Luo H, Jackson SA, Fagerlund RD, Summerfield TC, Eaton-Rye JJ (2014) The importance of
55 the hydrophilic region of PsbL for the plastoquinone electron acceptor complex of
56 Photosystem II. *Biochim Biophys Acta* 1837: 1435–1446.
57
58 <https://doi.org/10.1016/j.bbabi.2014.02.015>
59
60
61
62
63
64
65

- 1
2 Merry SAP, Nixon PJ, Barter LMC, Schilstra MJ, Porter G, Barber J, Durrant JR, Klug D
3 (1998) Modulation of quantum yield of primary radical pair formation in photosystem II by
4 site directed mutagenesis affecting radical cations and anions. *Biochemistry* 37: 17439–
5 17447. <https://doi.org/10.1021/bi980502d>
6
7
8 Müh F, Zouni A (2005) Extinction coefficients and critical solubilisation concentrations of
9 photosystems I and II from *Thermosynechococcus elongatus*. *Biochim Biophys Acta* 1708:
10 219–228. <https://doi.org/10.1016/j.bbabi.2005.03.005>
11
12
13
14 Müh F, Glöckner C, Hellmich J, Zouni A (2012) Light-induced quinone reduction in
15 photosystem II. *Biochim Biophys Acta* 1817: 44–65.
16
17 <https://doi.org/10.1016/j.bbabi.2011.05.021>
18
19
20
21 Mulo P, Sicora C, Aro E-M (2009) Cyanobacterial psbA gene family: optimization of
22 oxygenic photosynthesis. *Cell Mol Life Sci* 66: 3697–3710. [https://doi.org/10.1007/s00018-](https://doi.org/10.1007/s00018-009-0103-6)
23 [009-0103-6](https://doi.org/10.1007/s00018-009-0103-6)
24
25
26
27 Nowaczyk MM, Hebel R, Schlodder E, Meyer HE, Warscheid B, Rogner M (2006) Psb27,
28 a cyanobacterial lipoprotein, is involved in the repair cycle of photosystem II. *Plant Cell* 18:
29 3121–3131. <https://doi.org/10.1105/tpc.106.042671>
30
31
32
33 Nowaczyk MM, Krause K, Mieseler M, Sczibilanski A, Ikeuchi M, Rögner M (2012)
34 Deletion of psbJ leads to accumulation of Psb27–Psb28 photosystem II complexes in
35 *Thermosynechococcus elongatus*. *Biochim Biophys Acta* 1817: 1339–1345.
36
37 <http://dx.doi.org/10.1016/j.bbabi.2012.02.017>
38
39
40
41 Ohad I, Dal Bosco C, Herrmann RG, Meurer J (2004) Photosystem II proteins PsbL and PsbJ
42 regulate electron flow to the plastoquinone pool. *Biochemistry* 43: 2297–2308.
43
44 <https://doi.org/10.1021/bi0348260>
45
46
47
48 Rappaport F, Lavergne J (2009) Thermoluminescence: theory. *Photosynth Res* 101:205–216.
49
50 <https://doi.org/10.1007/s11120-009-9437-z>
51
52
53 Regel RE, Ivleva NB, Zer H, Meurer J, Shestakov SV, Herrmann RG, Pakrasi HB, Ohad I
54 (2001) Deregulation of electron flow within Photosystem II in the absence of the PsbJ protein.
55 *J Biol Chem* 276: 41473–41478. <https://doi.org/10.1074/jbc.M102007200>
56
57
58
59
60
61
62
63
64
65

1 Romero E, Novoderezhkin VI, van Grondelle R (2017) Quantum design of photosynthesis for
2 bio-inspired solar-energy conversion. *Nature* 543: 355–365.

3 <https://doi.org/10.1038/nature22012>
4

5
6 Roncel M, Boussac A, Zurita JL, Bottin H, Sugiura M, Kirilovsky D, Ortega J-M (2003)
7 Redox properties of the photosystem II cytochromes b559 and c550 in the cyanobacterium
8 *Thermosynechococcus elongatus*. *J Biol Inorg Chem* 8: 206–216.

9
10 <https://doi.org/10.1007/s00775-002-0406-7>
11

12
13
14 Roose JL, Pakrasi HB (2008) The Psb27 protein facilitates manganese cluster assembly in
15 photosystem II. *J Biol Chem* 283:4044–4050. <https://doi.org/10.1074/jbc.M708960200>

16
17
18 Roose JL, Frankel LK, Mummadisetti MP, Bricker TM (2016) The extrinsic proteins of
19 photosystem II: update. *Planta* 243: 889–908. <https://doi.org/10.1007/s00425-015-2462-6>
20
21

22
23 Rutherford AW, Crofts AR, Inoue Y (1982) Thermoluminescence as a probe of Photosystem
24 II photochemistry. The origin of the flash-induced glow peaks. *Biochim Biophys Acta* 682:
25 457–465. [https://doi.org/10.1016/0005-2728\(82\)90061-5](https://doi.org/10.1016/0005-2728(82)90061-5)
26
27

28
29 Rutherford AW, Zimmermann J-L (1984) A new EPR signal attributed to the primary
30 plastosemiquinone acceptor in Photosystem II. *Biochim Biophys Acta* 767: 168–175.

31
32 [https://doi.org/10.1016/0005-2728\(84\)90092-6](https://doi.org/10.1016/0005-2728(84)90092-6)
33

34
35
36 Rutherford AW, Zimmermann J-L, Mathis P (1983) The effect of herbicides on components
37 of the PS II reaction centre measured by EPR. *Febs Lett* 165: 156–162.

38
39 [https://doi.org/10.1016/0014-5793\(84\)80161-1](https://doi.org/10.1016/0014-5793(84)80161-1)
40

41
42 Rutherford AW, Krieger-Liszka A (2001) Herbicide-induced oxidative stress in photosystem
43 II. *Trends Biochem Sci* 26: 648–653. [https://doi.org/10.1016/S0968-0004\(01\)01953-3](https://doi.org/10.1016/S0968-0004(01)01953-3)
44

45
46 Sedoud A, Cox N, Sugiura M, Lubitz W, Boussac A, Rutherford AW (2011) The
47 semiquinone-iron complex of Photosystem II: EPR signals assigned to the low field edge of
48 the ground state doublet of $Q_A^{\bullet-}Fe^{2+}$ and $Q_B^{\bullet-}Fe^{2+}$. *Biochemistry* 50: 6012–6021.

49
50 <https://doi.org/10.1021/bi200313p>
51

52
53
54 Schatz GH, van Gorkom HJ (1985) Absorbance difference spectra upon charge transfer to
55 secondary donors and acceptors in Photosystem II, *Biochim Biophys Acta* 810: 283–294.

56
57 [https://doi.org/10.1016/0005-2728\(85\)90212-9](https://doi.org/10.1016/0005-2728(85)90212-9)
58
59
60
61
62
63
64
65

1 Shen JR (2015) The structure of Photosystem II and the mechanism of water oxidation in
2 photosynthesis. *Annu Rev Plant Biol* 66: 23–48. [https://doi.org/10.1146/annurev-arplant-
3 050312-120129](https://doi.org/10.1146/annurev-arplant-050312-120129)
4

5
6 Shen J-R, Qian M, Inoue Y, Burnap RL (1998) Functional characterization of *Synechocystis*
7 sp. PCC 6803 Δ psbU and Δ psbV mutants reveals important roles of cytochrome c-550 in
8 cyanobacterial oxygen evolution. *Biochemistry* 37: 1551-1558.
9
10 <https://doi.org/10.1021/bi971676i>
11

12
13
14 Sheridan KJ, Duncan EJ, Eaton-Rye JJ, Summerfield TC (2020) The diversity and
15 distribution of D1 proteins in cyanobacteria. *Photosynth Res* 145: 111–128.
16
17 <https://doi.org/10.1007/s11120-020-00762-7>
18

19
20
21 Shibuya Y, Takahashi R, Okubo T, Suzuki H, Sugiura M, Noguchi T (2010) Hydrogen bond
22 interaction of the pheophytin electron acceptor and its radical anion in Photosystem II as
23 revealed by Fourier Transform Infrared Difference Spectroscopy. *Biochemistry* 49: 493–501.
24
25 <https://doi.org/10.1021/bi9018829>
26

27
28
29 Styring S, Rutherford AW (1987) In the oxygen-evolving complex of photosystem II the S₀-
30 state is oxidized to the S₁-state by D⁺ (signal-II slow). *Biochemistry* 26: 2401–2405.
31
32 <https://doi.org/10.1021/bi00383a001>
33

34
35 Styring S, Rutherford AW (1988) The microwave power saturation of SII_{slow} varies with the
36 redox state of the oxygen-evolving complex in photosystem II. *Biochemistry* 27: 4915–4923.
37
38 <https://doi.org/10.1021/bi00413a049>.
39

40
41
42 Suga M, Akita F, Hirata K, Ueno G, Murakami H, Nakajima Y, Shimizu T, Yamashita K,
43 Yamamoto M, Ago H, Shen J-R (2015) Native structure of photosystem II at 1.95 angstrom
44 resolution viewed by femtosecond X-ray pulses. *Nature* 517: 99–103.
45
46 <https://doi.org/10.1038/nature13991>
47

48
49
50 Sugiura M, Rappaport F, Brettel K, Noguchi T, Rutherford AW, Boussac A (2004) Site-
51 directed mutagenesis of *Thermosynechococcus elongatus* photosystem II: the O₂ evolving
52 enzyme lacking the redox active tyrosine D. *Biochemistry* 43: 13549–13563.
53
54 <https://doi.org/10.1021/bi048732h>
55

1 Sugiura M, Boussac A (2014) Some Photosystem II properties depending on the D1 protein
2 variants in *Thermosynechococcus elongatus*. *Biochim Biophys Acta* 1837: 1427–1434.

3 <https://doi.org/10.1016/j.bbabbio.2013.12.011>
4

5
6 Sugiura M, Inoue Y (1999) Highly purified thermo-stable oxygen evolving Photosystem II
7 core complex from the thermophilic cyanobacterium *Synechococcus elongatus* having His-
8 tagged CP43. *Plant Cell Physiol* 40: 1219–1231.

9
10 <https://doi.org/10.1093/oxfordjournals.pcp.a029510>
11

12
13
14 Sugiura M, Harada S, Manabe T, Hayashi H, Kashino Y, Boussac A (2010a) Psb30
15 contributes to structurally stabilise the Photosystem II complex in the thermophilic
16 cyanobacterium *Thermosynechococcus elongatus*. *Biochim Biophys Acta* 1797: 1546–1554.

17
18 <https://doi.org/10.1016/j.bbabbio.2010.03.020>
19

20
21
22 Sugiura M, Iwai E, Hayashi H, Boussac A (2010b) Differences in the interactions between the
23 subunits of Photosystem II dependent on D1 protein variants in the thermophilic
24 cyanobacterium *Thermosynechococcus elongatus*. *J Biol Chem* 285: 30008–30018.

25
26 <https://doi.org/10.1074/jbc.M110.136945>
27

28
29
30 Sugiura M, Azami C, Koyama K, Rutherford AW, Rappaport F, Boussac A (2014)
31 Modification of the pheophytin redox potential in *Thermosynechococcus elongatus*
32 Photosystem II with PsbA3 as D1. *Biochim Biophys Acta* 1837: 139–148.

33
34 <https://doi.org/10.1016/j.bbabbio.2013.09.009>
35

36
37
38 Sugiura M, Taniguchi T, Tango N, Nakamura M, Sellés J, Boussac A (2020) Probing the role
39 of arginine 323 of the D1 protein in photosystem II function. *Physiol Plant* 171: 183–199.

40
41 <https://doi.org/10.1111/ppl.13115>
42

43
44
45 Suhai T, Dencher NA, Poetsch A, Seelert H (2008) Remarkable stability of the proton
46 translocating F1F0-ATP synthase from the thermophilic cyanobacterium
47 *Thermosynechococcus elongatus* BP-1. *Biochim Biophys Acta* 1778: 1131-1140.

48
49 <https://doi.org/10.1016/j.bbammem.2007.12.017>
50

51
52
53 Takasaka K, Iwai M, Umena Y, Kawakami K, Ohmori Y, Ikeuchi M, Takahashi Y, Kamiya
54 N, Shen JR (2010) Deletion Structural and functional studies on Ycf12 (Psb30) and PsbZ-
55 deletion mutants from a thermophilic cyanobacterium. *Biochim Biophys Acta* 1797: 278–284.

56
57 <https://doi.org/10.1016/j.bbabbio.2009.11.001>
58
59
60
61
62
63
64
65

1 Umena Y, Kawakami K, Shen J-R, Kamiya N (2011) Crystal structure of oxygen-evolving
2 Photosystem II at a resolution of 1.9 angstrom. *Nature* 473: 55–60.

3 <https://doi.org/10.1038/nature09913>
4

5
6 Uto S, Kawakami K, Umena Y, Iwai M, Ikeuchi M, Shen JR, Kamiya N (2017) Mutual
7 relationships between structural and functional changes in a PsbM-deletion mutant of
8 photosystem II. *Faraday Discuss* 198: 107–120. <https://doi.org/10.1039/C6FD00213G>
9

10 van Eerden FJ, Melo MN, Frederix PWJM, Periole X, Marrink SJ (2017) Exchange pathways
11 of plastoquinone and plastoquinol in the photosystem II complex. *Nature Comm* 8:15214.

12 <https://doi.org/10.1038/ncomms15214>
13

14 Velthuys BR (1981) Electron-dependent competition between plastoquinone and inhibitors
15 for binding to Photosystem-II. *Feb let* 126: 277–281. <https://doi.org/10.1016/0014->

16 [5793\(81\)80260-8](https://doi.org/10.1016/0014-5793(81)80260-8)
17

18
19 Xiao Y, Huang G, You X, Zhu Q, Wang W, Kuang T, Han G, Sui S-F, Shen J-R (2021)
20 Structural insights into cyanobacterial photosystem II intermediates associated with Psb28
21 and Tsl0063. *Nature Plants*, 7: 1132–1142. <https://doi.org/10.1038/s41477-021-00961-7>
22

23
24
25 Zabret J, Bohn S, Schuller SK, Arnolds O, Möller M, Meier-Credo J, Liauw P, Chan A,
26 Tajkhorshid E, Langer JD, Stoll R, Krieger-Liszkay A, Engel BD, Rudack T, Schuller JM,
27 Nowaczyk MM (2021) Structural insights into photosystem II assembly. *Nature Plants* 7:
28 524–538. <https://doi.org/10.1038/s41477-021-00895-0>
29
30
31
32
33
34
35
36
37
38
39
40
41
42
43
44
45
46
47
48
49
50
51
52
53
54
55
56
57
58
59
60
61
62
63
64
65

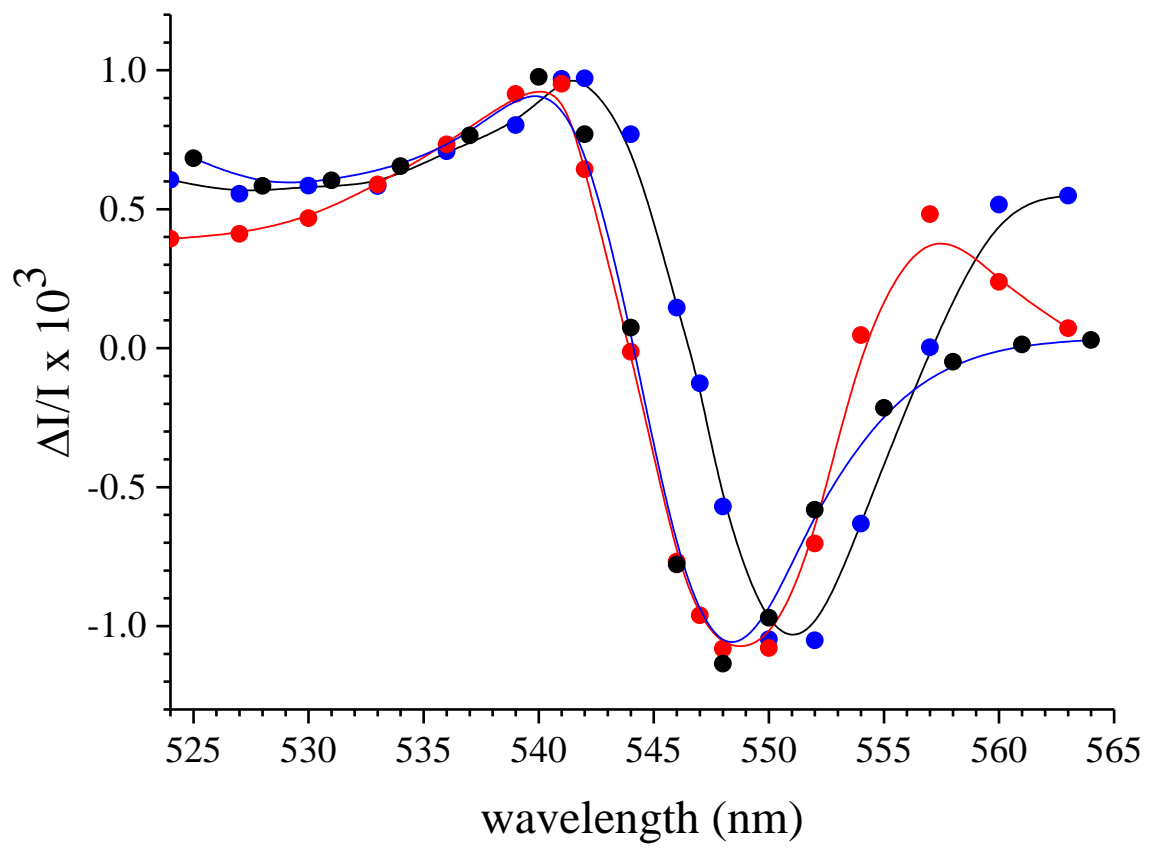
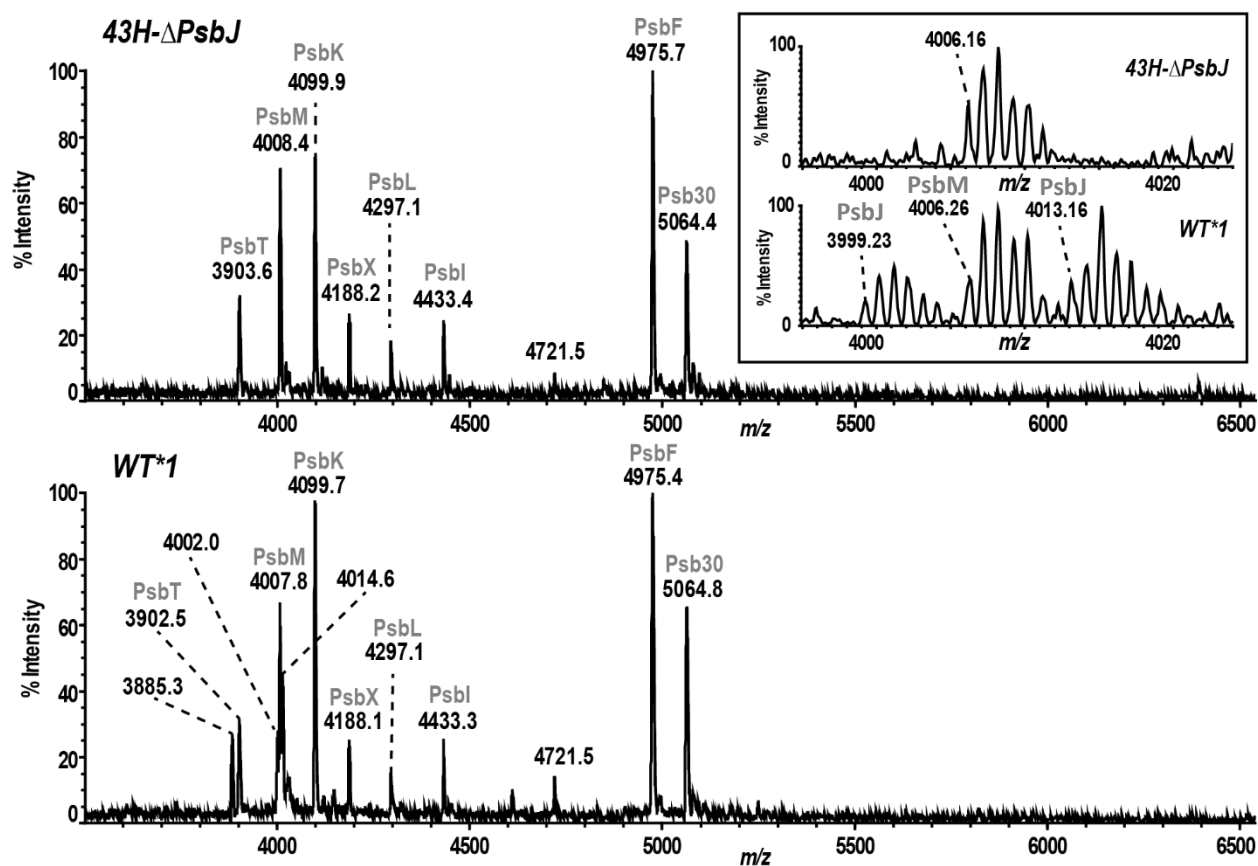


Fig. 1

A



B

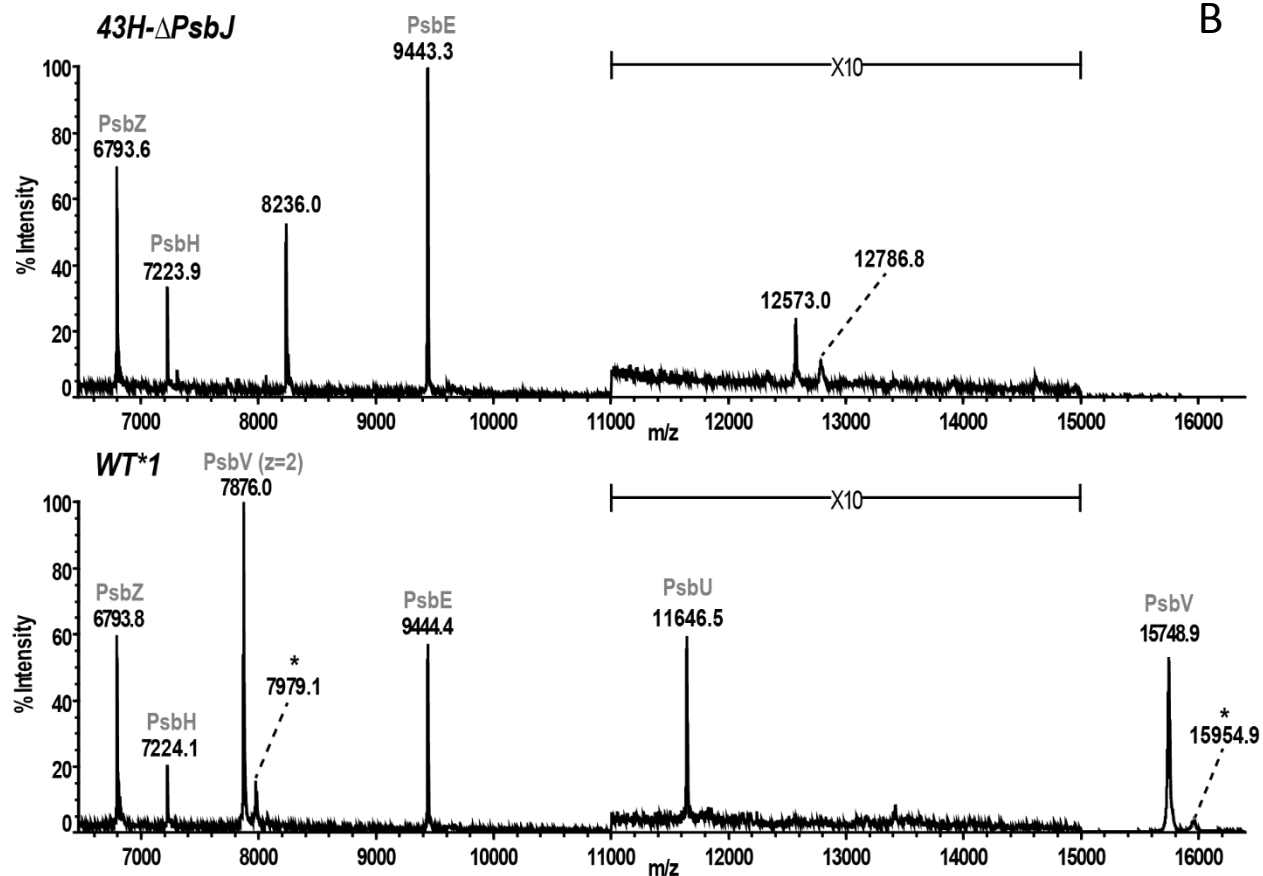


Fig. 2

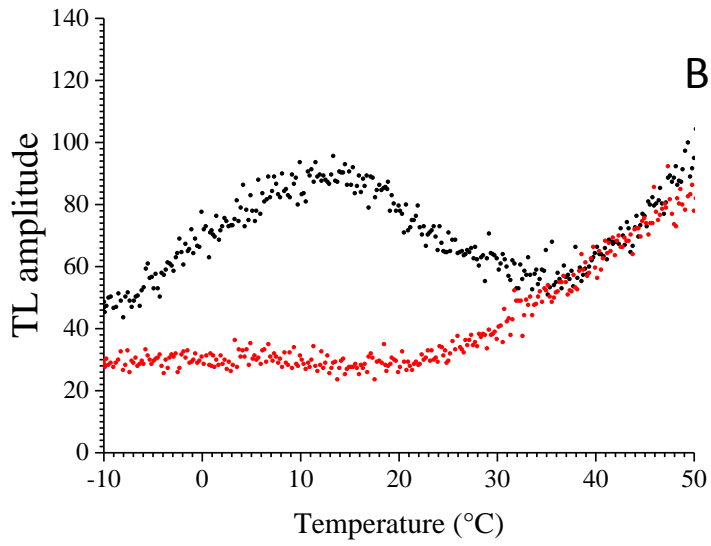
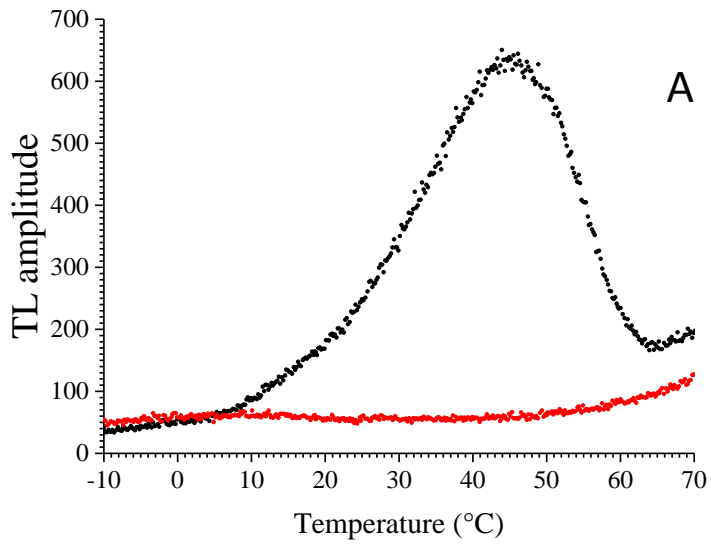


Fig. 3

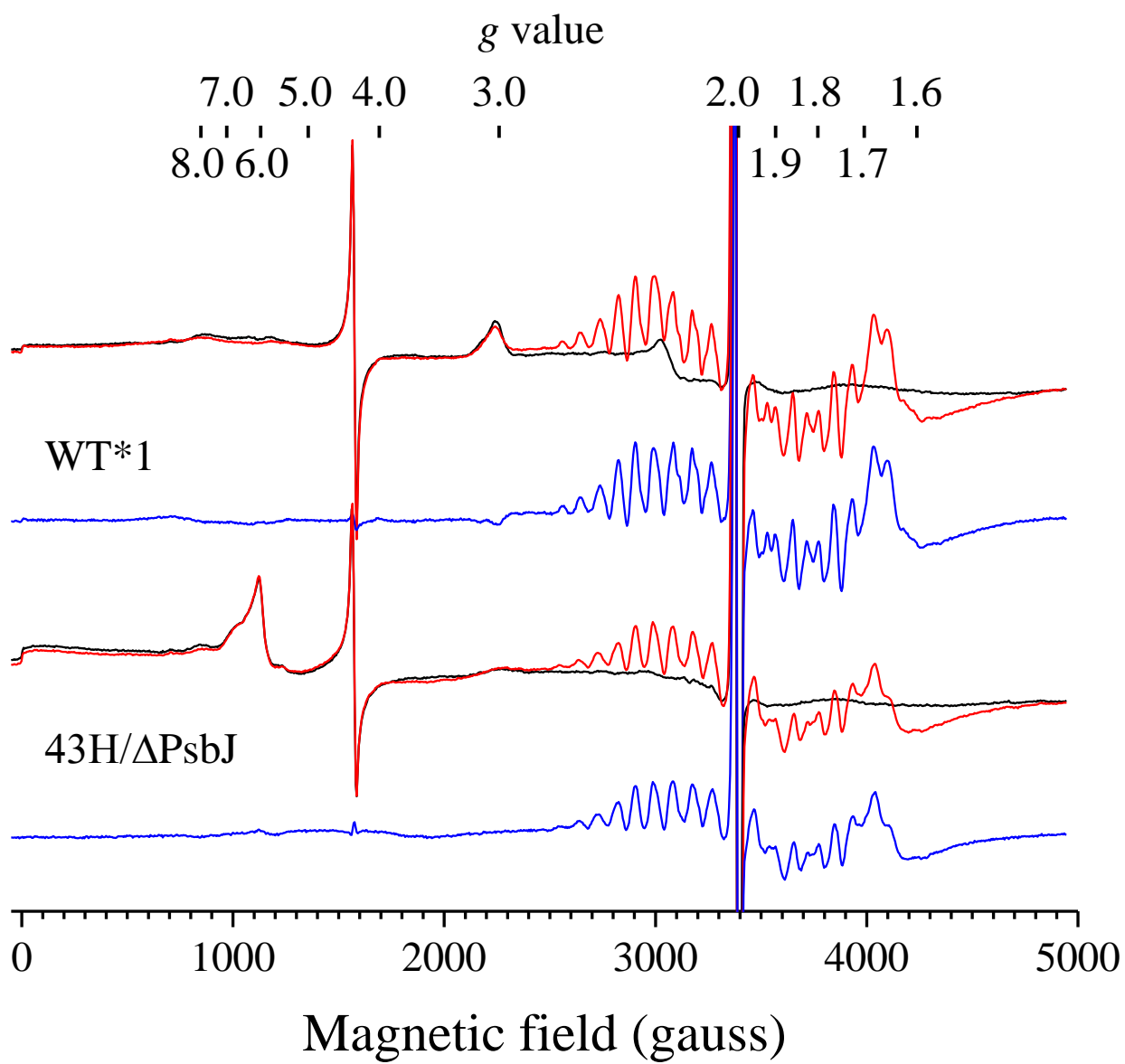


Fig. 4

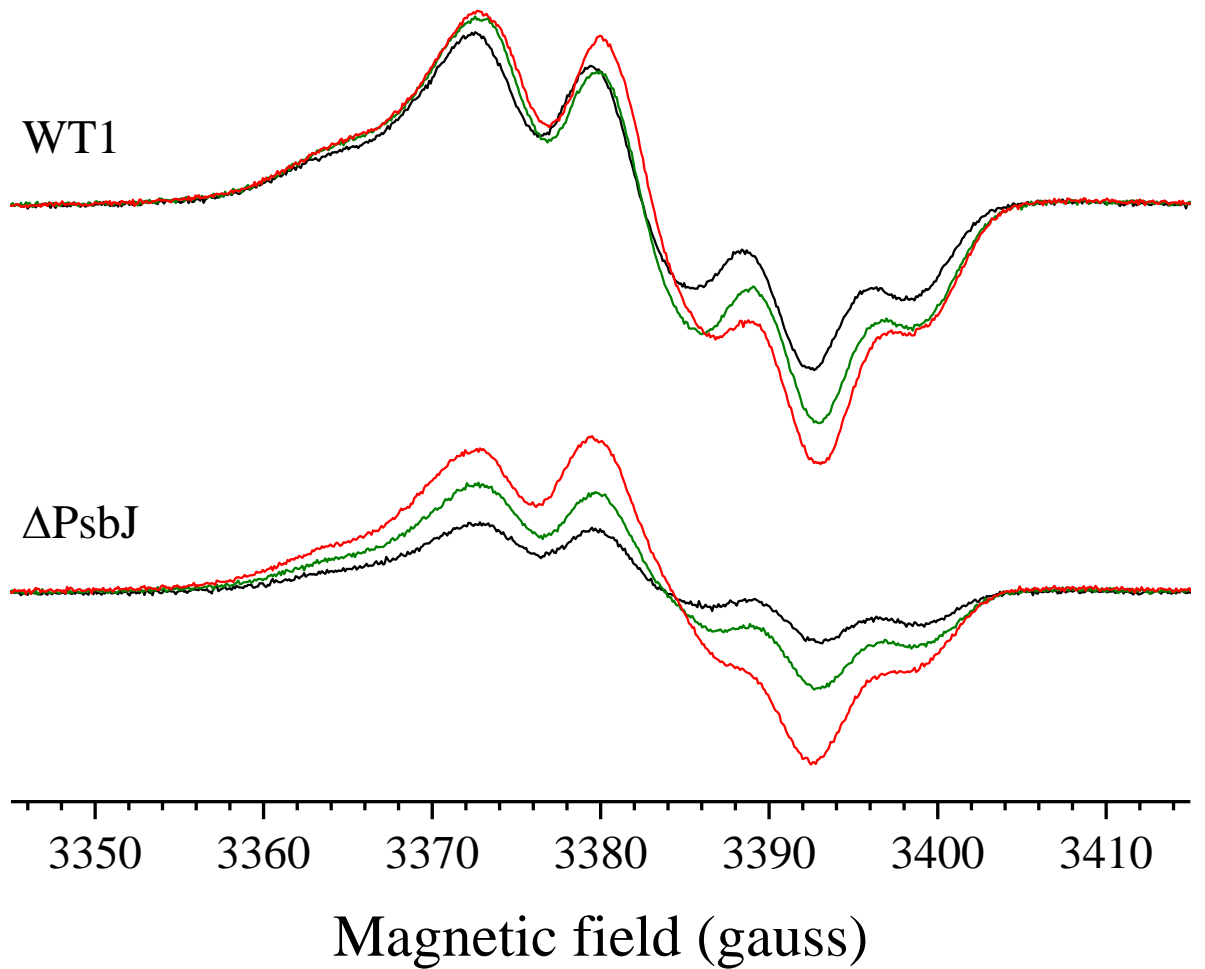
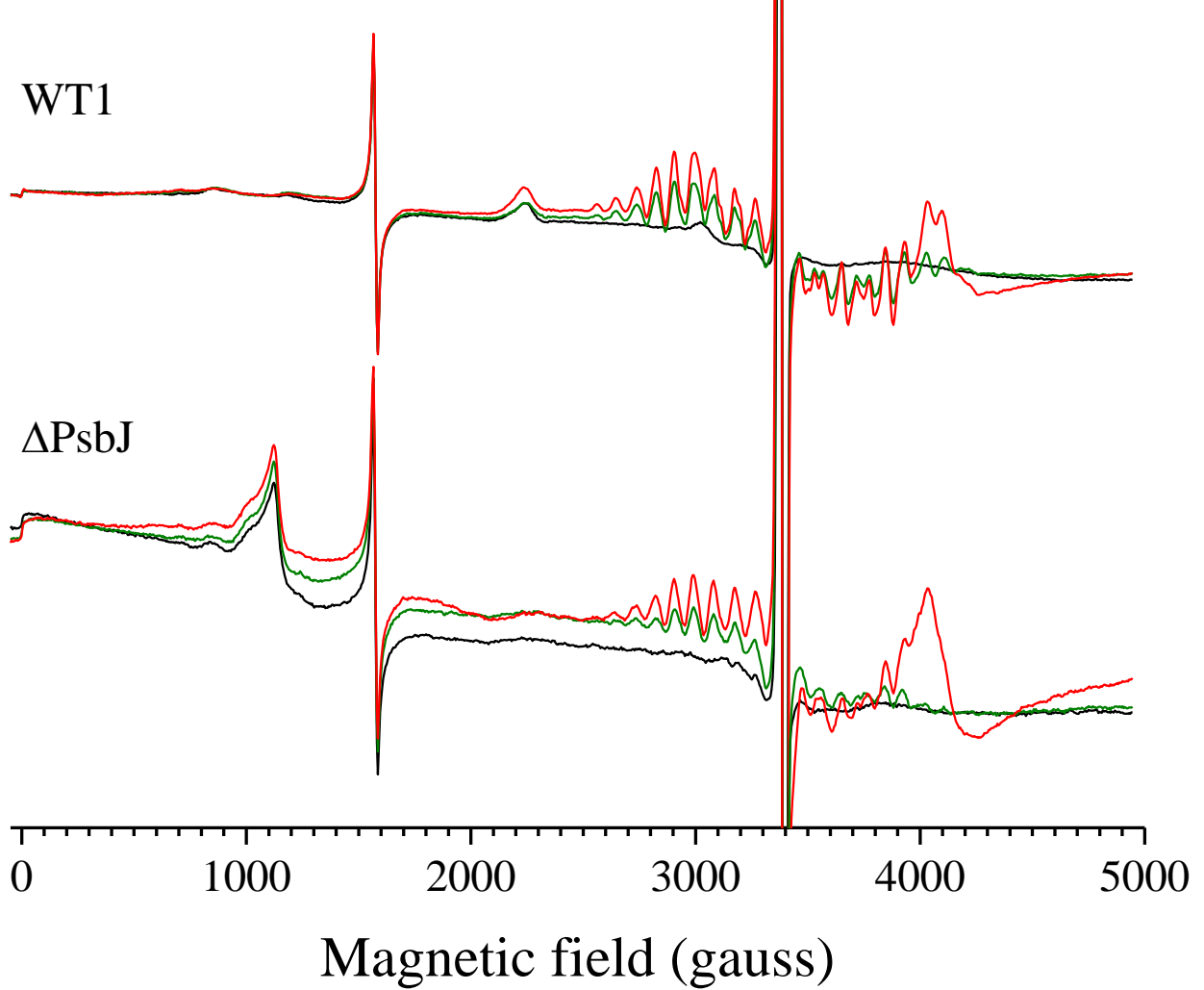


Fig. 5

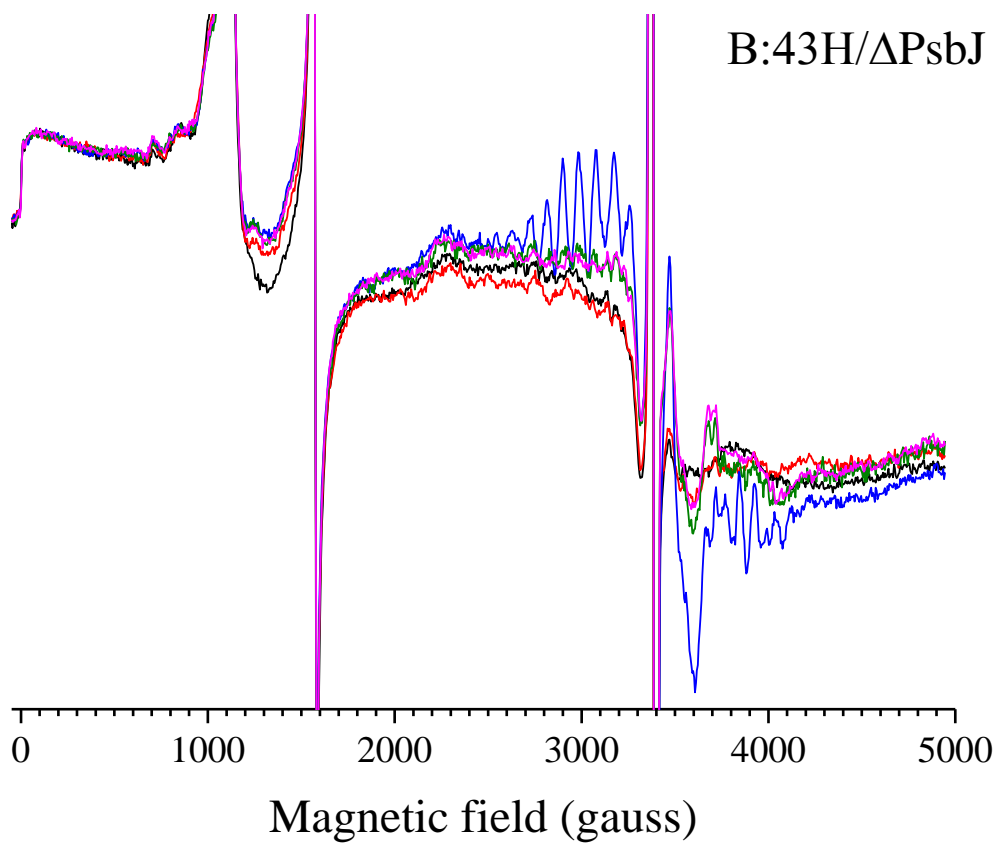
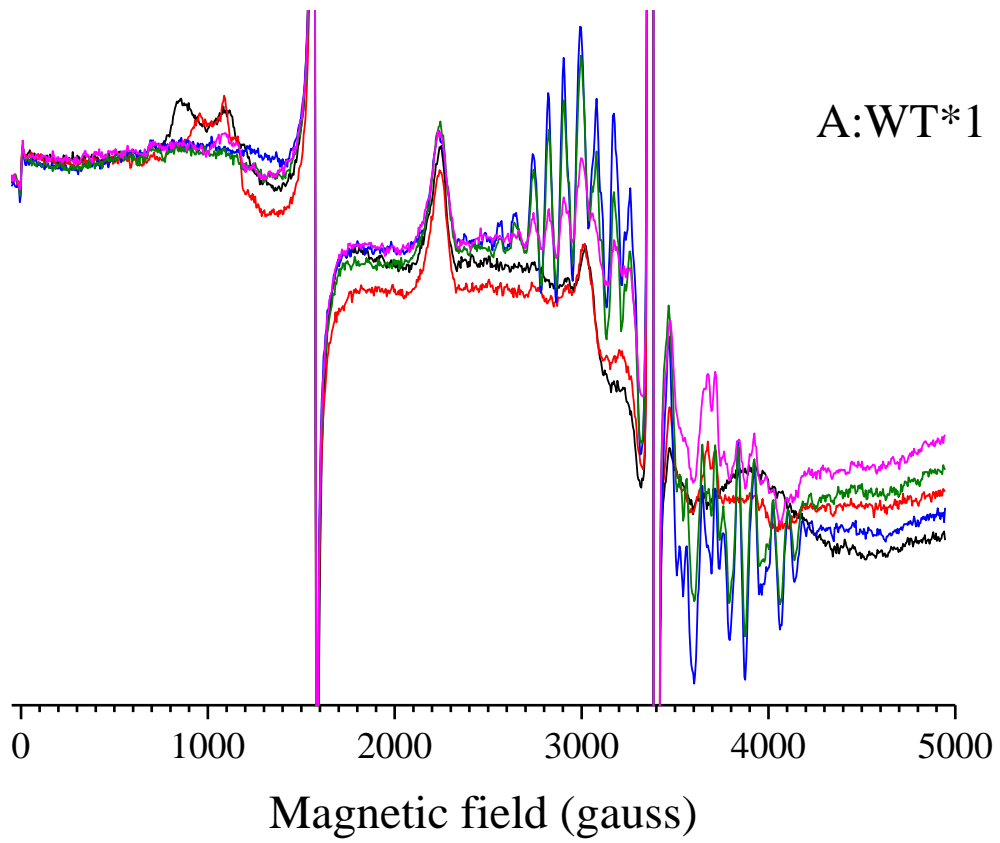


Fig. 6

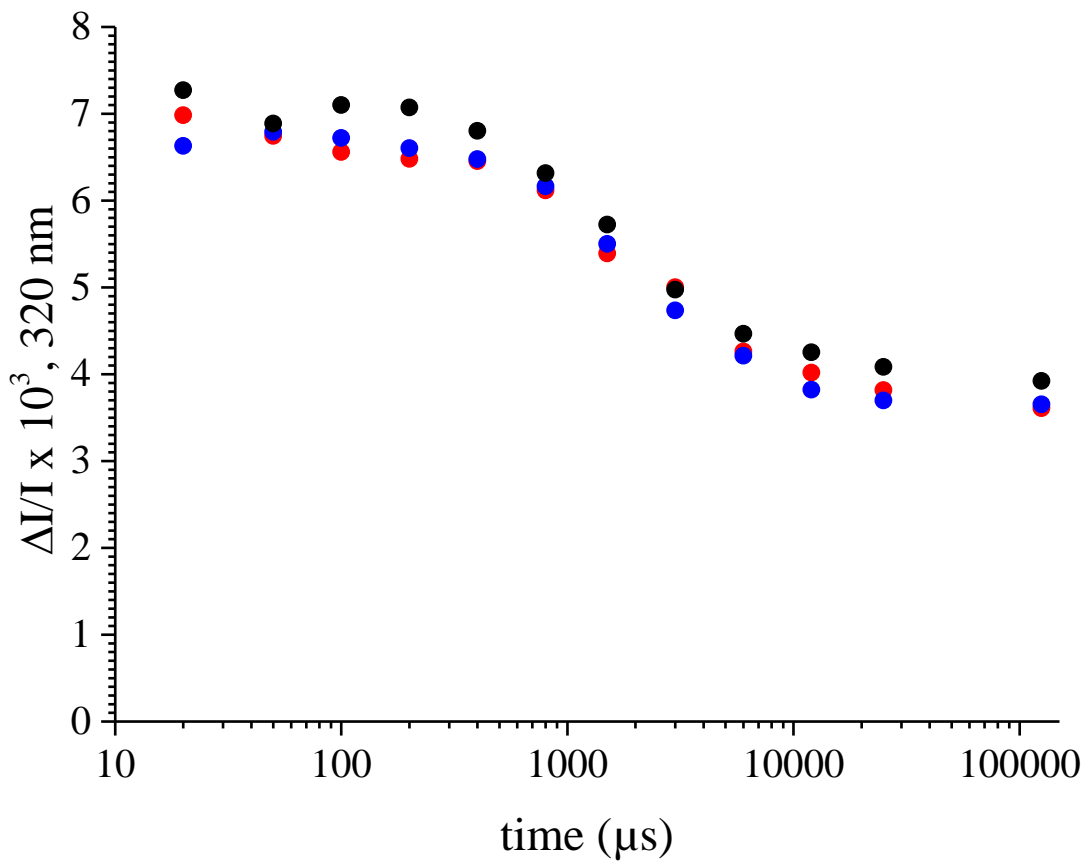


Fig. 7

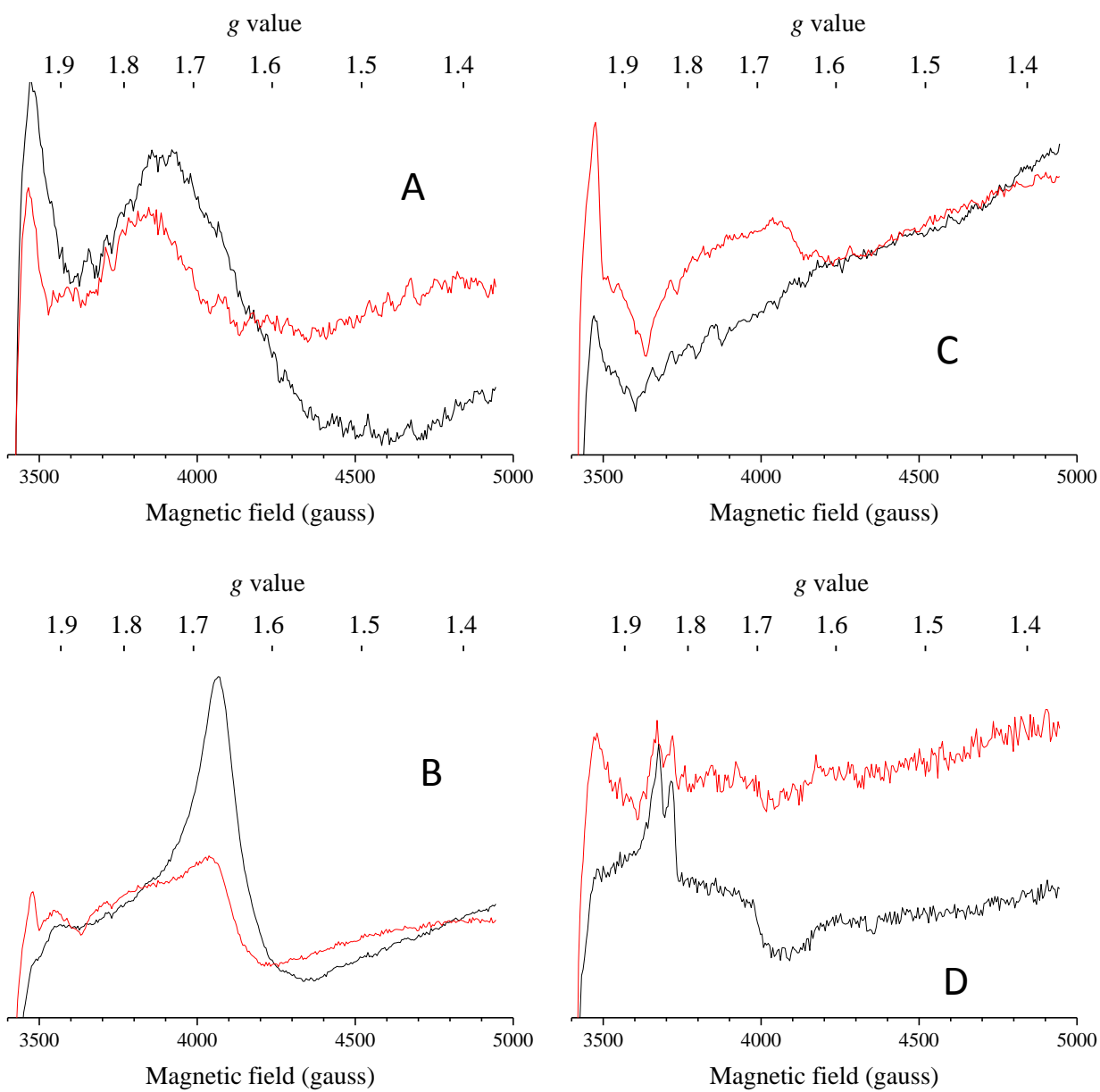


Fig. 8

Properties of Photosystem II lacking the PsbJ subunit.

Alain Boussac¹, Julien Sellés², Marion Hamon³, Miwa Sugiura⁴

¹ I²BC, UMR CNRS 9198, CEA Saclay, 91191 Gif-sur-Yvette, France.

² Institut de Biologie Physico-Chimique, UMR CNRS 7141 and Sorbonne Université, 13 rue Pierre et Marie Curie, 75005 Paris, France.

³ Institut de Biologie Physico-Chimique, UMR8226/FRC550 CNRS and Sorbonne-Université, 13 rue Pierre et Marie Curie, 75005 Paris, France.

⁴ Proteo-Science Research Center, and Department of Chemistry, Graduate School of Science and Technology, Ehime University, Bunkyo-cho, Matsuyama, Ehime 790-8577, Japan.

*Corresponding authors: alain.boussac@cea.fr, miwa.sugiura@ehime-u.ac.jp

The authors declare that they have no conflict of interest.

ORCID numbers:

Alain Boussac, 0000-0002-3441-3861

Julien Sellés, 0000-0001-9262-8257

Keywords: Photosystem II, PsbJ, plastoquinone, assembly, photoinhibition.

Acknowledgments

This work has been in part supported by i) the French Infrastructure for Integrated Structural Biology (FRISBI) ANR-10-INBS-05, ii) the Labex Dynamo (ANR-11-LABX-0011-01), iii) EQUIPEX (CACSICE ANR-11-EQPX-0008), notably through funding of the Proteomic Platform of IBPC (PPI). MS was supported by the JSPS-KAKENHI grant in Scientific Research on Innovative Areas JP17H06435 and a JSPS-KAKENHI grant 21H02447.

Abbreviations:

Chl, chlorophyll; Chl_{D1}/Chl_{D2}, accessory Chl's on the D1 or D2 side, respectively; DCMU, 3-(3,4-dichlorophenyl)-1,1-dimethylurea; PSII, Photosystem II; MES, 2-(*N*-morpholino) ethanesulfonic acid; P₆₈₀, primary electron donor; P_{D1} and P_{D2}; Chl monomer of P₆₈₀ on the D1 or D2 side, respectively, Phe_{D1} and Phe_{D2}, pheophytin on the D1 or D2 side, respectively; Q_A, primary quinone acceptor; Q_B, secondary quinone acceptor; Tyr_D, redox active tyrosine 160 of D2; Tyr_Z, redox active tyrosine 161 of D1; TL, thermoluminescence; WT*3, *T. elongatus* mutant strain containing only the *psbA₃* gene and a His₆-tag on the C-terminus of CP43. EPR, Electron Paramagnetic Resonance spectroscopy; MALDI-TOF, Matrix Assisted Laser Desorption Ionization - Time of Flight.

Abstract

Photosystem II (PSII), the oxygen-evolving enzyme, consists of 17 trans-membrane and 3 extrinsic membrane proteins. Other subunits bind to PSII during assembly, like Psb27, Psb28, Tsl0063. The presence of Psb27 has been proposed (Zabret et al. 2021 [Nature Plants 7: 524–538](#); Huang et al. 2021 [Proc Natl Acad Sci USA 118: e2018053118](#); Xiao et al. 2021 [7: 1132–1142](#)) to prevent the binding of PsbJ, a single transmembrane α -helix close to the quinone Q_B binding site. Consequently, a PSII rid of Psb27, Psb28 and Tsl0034 prior to the binding of PsbJ would logically correspond to an assembly intermediate. The present work describes experiments aiming at further characterizing such a Δ PsbJ-PSII, purified from the thermophilic *Thermosynechococcus elongatus*, by means of MALDI-TOF spectroscopy, Thermoluminescence, EPR spectroscopy and UV-visible time-resolved spectroscopy. In the purified Δ PsbJ-PSII, an active Mn_4CaO_5 cluster is present in 60-70 % of the centers. In these centers, although the forward electron transfer seems not affected, the E_m of the Q_B/Q_B^- couple increases by ≥ 120 mV thus disfavoring the electron coming back on Q_A . The increase of the energy gap between Q_A/Q_A^- and Q_B/Q_B^- could contribute in a protection against the charge recombination between the donor side and Q_B^- , identified at the origin of photoinhibition under low light (Keren et al. 1997 [Proc Natl Acad Sci USA 94: 1579–1584](#)), and possibly during the slow photoactivation process.

Introduction

Photosystem II (PSII), the water-splitting enzyme in cyanobacteria, algae and higher plants, is responsible for the production of the atmospheric O₂ that is essential for aerobic organisms and it is the first step in the production of food, fibers and fossil fuels. The mature Photosystem II, in cyanobacteria, consists of 20 subunits (Umena et al. 2011; Suga et al. 2015) with 17 trans-membrane and 3 extrinsic membrane proteins (Roose et al. 2016). The PSII also binds 35 chlorophylls, 2 pheophytins, 2 hemes, 1 non-heme iron, 2 plastoquinones (Q_A and Q_B), the Mn₄CaO₅ cluster, 2 Cl⁻, 12 carotenoids and 25 lipids (Umena et al. 2011; Suga et al. 2015). Most of the cofactors involved in the water oxidation and electron transfer bind to the reaction center subunits, PsbA (also called D1) and PsbD (also called D2).

After the absorption of a photon by one of the antenna chlorophylls, the excitation is transferred from chlorophyll to chlorophyll to the photochemical trap formed by the four chlorophylls P_{D1}, P_{D2}, Chl_{D1} and Chl_{D2}. A few picoseconds later, a charge separation occurs forming the Chl_{D1}⁺Phe_{D1}⁻ and then the P_{D1}⁺Phe_{D1}⁻ radical pairs (Holzwarth et al. 2006; Romero et al. 2017). In the ns time range, P_{D1}⁺ oxidizes Tyr_Z, the Tyr161 of the D1 polypeptide. In the μs to ms time range, the radical Tyr_Z[•] oxidizes the Mn₄CaO₅ cluster, see (Shen 2015, Cox et al. 2020) for reviews. On the electron acceptor side, Phe_{D1}⁻ reduces the primary quinone electron acceptor Q_A. The electron on Q_A⁻ is in turn transferred to the second quinone electron acceptor Q_B. Whereas Q_A is only singly reduced under normal conditions, Q_B can be doubly reduced and can bind two protons before to leave its binding site, reviewed in (de Causmaecker et al. 2019). The Mn₄CaO₅ complex is oxidised sequentially in four successive charge separations. In doing so, it passes through five redox states denoted by S_n, where n represents the number of stored oxidative equivalents (Kok et al. 1970; Joliot and Kok 1975). When the S₄-state is formed, *i.e.* after the 3rd flash of light given on dark-adapted PSII that is in the S₁-state, the two water molecules bound to the cluster are oxidized, the O₂ is released and the S₀-state is reformed. The first step in the photosynthetic electron transfer chain is the absorption of a photon by the antenna chlorophyll. Then, the excitation is transferred to the photochemical trap that includes the four chlorophylls P_{D1}, P_{D2}, Chl_{D1} and Chl_{D2}. After a few picoseconds following the light-absorption process a charge separation occurs forming the Chl_{D1}⁺Phe_{D1}⁻ and then the P_{D1}⁺Phe_{D1}⁻ radical pairs (Holzwarth et al. 2006; Romero et al. 2017). Then, P_{D1}⁺ oxidizes Tyr_Z, the Tyr161 of the D1 polypeptide, which in turn oxidizes the Mn₄CaO₅ cluster, see (Shen 2015, Cox et al. 2020) for reviews. The electron on Phe_{D1}⁻ is then transferred to Q_A, the primary quinone electron acceptor and then to Q_B, the

~~second quinone electron acceptor. Whereas Q_A is only singly reduced under normal conditions, Q_B accepts two electrons and two protons before to leave its binding site, reviewed in (de Causmaecker et al. 2019). The Mn_4CaO_5 cluster is sequentially oxidized following each charge separation so that it cycles through five redox states denoted S_n , where n stands for the number of stored oxidizing equivalents (Kok et al. 1970; Joliot and Kok 1975). When the S_4 state is formed, i.e. after the 3rd flash of light given on dark adapted PSII that is in the S_1 state, the two water molecules bound to the cluster are oxidized, the O_2 is released and the S_0 state is reformed.~~

In cyanobacteria, in addition to the subunits involved in the cofactors binding (PsbA, PsbD, CP43, CP47, PsbE, PsbF), there are several small subunits consisting in only a transmembrane α -helix as PsbT, PsbM, PsbJ, PsbK, PsbL, PsbI, PsbX, PsbY, Psb30 (formerly Ycf12), e.g. (Kashino et al. 2002, 2007; Nowaczyk et al. 2012; Sugiura et al. 2012). Some roles have been attributed to these low molecular weight subunits either upon site directed mutagenesis, mainly for PsbT, or upon the deletion of the protein as for PsbM, PsbJ, Psb30, PsbK, PsbX, PsbZ.

It has been proposed that the interaction between Phe239 of PsbA and the PsbT subunit is required to restrict the movement of the DE loop of PsbA. In turn, the disruption of this interaction may perturb the binding of bicarbonate to the non-heme iron that could contribute to the signal for PSII to undergo a repair following photodamages (Forsman and Eaton-Rye 2021). Deletion of PsbM has been reported to mainly affect the Q_B environment (Uto et al. 2017). PSII depleted of Psb30 exhibited a lower efficiency under high light conditions and Psb30 favors the stabilization of the PSII complex (Sugiura et al. 2010a; Inoue-Kashino et al. 2011). Deletion of PsbK has been proposed to destabilize the association of PsbZ and Psb30 (Ycf12) with PSII complex and to alter the Q_B function (Iwai et al. 2010). PsbZ has been proposed to stabilize the binding of Psb30 (Takasaka et al. 2010). Deletion of PsbX has been shown to affect the PSII integrity in both *Arabidopsis thaliana* (Garcia-Cerdan et al. 2009) and *Synechocystis sp.* PCC 6803 (Funk 2000). In plant PSII, the PsbL subunit seems to prevent the back electron flow from the reduced plastoquinol pool thus protecting the PSII from photoinactivation (Ohad et al. 2004). In *Synechocystis sp.* PCC 6803, PsbL also influences forward electron transfer from Q_A^- to Q_B (Luo et al. 2014).

The *psbJ* gene belongs to the *psbEFLJ* operon coding for the PsbE and PsbF subunits bearing the two histidine residues His23 and His24, respectively, which are the heme iron axial ligands of the Cyt b_{559} (Umena et al. 2011). The PsbJ subunit is close to PsbK and its possible involvement in the exchange of the plastoquinone has been discussed (Kaminskaya

et al. 2007; Müh et al. 2012; van Eerden et al. 2017) with a role in the efficiency of forward electron flow following the charge separation process by affecting the Q_A and Q_B properties (Ohad et al. 2004; Regel et al. 2001). In *Synechocystis sp.* PCC 6803, double mutants lacking PsbJ and either PsbV or PsbO are unable to grow photoautotrophically (Choo et al. 2021).

In most of the deletion mutants, the observed phenotype is an alteration of the acceptor side. However, it is difficult to attribute these changes more to a specific role of the deleted subunits, rather than to perturbations in the overall structure of PSII. Cyanobacteria have several PsbA isoforms (Mulo et al. 2009; Sugiura and Boussac, 2014; Sheridan et al. 2020). In *Thermosynechococcus elongatus*, the deletion of the *psbJ* gene has different consequences with either PsbA1 or PsbA3 as the D1 protein. In PsbA3-PSII, the effects are minor whereas in the purified Δ PsbJ-PsbA1/PSII several other subunits including PsbY, PsbU, and PsbV are lacking (Sugiura et al. 2010b). In contrast, Psb27, Psb28 and Tsl0063, have been found to be associated to a proportion of the Δ PsbJ-PsbA1/PSII (Nowaczyk et al. 2012). These three proteins are known to be PSII assembly factors (Nowaczyk et al. 2006; Roose and Pakrasi 2008; Komenda et al. 2012; Liu et al. 2013; Huang et al. 2021; Zabret et al. 2021). It should be noted that Tsl0063 is named either Psb34 in (Zabret et al. 2021) or Psb36 in (Xiao et al. 2021). Structures of PSII corresponding to assembly intermediates have been recently solved by using cryo-EM by using different strategies (Zabret et al. 2021; Huang et al. 2021; Xiao et al. 2021). Upon deletion of the *psbJ* gene it became possible to isolate a “PSII-I” intermediate with Psb27, Psb28 and Tsl0063 bound and in which the major conformational change was a distortion of the Q_B binding site and the replacement of bicarbonate with glutamate as a ligand of the non-heme iron (Zabret et al. 2021). From a *psbV* deletion mutant a dimeric Psb27-PSII (Huang et al. 2021) and Psb28-PSII (Xiao et al. 201) have also been purified in which the dissociation of PsbJ occurs. Such changes are proposed to protect the PSII from damage during biogenesis until an active Mn_4CaO_5 cluster is assembled (Zabret et al. 2021; Xial et al. 2021).

Since the presence of Psb27 prevents the binding of PsbU and induces the dissociation of PsbJ and PsbY (Huang et al. 2021) and since PsbJ also seems to trigger the release of Psb28 (Zabret et al. 2021), the binding of PsbJ during the PSII assembly process very likely occurs *after* the release of Psb27 and Psb28. Consequently, a PSII without Psb27, Psb28, Tsl0063, and without PsbJ would logically also correspond to an assembly intermediate. In the present work, we describe the results of experiments aiming at further characterizing the Δ PsbJ-PsbA1/PSII purified from *Thermosynechococcus elongatus* by means of MALDI-TOF

spectroscopy, Thermoluminescence, EPR spectroscopy and UV-visible time-resolved spectroscopy.

Materials and Methods

Samples used

The *Thermosynechococcus elongatus* strains used were; *i*) the $\Delta psbA_2$, $\Delta psbA_3$ deletion mutant, referred to as either WT*1-PSII or PsbA1-PSII, *ii*) the $\Delta psbA_1$, $\Delta psbA_2$ deletion mutant, referred to as either WT*3-PSII or PsbA3-PSII (Sugiura et al. 2010b), and *iii*) the $\Delta PsbJ$ -43H deletion mutant (Sugiura et al. 2010b) which has the three *psbA* genes but in which only the PsbA1-PSII is produced under the culture conditions used in this work, see thereafter. These strains were constructed from the *T. elongatus* 43-H strain that had a His₆-tag on the carboxy terminus of CP43 (Sugiura and Inoue 1999). PSII purification was achieved as previously described (Sugiura et al. 2014). The final resuspending medium contained 1 M betaine, 15 mM CaCl₂, 15 mM MgCl₂, 40 mM Mes, pH 6.5 adjusted with NaOH.

MALDI-TOF measurements

All reagents and solvents were purchased from Sigma-Aldrich (Saint Quentin-Fallavier, France) with the highest purity available. Peptides and protein used for calibration were purchased from LaserBio Labs (TOF Mix) and Sigma (equine apomyoglobin), respectively. For intact mass analysis, 1 μ L of PSII complex prepared at a concentration of \sim 100 μ g Chl /mL in the medium mentioned above was mixed with 2 μ L of a saturated solution of sinapinic acid in 60/0.1 acetonitrile/trifluoroacetic acid. Two microliters of this premix were spotted onto the sample plate and allowed to dry under a gentle air stream. Spectra were acquired in positive reflectron and linear mode on an Axima Performance MALDI-TOF/TOF mass spectrometer (Shimadzu, Manchester, UK) with a pulse extraction fixed at 4000 for 3000-10000 m/z range and at 10000 for 6000-20000 m/z range acquisitions. All spectra were externally calibrated using a homemade calibrant mixture prepared by mixing 1 μ L of 50 μ M apomyoglobine in water with 2 μ L of TOF Mix solution containing ACTH [7-38] peptide at a concentration of 6 μ M.

UV-visible time-resolved absorption change spectroscopy

Absorption changes measurements have been performed with a lab-built spectrophotometer (Béal et al. 1999) slightly modified as previously described (Sugiura et al. 2020) in which the absorption changes were sampled at discrete times by short analytical flashes. These analytical flashes were provided by an optical parametric oscillator (Horizon OPO, Amplitude Technologies) pumped by a frequency tripled Nd:YAG laser (Surelite II, Amplitude Technologies), producing monochromatic flashes (355 nm, 2 nm full-width at half maximum) with a duration of 5 ns. Actinic flashes were provided by a second Nd:YAG laser (Surelite II, Amplitude Technologies) at 532 nm, which pumped an optical parametric oscillator (Surelite OPO plus) producing monochromatic saturating flashes at 695 nm with the same pulse length. The two lasers were working at a frequency of 10 Hz. The time delay between the laser delivering the actinic flashes and the laser delivering the detector flashes was controlled by a digital delay/pulse generator (DG645, jitter of 1 ps, Stanford Research). The path-length of the cuvette was 2.5 mm.

The samples were diluted in 1 M betaine, 15 mM CaCl₂, 15 mM MgCl₂, and 40 mM Mes (pH 6.5). PSII samples were dark-adapted for ~ 1 h at room temperature (20–22°C) before, when indicated, the addition of 0.1 mM phenyl *p*-benzoquinone (PPBQ) dissolved in dimethyl sulfoxide. The chlorophyll concentration of all the samples was ~ 25 µg of Chl/mL. After the ΔI/I measurements, the absorption of each diluted batch of samples was precisely controlled to avoid errors due to the dilution of concentrated samples and the ΔI/I values were normalized to $A_{673} = 1.75$, with $\epsilon \sim 70 \text{ mM}^{-1}\cdot\text{cm}^{-1}$ at 674 nm for dimeric PSII (Müh and Zouni 2005).

EPR spectroscopy

X-band cw-EPR spectra were recorded with a Bruker Elexsys 500 spectrometer previously described (Sugiura et al. 2020) equipped with a standard ER 4102 (Bruker) X-band resonator, a Bruker teslameter, an Oxford Instruments cryostat (ESR 900) and an Oxford ITC504 temperature controller. Flash illumination at room temperature was provided by a neodymium:yttrium–aluminum garnet (Nd:YAG) laser (532 nm, 550 mJ, 8 ns Spectra Physics GCR-230-10). Illumination at 198 K with visible light was done in a non-silvered Dewar filled with ethanol cooled with dry ice for approximately 5-10 seconds with a 800 W tungsten lamp filtered by water and infrared cut-off filters. Illumination at 4.2 K was done in the EPR cavity using a low-voltage halogen lamp (24V, 250W, Philips Type 13163) filtered by water and infrared cut-off filters. After a 1 h dark-adaptation at room temperature the samples were

frozen in the dark to 198 K in a dry ice ethanol bath and then transferred to 77 K in liquid N₂. Prior to the recording of the spectra the samples were degassed at 198 K.

Thermoluminescence measurements

Thermoluminescence (TL) curves were measured with a lab-built apparatus (Ducruet 2003; Ducruet and Vass 2009). PSII samples were diluted in 1 M betaine, 40 mM MES, 15 mM MgCl₂, 15 mM CaCl₂, pH 6.5 and then dark-adapted for at least 1 h at room temperature. When used, DCMU (100 μM, final concentration), dissolved in ethanol, was added after the dark-adaptation. Flash illumination was given at -10°C by using a saturating xenon flash. Two reasons justifies the choice of this temperature. Firstly, with the resuspending medium used, the freezing/melting of the samples occurs at ~ -15°C. Since the frozen samples are strongly diffusing, the flash illumination was done at a temperature slightly above -15°C. Secondly, an artefact occurs in the melting region which makes difficult the detection of small signals. It has been checked after the dilutions that the PSII samples had the same OD at 673 nm equal to 0.70 *i.e.* ~ 10 μg Chl/mL.

The measurements have been done on two different ΔPsbJ-PSII preparations with at least two measurements on each PSII samples except for the period 4 oscillation experiment at 291 nm done on only one PSII preparation. In addition to MALDI-TOF analysis, the protein content of the ΔPsbJ-PSII has been previously monitored with SDS-page and the oligomeric state of PSII was also analyzed by gel permeation (Sugiura et al. 2010b). Most of the ΔPsbJ-PSII, although not all, was in monomeric form and there was no evidence for the presence of any of the 3 proteins Psb28, Psb27 and Tsl0063 in significant amounts. For the spectroscopic measurements all samples were dark-adapted for one hour at room temperature before the measurements for allowing a full decay of S₂ and S₃ into S₁ (Sugiura et al. 2004).

Results

Before ~~to~~ studying the effects of the PsbJ deletion some control experiments were performed. Indeed, it has been reported (Nowaczyk et al. 2012) that in *T. elongatus* cells having all the *psbA1*, *psbA2* and *psbA3* genes, and the *psbJ* gene inactivated by insertion of a cassette, PsbA1 was replaced by PsbA3 in the ΔPsbJ-PSII. Although this substitution was not observed in the most recent work done by the same group (Zabret et al. 2021) it seemed important to us to verify that the D1 subunit was indeed PsbA1 in our ΔPsbJ-43H/PSII which

also contains the 3 genes, *psbA1*, *psbA2* and *psbA3*. For that, we have recorded the electrochromic blue shift undergone by Phe_{D1} in the Q_X spectral region upon the formation of Q_A⁻. This electrochromic C-550 band shift is well known to be red shifted by ~ 3.0 nm from 544 nm in PsbA1-PSII to 547 nm in PsbA3-PSII. This shift reflects a hydrogen bond from the 13¹-keto C=O group of Phe_{D1} stronger with the carboxylate group of E130 in PsbA3-PSII than with the amine group of Q130 in PsbA1-PSII (Merry et al. 1998; Cuni et al. 2004; Hughes et al. 2010; Shibuya et al. 2010).

Figure 1 shows the C-550 bandshift with PsbA1-PSII (black spectrum), in PsbA3-PSII (blue spectrum) and in ΔPsbJ-43H/PSII (red spectrum). For these measurements, the samples were first dark-adapted for one hour at room temperature. Then, the absorption changes were measured 15 μs after each actinic flash in a series in the presence of PPBQ. The data points are the average of the individual absorption changes induced by the 2nd to 7th flashes. In the ΔPsbJ-43H/PSII the electrochromic band shift was similar to that in the PsbA1/PSII sample, showing unambiguously that the D1 protein is PsbA1 in the ΔPsbJ-43H/PSII.

Secondly, the polypeptide content was analysed in WT*1-PSII and ΔPsbJ-43H/PSII with MALDI-TOF spectroscopy. Panel A in Figure 2 shows the *m/z* region from 3500 to 6500. The inset in Panel A shows the *m/z* region corresponding to PsbM (4009 Da calc.) and PsbJ (4002 Da calc.) by using the reflection mode. The different peaks for one protein correspond to the different proportions of ¹³C in the proteins starting from no ¹³C (100% ¹²C) to 1, 2, 3, and so on, ¹³C per protein. The two peaks for PsbJ spaced by ~16 *m/z* likely correspond to an oxygen adduct for the larger *m/z* value, also seen in earlier reports as in (Sugiura et al. 2010b; Nowaczyk et al. 2012). Panel B in Figure 2 shows the *m/z* region from 6500 to 16000. The PsbJ subunit, as expected, is missing in the ΔPsbJ-43H/PSII (Sugiura et al. 2010b; Nowaczyk et al. 2012). In ΔPsbJ-43H/PSII, other subunits are missing as PsbY, PsbU, PsbV (the Cyt_{c550}) as previously observed. However, PsbM and PsbF are now detected in 43H/ΔPsbJ-PSII exhibiting a peak with an amplitude comparable to that in WT*1-PSII and with a single peak for PsbM while two peaks (native and formylated) were previously observed in (Sugiura et al. 2010b). The reasons for such a difference between the two observations is at present unclear. A reexamination of the raw data in (Sugiura et al. 2010b) indicates that at that time we did not pay attention to the possible presence of Psb28 in a very small proportion of our ΔPsbJ-43H/PSII. Indeed, a very small peak at *m/z* ~ 12787 was present (Sugiura et al. 2010b). Panel B in Figure 2 also shows a very small peak at 12787 that could well correspond to Psb28. However, the amplitude of this peak is close to the limit of

the detection. A small peak detected at $m/z=13424$ in some traces could correspond to Psb27 (not shown). A peak at $m/z=5936$, not attributed in (Sugiura et al. 2010b) could originate from Tsl0063 recently detected in Δ PsbJ-PsbA1/PSII (Zabret et al. 2021). This protein is however not detected in Figure 2. The MALDI-TOF data described above in comparison with those in literature show that upon the deletion of PsbJ in PsbA1-PSII, the PSII composition may slightly vary from prep to prep. If present, the 3 proteins Psb27, Psb28 and Tsl0063 are in a so minor proportion of the Δ PsbJ-43H/PSII studied here that this proportion will not contribute significantly to the results described thereafter. We cannot eliminate the possibility that these 3 proteins are removed during the PSII purification. This, however, does not modify the fact that the studied Δ PsbJ-43H/PSII does not bind Psb27, Psb28 and Tsl0063.

In *Synechocystis* 6803, the deletion of PsbJ has been proposed to alter both the forward electron flow from Q_A^- to the plastoquinone pool and the back reaction between Q_A^- and the oxidized Mn_4CaO_5 cluster (Regel et al. 2001). These conclusions were done in part from thermoluminescence experiments (Rutherford et al. 1982) in whole cells. Here, similar measurements have been done but in purified WT*1-PSII and Δ PsbJ-43H/PSII. Figure 3 shows the TL curves after 1 flash given at -10°C in WT*1-PSII, black traces, and Δ PsbJ-43H/PSII, red traces. In Panel A, the TL measurements were done without any addition whereas in Panel B they were done in the presence of DCMU. The TL curves in WT*1-PSII arising from the $S_2Q_B^-$ charge recombination in Panel A with a peak temperature at $\sim 43^\circ\text{C}$ and from the $S_2Q_A^-$ /DCMU charge recombination in Panel B with a peak temperature at $\sim 13^\circ\text{C}$ are those expected in *T. elongatus* with an heating rate of 0.4°C/s . In Δ PsbJ-43H/PSII, no signal was detected both in Panels A and B. The very small signal around 0°C in Panels A and B is very similar in the absence and the presence of DCMU and therefore cannot arise from the $S_2Q_B^-$ and $S_2Q_A^-$ /DCMU charges recombinations studied here. The TL results in Figure 3 differ significantly from those in *Synechocystis* whole cells where in the Δ PsbJ mutant a small TL signal was detected at a slightly lower temperature for the $S_2Q_B^-$ charge recombination and at a slightly higher temperature for the $S_2Q_A^-$ /DCMU charge recombination (Regel et al. 2001). However, the amplitude of a TL signal depends on the proportion of centers with Q_B^- in the dark-adapted state, something that is difficult to control in whole cells. The lack of a TL signal in Δ PsbJ-43H/PSII both with and without DCMU may be explained if 100% of the centers are in the Q_B^- state upon the dark adaptation. As ~~this~~ will be shown later, ~~this~~ is not the case in the Δ PsbJ-43H/PSII studied here and so we have to find another explanation is needed.

The first simple explanation is that the radiative charge recombination in the Δ PsbJ-43H/PSII occurs either *i*) at a temperature much above a bearable temperature for PSII (*i.e.* $\gg 60^\circ\text{C}$) or *ii*) at a temperature much lower than 0°C . In the first case, the Em of the Q_A/Q_A^- couple, upon the deletion of PsbJ, would be strongly increased and, in the second case, strongly decreased. The second possibility could be a situation in which the Mn_4CaO_5 cluster in the Δ PsbJ-43H/PSII is inactive or lost because we know that under continuous illumination the activity is significantly decreased (Sugiura et al. 2010b).

Before ~~to~~going further in the interpretation of the TL experiments, we have therefore performed some EPR measurements for clarifying the situation.

Figure 4 shows the EPR spectra recorded at 8.6 K in dark-adapted samples (black spectra) and after a continuous illumination at 198 K (red spectra). The blue spectra are the light-*minus*-dark spectra. At 198 K, the electron transfers from Q_A^- to Q_B and from Q_A^- to Q_B^- are blocked so that only one charge separation may occur (Fufezan et al. 2005). In WT*1-PSII, the black spectrum is very similar to the spectrum recorded in PsbA3-PSII under the same conditions, see (Boussac et al. 2011) for a detailed description of the spectra. The signal between 3600 and 5000 gauss originates from $\text{Fe}^{2+}Q_B^-$ (Fufezan et al. 2005; Boussac et al. 2011; Sedoud et al. 2011). After illumination at 198 K for ~ 5 -10 s, the S_2 multiline signal was formed together with a signal at $g = 1.6$ (~ 4100 gauss). The $g = 1.6$ signal originates from the $Q_A^-\text{Fe}^{2+}Q_B^-$ state. The $Q_A^-\text{Fe}^{2+}$ signal formed in centers with Q_B oxidized prior to the illumination is difficult to detect in the presence of the multiline signal. A careful examination of the blue spectrum in the $g = 6$ to $g = 8$ region indicates that the non-heme iron was oxidized in a very small fraction of the dark-adapted centers and was reduced upon the 198 K illumination (Boussac et al. 2011). The spectrum in the dark-adapted Δ PsbJ-43H/PSII also exhibits a $\text{Fe}^{2+}Q_B^-$ signal with a somewhat smaller amplitude (see also Figure 7) than in WT*1-PSII. This observation rules out the hypothesis that the lack of a TL signal is due to centers with 100% Q_B^- in the dark-adapted state. In agreement with the MALDI-TOF data above, and as previously reported (Sugiura et al. 2010b), the EPR also shows that the Cyt c_{550} (PsbV) is missing in the purified PSII as evidenced by the much smaller signals at $g \sim 3$ and $g \sim 2.2$ (3000 gauss) corresponding to the g_z and g_y resonances of cytochrome signals, respectively (the g_x feature is difficult to detect under the conditions used for the recording of these spectra). We have nevertheless previously shown that PsbV was detectable in the Δ PsbJ-43H/thylakoids (Sugiura et al. 2010b). Cyt b_{559} is detected because it is in the low potential oxidized form in Δ PsbJ-43H/PSII (Sugiura et al. 2010). The detection of a signal at g

= 6 (~1100 gauss) indicates that a proportion of $\text{Cyt}b_{559}$ is also present in an oxidized high spin ($S = 5/2$) configuration. Importantly, the S_2 multiline signal is detectable upon the 198 K illumination with an amplitude close to 60-70 % of that in WT*1-PSII. Therefore, the total absence of a TL signal in this sample is also not due to an inactive or missing Mn_4CaO_5 cluster. The proportion of $\Delta\text{PsbJ-43H/PSII}$ in which the Mn_4CaO_5 is able to progress to the S_2 state upon an illumination at 198 K is higher than the O_2 evolution activity found in this PSII that is about 30% (Sugiura et al. 2010b). However, it is well known that the O_2 activity under continuous illumination does not necessarily correlate with the proportion of active centers. For example, upon the substitution of Ca^{2+} for Sr^{2+} the O_2 activity under continuous illumination is decreased by a least of factor of 2 whereas all the centers are fully active (Ishida et al. 2008). In an additional control experiment (not shown) aiming at following the period four oscillation measured at 291 nm and 100 ms after each flash of a series (Lavergne 1991; Ishida et al. 2008) it has been found that in the $\Delta\text{PsbJ-43H/PSII}$ the miss parameter is close to 20% instead of ~ 8% in the PsbA1-PSII .

The remaining possible explanations for the lack of a TL signal in $\Delta\text{PsbJ-43H/PSII}$ are either *i*) an inefficient charge separation after one flash illumination in contrast to the continuous illumination at 198 K, and/or *ii*) a too fast, even at -10°C , or too slow charge recombination in the temperature range probed by the TL thus preventing the detection of the signal. These possibilities have been tested in the EPR experiments reported in Figure 5 and Figure 6.

Panel A in Figure 5 shows the magnetic field range in which most of the EPR signals are detectable except Tyr_D^\bullet . The Tyr_D^\bullet signal is shown in Panel B. The black spectra were recorded in dark-adapted PSII and they are, of course, similar to those described in Figure 4. The green spectra have been recorded after one saturating flash given at room temperature (~20-22 °C) followed by an as-fast-as possible freezing of the sample (~2 s) in a dry ice bath at 198 K. Then, the red spectra were recorded after a further continuous illumination at 198 K following the one flash illumination. In WT*1-PSII, the difference in the amplitude of the S_2 multiline between the green and red spectra is mainly due to the proportion of centers in which the $S_0\text{Tyr}_D^\bullet$ to $S_1\text{Tyr}_D^\bullet$ transition occurs with the one flash illumination. As the Tyr_D^\bullet signal (Panel B) does not vary significantly, this suggests that the proportion of centers in which the $S_1\text{Tyr}_D$ to $S_1\text{Tyr}_D^\bullet$ transition occurs is negligible (Styring and Rutherford 1987).

In contrast, in $\Delta\text{PsbJ-43H/PSII}$, upon the illumination at 198 K, the increase of the S_2 multiline and Tyr_D^\bullet signals was much more pronounced than in WT*1-PSII. This results

shows that in dark-adapted Δ PsbJ-43H/PSII there is a proportion of centers in the S_1 Tyr_D state and a larger proportion of centers in the S_0 Tyr_D[•] state than in WT*1-PSII. Since the proportion of centers in the Q_A Fe²⁺Q_B⁻ state is smaller in the Δ PsbJ-43H/PSII than in WT*1-PSII after the dark adaptation, this ratio is inverted after the one flash illumination. Consequently, the illumination at 198 K is expected to induce a larger Q_A Fe²⁺Q_B⁻ in Δ PsbJ-43H/PSII than in WT*1-PSII and that is indeed what is observed here. It should be mentioned that, normally, an illumination at 198 K is unable to oxidize Tyr_D in active centers. The increase seen in Panel B therefore likely occurs in the proportion of inactive Δ PsbJ-43H/PSII. The important result in this experiment is that the one-flash illumination is able to induce the S_2 state in the Δ PsbJ-43H/PSII although to a slightly less extent than in WT*1-PSII due to a higher proportion of centers in the S_1 Tyr_D and S_0 Tyr_D[•] states and also to a higher miss parameter. The stability of the S_2 state has then been monitored in an experiment corresponding to the TL experiment in the presence of DCMU.

In Figure 6, the black spectra were recorded in dark-adapted PSII without any addition and the red spectra after the addition of DCMU. Two observations can be made here. Firstly, in both WT*1-PSII and Δ PsbJ-43H/PSII, the addition of DCMU resulted in the formation of Q_A Fe²⁺/DCMU to the detriment of Fe²⁺Q_B⁻ (Velthuys 1981). In both samples, Q_A Fe²⁺/DCMU exhibited either the $g = 1.9$ signal or the $g = 1.82$ signal (Rutherford et al. 1983, Rutherford and Zimmermann 1984), see below for a better description of the signals in Figure 6. Secondly, in WT*1-PSII, the addition of DCMU also modified the non-heme iron signal as previously observed (Diner and Petrouleas 1987). The blue spectra were then recorded after a continuous illumination at 198 K. The S_2 multiline signal was formed in the open centers, *i.e.* in those with no Q_B⁻ prior to the addition of DCMU. The larger Q_A Fe²⁺ signal at $g = 1.9$ in Δ PsbJ-43H/PSII than in WT*1-PSII have two possible explanations: *i*) a lower amount of Q_B⁻ before the addition of DCMU and *ii*) a smaller proportion of oxidized non-heme iron. Indeed, the oxidation of Q_A by the oxidized non-heme iron results in the disappearance of the non-heme iron signal in WT*1-PSII. Unfortunately, in Δ PsbJ-43H/PSII, the presence of the high spin Cyt_b₅₅₉ signal does not allow the detection of the non-heme iron signal.

After the illumination at 198 K, the samples were immersed for 1 to 2 seconds, in total darkness, in an ethanol bath at 0°C and immediately refrozen in a dry ice bath at 198 K and the green spectra were recorded. In WT*1-PSII, the brief passage at 0°C induced almost no change in the amplitude of the S_2 multiline signal. In contrast, in Δ PsbJ-43H/PSII, almost all the S_2 multiline signal and the $g = 1.9$ quinone signal disappeared thus showing that the

recombination in the $S_2Q_A^-/DCMU$ state is very fast at 0°C in this sample. This very likely explains the lack of a TL signal in Figure 3B. The proportion of the $g = 1.9$ signal which decayed during the warming at 0°C appears larger than the proportion the $g = 1.82$ signal which decayed. This suggests that the recombination was more efficient with the quinone in the $g = 1.9$ state than in the $g = 1.82$ state (Demeter al. 1993; Rutherford, personal communication). Finally, the samples were immersed, in the dark, in an ethanol bath at 20°C and immediately refrozen in a dry ice bath at 198 K and the spectra in magenta were recorded. In WT*1-PSII, the S_2 multiline now decreased significantly as expected from the peak temperature observed in this sample. In $\Delta\text{PsbJ-43H/PSII}$, the spectrum was not significantly different from that one after the thawing at 0°C . The recording of the Tyr_D^\bullet spectra as in Panel B of Figure 5 showed again that Tyr_D^\bullet could be induced at 198 K and that a decay occurs upon the short incubation at 0°C (not shown). The experiments described above focused on the charge recombinations. In the following, we will address the forward electron transfer.

Figure 7 shows the flash-induced $\Delta I/I$ and its decay at 320 nm after the 2nd flash given on dark-adapted WT*3-PSII (blue), WT*1-PSII (black) and $\Delta\text{PsbJ-43H/PSII}$ (red). The Q_A^- -*minus*- Q_A and Q_B^- -*minus*- Q_B difference spectra are similar and have their maximum amplitude at around 320 nm (Schatz and van Gorkom 1985). After the 1st flash and the 3rd flash, the S_1 to S_2 and S_3 to S_0 transitions also contribute significantly to the flash induced absorption changes at 320 nm (Lavergne 1991). In addition, the first flash is also complicated by the Q_A^- to Fe^{2+} electron transfer (Boussac et al. 2011) with possible contribution in this spectral range of the $\text{Fe}^{3+}/\text{Fe}^{2+}$ couple (Sellés and Boussac, unpublished) and with the formation of the Tyr_Z^\bullet radical in inactive centers (with a flash spacing of 300 ms, the dead centers contribute mainly on the first flash due to the slow decay of Tyr_Z^\bullet). For all these reasons, Figure 7 only shows the data after the second flash which is the easiest kinetics to analyze. In centers with Q_B oxidized in the dark-adapted state the flash illumination forms the $Q_A^-Q_B$ state and then the $Q_AQ_B^-$ state. In these centers, the flash-induced $\Delta I/I$ does not decay and it is responsible for the remaining stable $\Delta I/I$ at the longest times. In dark-adapted centers with Q_B^- present, the flash illumination forms the $Q_A^-Q_B^-$ state and then the $Q_AQ_BH_2$ state. This reaction is at the origin of the decay in Figure 7 and ~~these~~ kinetics ~~is~~-are similar in the 3 samples with a $t_{1/2}$ of 2-3 ms. The similar apparent lag phase with a duration of ~ 1 ms likely corresponds to the electron transfer between Q_A^- and either Q_B or Q_B^- . This experiment shows that the forward electron transfer is not affected by the deletion of PsbJ.

Finally, Figure 8 shows EPR spectra in WT*1-PSII (black spectra) and Δ PsbJ-43H/PSII (red spectra) recorded with a magnetic field scale allowing a better observation of the quinone signals. Panel A shows the $\text{Fe}^{2+}\text{Q}_\text{B}^-$ signal recorded in the dark-adapted samples. The signal is smaller in the Δ PsbJ-43H/PSII as mentioned previously and very slightly shifted. Panel B shows the spectra after a further illumination at 4.2 K. In centers with Q_B^- present in the dark this 4.2 K illumination resulted in the formation of the $\text{Q}_\text{A}^-\text{Fe}^{2+}\text{Q}_\text{B}^-$ signal that is larger in the WT*1-PSII. In the Δ PsbJ-43H/PSII, consequently to the larger proportion of centers with Q_B^- in the dark-adapted state, the 4.2 K illumination resulted in a larger proportion of $\text{Q}_\text{A}^-\text{Fe}^{2+}\text{Q}_\text{B}^-$ giving rise to the $g = 1.9$ signal between 3500 and 3700 gauss. Panel C shows the spectra recorded after an illumination at 4.2 K of samples in which a low amount of ferricyanide has been added (less than 100 μM) upon the dark adaptation to have the highest proportion of Q_B^- without the risk to oxidize the non-heme iron. Although there was still a low amount of $\text{Q}_\text{A}^-\text{Fe}^{2+}\text{Q}_\text{B}^-$ signal in Δ PsbJ-43H/PSII, in both samples such a procedure resulted in the formation of a similar $\text{Q}_\text{A}^-\text{Fe}^{2+}\text{Q}_\text{B}^-$ characterized by the $g = 1.9$ signal. Finally, in Panel D the spectra were recorded after the addition of DCMU which resulted in the formation of $\text{Q}_\text{A}^-\text{Fe}^{2+}/\text{DCMU}$ in centers with Q_B^- present in the dark. Two signals are observed in the two samples, the signal at $g = 1.9$ and a much broader ~ 300 gauss-width signal reminiscent of a signal previously observed (Sedoud et al. 2011). The larger amplitude of these two signals in WT*1-PSII resulted of the higher concentration of Q_B^- in the dark in this PSII.

Discussion

In PSII lacking the PsbJ subunit it is possible to observe a proportion of the enzyme associated to polypeptides known to be assembly cofactors such as Psb27, Psb28 and Tsl0063, and which are not detected in the mature PSII, *e.g.* (Nowaczyk et al. 2006; Roose and Pakrasi 2008; Komenda et al. 2012; Liu et al. 2013; Huang et al. 2021; Zabret et al. 2021). The cryo-EM structure of an intermediate state was resolved (Zabret et al. 2021) with the interesting observation that the bicarbonate ligand of non-heme iron is replaced with a glutamate (glu241 of PsbD), a structural motif found in purple bacteria. Such a motif was further proposed to protect PSII from damage during biogenesis. Although the 3 proteins Psb27, Psb28 and Tsl0063 are possibility detected in the Δ PsbJ-43H/PSII studied here, the MALDI-TOF signals are so weak that we can reasonably consider that the purified PSII

studied here is devoid of these assembly cofactors, see also (Sugiura et al. 2010b). The main peptides which are missing in this Δ PsbJ-43H/PSII are PsbY, PsbU and PsbV. Although PsbV is present in the Δ PsbJ-thylakoids (Sugiura et al. 2010b), the g_z value is lower than in intact PSII. This indicates (Roncel et al. 2003) that PsbV is not properly bound to PSII in thylakoids in the absence of PsbJ. Therefore, PsbJ very likely stabilizes the binding of the extrinsic peptides PsbU and PsbV and possibly of the trans-membrane α -helix PsbY as previously suggested (Zabret et al. 2021; Huang et al. 2021; Xiao et al. 2021). The Δ PsbJ-43H/PSII is essentially monomeric (Sugiura et al. 2010b) and in agreement with such a destabilization for PsbY, it was observed that although present, no electron density corresponding to PsbY was found in a crystal of monomeric PSII (Broser et al. 2010).

Despite the close proximity of PsbJ with the Q_B binding pocket, from the data in Figure 8, the lack of this subunit does not dramatically perturb, from an EPR point of view, any of the four states $Q_A Fe^{2+} Q_B^-$, $Q_A^- Fe^{2+} Q_B$, $Q_A^- Fe^{2+} Q_B^-$ and $Q_A^- Fe^{2+}/DCMU$. The quinone Q_B is present and DCMU binds in the Q_B pocket, with the same consequences, as in the wild type PSII. Nevertheless, despite the lack of strong structural changes/modifications, the energetics is strongly modified. Since a great proportion of Δ PsbJ-43H/PSII has an intact Mn_4CaO_5 cluster, this allowed us to probe these changes by using thermoluminescence (Rutherford 1982; Johnson et al. 1995; Cser and Vass 2007; Rappaport and Lavergne 2009).

In WT*1-PSII, the TL peak corresponding to the $S_2 Q_A^- /DCMU$ recombination is downshifted by $\sim 32^\circ C$, from $45^\circ C$ to $13^\circ C$, when compared to the $S_2 Q_B^-$ recombination. According to a correspondence of $0.3-0.4^\circ C/mV$ estimated by Rappaport and Lavergne (2009), see also (Cser and Vass 2007), this locates the energy level of the $S_2 Q_A^- /DCMU$ state at least $80 mV (= 32/0.4)$ above the energy level of the $S_2 Q_B^-$ state in WT*1-PSII. If we assume that the Em of the Q_A/Q_A^- couple is increased by about $50 mV$ with DCMU bound as in plant PSII (Krieger et al. 1995), this would locate the energy level of the $S_2 Q_A^-$ state at least $80 + 50 = 130 mV$ above that of the $S_2 Q_B^-$ state in WT*1-PSII.

In Δ PsbJ-43H/PSII neither the $S_2 Q_A^- /DCMU$ nor the $S_2 Q_B^-$ charge recombinations are detectable in the temperature range from $-10^\circ C$ to $70^\circ C$. The same reasoning done above for the WT*1-PSII would locate the energy level of the $S_2 Q_A^- /DCMU$ state at least $200 mV (= 80/0.4)$ above the $S_2 Q_B^-$ state in Δ PsbJ-43H/PSII, $80^\circ C$ being the lower limit for the difference in the TL peaks corresponding to the $S_2 Q_A^- /DCMU$ and $S_2 Q_B^-$ charge recombinations in this sample.

We cannot totally discard the possibility that the release of PsbV affects the stability of S_2 in the Δ PsbJ-43H/PSII. However, *Synechocystis* mutants lacking PsbV exhibit TL peaks at a slightly higher temperature than in the wild type (Shen et al. 1998) suggesting an increase of the S_2 stability that is the opposite of what is seen here.

For analyzing the TL data, two extreme cases will be considered assuming that the effect of the deletion occurs mainly on the acceptor side. In the first one, the deletion of PsbJ would only affect the Em of the Q_A/Q_A^- couple whereas in the second case, only the Em of the Q_B/Q_B^- couple would be affected. We cannot discard a possible effect on both Q_A and Q_B . In this case, the changes will apply on Q_A and Q_B but to a less extent on each of them.

In the first case, we will assume that in Δ PsbJ-43H/PSII the binding of DCMU also increases the Em of the Q_A/Q_A^- couple by ~ 50 mV as supposed above for WT*1/PSII. Therefore, with an energy level of the $S_2Q_A^-/DCMU$ state at least 200 mV above that of the $S_2Q_B^-$ state this would locate the energy level of the $S_2Q_A^-$ state (without DCMU) at least $200+50=250$ mV above the $S_2Q_B^-$ state in Δ PsbJ-43H/PSII instead of 130 mV in WT*1-PSII. Although the value of 250 mV could be overestimated, this high value explains the lack of the $S_2Q_B^-$ charge recombination experimentally observed in the TL experiment and the very fast $S_2Q_A^-/DCMU$ charge recombination. The decrease in the Em of the Q_A/Q_A^- couple could also explain the faster charge recombination observed in *Synechocystis* 6803 (Regel et al. 2001) in the absence of PsbJ if we are in conditions with a large proportion of the quinone pool fully reduced as often observed with whole cells.

In the second case, the Em of the Q_B/Q_B^- couple would reach a value disfavoring the electron coming back on Q_A . However, the energy level of the $S_2Q_A^-/DCMU$ also needs to be much higher in Δ PsbJ-43H/PSII than in WT*1-PSII to explain the lack of a TL signal in the presence of DCMU above -10°C . Since the peak in WT*1-PSII is observed at 13°C , a peak at a temperature below -10°C correspond to a decrease by at least ~ -58 mV ($-23/0.4$) for the Em of the Q_A/Q_A^- couple in the presence of DCMU when compared to WT*1-PSII. Since PsbJ is close to the Q_B pocket and therefore close to the DCMU binding site, a DCMU effect on the Em of the Q_A/Q_A^- couple different in Δ PsbJ-43H/PSII than in plant PSII would not be unlikely. If we further push the reasoning assuming no change in the Em Q_A/Q_A^- couple in the Δ PsbJ-43H/PSII, the effect of the DCMU binding could be negligible. Indeed, the Em of the Q_A/Q_A^- couple with DCMU bound in the Δ PsbJ-43H/PSII would be the same than for the Q_A/Q_A^- couple in the absence of DCMU in WT*1/PSII. A higher Em of the Q_B/Q_B^- couple may also explain the lower O_2 evolution under continuous illumination by the Δ PsbJ-

43H/PSII (Sugiura et al. 2010b) by decreasing the efficiency of the electron transfer between Q_B^- and the added quinone.

Alone, a low Em of the Q_A/Q_A^- couple in Δ PsbJ-43H/PSII is expected to increase the damages due to the repopulation of triplet states in the functional enzyme. For that reason we would favor the model in which only the Em of the Q_B/Q_B^- couple is affected (increased) in Δ PsbJ-43H/PSII. The increase of the ΔEm between Q_A/Q_A^- and Q_B/Q_B^- , and without affecting the forward electron transfer, could contribute in a protection against the charge recombinations between the donor side and Q_B^- . Such a charge recombination was identified ~~as~~ the origin of the damage by about 2 orders of magnitude higher than ~~that~~-induced by the same amount of energy delivered by continuous light (Keren et al. 1997) and a protection against it would favor the photoactivation process, see (Bao and Burnap 2016) for a recent review on photoactivation.

Legends of the figures

Figure 1: Light-induced difference spectra around 545 nm. The flash-induced absorption changes were measured in PsbA1/PSII (black spectrum), Δ PsbJ-43H/PSII (red spectrum) and PsbA3-PSII (blue spectrum). The data points are the average of the $\Delta I/I$ values detected 15 μ s after the 2nd to 7th actinic flashes given to dark-adapted PSII. After dark adaptation for 1 h at room temperature, 100 μ M PPBQ (dissolved in dimethyl sulfoxide) was added to the samples. The amplitude of the spectra were normalized to a Chl concentration corresponding to $OD_{673nm}=1.75$.

Figure 2: MALDI-TOF MS profiling of PSII subunits. (A) Linear mode MALDI-TOF spectra of subunits from Δ PsbJ-43H/PSII (upper panel) and WT*1-PSII (lower panel) strains. For presentation, both spectra were internally recalibrated on known peaks of PSII subunits using their theoretical average masses (formylated PsbT, $m/z = 3902.67$ Da; PsbK, $m/z = 4099.88$ Da; PsbL, $m/z = 4297.02$ Da; acetylated PsbF, $m/z = 4975.66$ Da; formylated PsbZ, $m/z = 6792.18$ Da; PsbE, $m/z = 9441.53$ Da) according to (Sugiura et al. 2010a 2010b, Boussac et al. 2013, Nowaczyk et al. 2012). In the inset, zoom of the 3090-4025 m/z range of high-resolution MALDI-TOF spectra from Δ PsbJ-43H/PSII mutant (upper panel) and WT*1-PSII wild-type (lower panel) strains acquired in reflection mode. Both spectra were internally recalibrated on known mono-isotopic peaks of PSII subunits using their theoretical mono-isotopic masses (formylated PsbT, $m/z = 3900.09$ Da; PsbK, $m/z = 4097.32$ Da; PsbL, $m/z = 4294.32$ Da; acetylated PsbF, $m/z = 4972.61$ Da). (B) Linear mode MALDI-TOF spectra of Δ PsbJ-43H/PSII mutant (upper panel) and WT*1/PSII (lower panel) strains. In the upper panel which shows the 11000-15000 m/z range for the Δ PsbJ-43H/PSII mutant spectrum, the amplitude was magnified 10 times. (*) this 206 Da mass shift could correspond to farnesyl adduct find in mono-charged and discharged PsbV. There is no peak at 16472 m/z which suggests that the peak at 8236 m/z does not correspond to a double charged ion. Instead, it could correspond to a contamination by the subunit c of the ATP synthase (Suhai et al. 2008).

Figure 3: Thermoluminescence curves after one flash given at -10°C either without any addition (Panel A) or in the presence of DCMU (Panel B). Black curve, WT*1/PSII; red curve, Δ PsbJ-43H/PSII. The concentration of the samples was adjusted exactly to $OD_{673nm}=0.7$ (~ 10 μg Chl/mL) before to be dark-adapted at room temperature for at least 1 h.

In Panel B, the final concentration of DCMU, dissolved in ethanol, was 100 μM . After the addition of DCMU, the samples were immediately loaded into the cuvette in total darkness. The heating rate was 0.4°C/s.

Figure 4: EPR spectra recorded in WT*1-PSII and $\Delta\text{PsbJ-43H/PSII}$. The spectra were recorded after dark-adaptation for 1 hour at room temperature (black spectra) and after a continuous illumination at 198 K (red spectra). The blue spectra are the light-*minus*-dark spectra. The concentration was 1.1 mg Chl/mL. Instrument settings: temperature, 8.6 K; modulation amplitude, 25 G; microwave power, 20 mW; microwave frequency, 9.4 GHz; modulation frequency, 100 kHz.

Figure 5: EPR spectra recorded in WT*1/PSII and $\Delta\text{PsbJ-43H/PSII}$. The spectra were recorded after dark-adaptation for 1 hour at room temperature (black spectra), after illumination by one flash at room temperature (green spectra) and after a further continuous illumination at 198 K (red spectra). The concentration was 1.1 mg Chl/mL. Instrument settings: temperature, 8.6 K; microwave frequency, 9.4 GHz; modulation frequency, 100 kHz. Modulation amplitude, 25 G and microwave power, 20 mW in Panel A and modulation amplitude, 2.8 G and microwave power, 2 μW in Panel B. In the conditions used for the recording of the Tyr_D[•] spectra, the microwave power is still slightly saturating so that an increase in the relaxation properties upon the formation of S₂ induces an increase of the signal amplitude (Styring and Rutherford 1988). This effect is larger in the negative part of the signal and is less when using a smaller modulation frequency (not shown) which is indicative of a rapid-passage effect (Styring and Rutherford 1988).

Figure 6: EPR spectra recorded in WT*1-PSII (Panel A) and $\Delta\text{PsbJ-43H/PSII}$ (Panel B). The spectra were recorded after dark-adaptation for 1 hour at room temperature (black spectra) and after the addition (100 μM) dissolved in ethanol (red spectra). Then, the blue spectra were recorded after an illumination at 198 K. The green spectra were recorded after a brief (1-2 s) warming of the samples at 0°C and the spectra in magenta were recorded after a second brief warming at 20°C. The concentration was 1.1 mg Chl/mL. Instrument settings: temperature, 8.6 K; microwave frequency, 9.4 GHz; modulation frequency, 100 kHz; modulation amplitude, 25 G; microwave power, 20 mW.

Figure 7: Time-courses of the $\Delta I/I$ changes at 320 nm after the 2nd flash given on dark-adapted WT*1-PSII (black points), Δ PsbJ-43H/PSII (red points) and WT*3-PSII (blue data points). Flashes spaced 300 ms apart. Chl concentration adjusted to $OD_{673nm}=1.75$.

Figure 8: EPR spectra recorded in WT*1-PSII (black spectra) and Δ PsbJ-43H/PSII (red spectra). Panel A, the spectra were recorded after dark-adaptation for 1 hour at room temperature. Panel B, the spectra were recorded after a further illumination at 4.2 K. Panel C, the spectra were recorded after the addition of 100 μ M of ferricyanide on dark-adapted samples followed by an illumination at 4.2 K. Panel D, the spectra were recorded after the addition of DCMU (100 μ M) dissolved in ethanol to dark-adapted samples. The concentration was 1.1 mg Chl/mL. Instrument settings: temperature, 4.2 K except for Panel A in which T = 8.6 K; microwave frequency, 9.4 GHz; modulation frequency, 100 kHz; modulation amplitude, 25 G; microwave power, 20 mW.

References

- Bao H, Burnap RL (2016) Photoactivation: The light-driven assembly of the water oxidation complex of Photosystem II. *Front Plant Sci* 7:article 578.
<https://doi.org/10.3389/fpls.2016.00578>
- Beal D, Rappaport F, Joliot P (1999) A new high-sensitivity 10-ns time-resolution spectrophotometric technique adapted to in vivo analysis of the photosynthetic apparatus. *Rev Sci Instrum* 70: 202–207. <https://doi.org/10.1063/1.1149566>
- Boussac A, Sugiura M, Rappaport F (2011) Probing the quinone binding site of photosystem II from *Thermosynechococcus elongatus* containing either PsbA1 or PsbA3 as the D1 protein through the binding characteristics of herbicides. *Biochim Biophys Acta* 1807:119–129.
<https://doi.org/10.1016/j.bbabi.2010.10.004>
- Broser M, Gabdulkhakov A, Kern J, Guskov A, Muh F, Saenger W, Zouni A (2010) Crystal structure of monomeric Photosystem II from *Thermosynechococcus elongatus* at 3.6-Å resolution. *J Biol Chem* 285: 26255–26262. <https://doi.org/10.1074/jbc.M110.127589>.
- Choo P, Forsman JA, Hui LL, Khaing EP, Summerfield TC, Eaton-Rye JJ (2021) The PsbJ protein is required for photosystem II activity in centers lacking the PsbO and PsbV luminal subunits. *Photosynth Res*, early access. <https://doi.org/10.1007/s11120-021-00862-y>
- Cox N, Pantazis DA, Lubitz W (2020) Current understanding of the mechanism of water oxidation in Photosystem II and its relation to XFEL data. *Annu. Rev. Biochem.* 89:795–820.
<https://doi.org/10.1146/annurev-biochem-011520-104801>
- Cser K, Vass I (2007) Radiative and non-radiative charge recombination pathways in Photosystem II studied by thermoluminescence and chlorophyll fluorescence in the cyanobacterium *Synechocystis* 6803. *Biochim Biophys Acta* 1767: 233–243.
<https://doi.org/10.1016/j.bbabi.2007.01.022>
- Cuni A, Xiong L, Sayre R, Rappaport F, Lavergne J (2004) Modification of the pheophytin midpoint potential in Photosystem II: modulation of the quantum yield of charge separation and of charge recombination pathways. *Phys Chem Chem Phys* 6: 4825–4831
<https://doi.org/10.1039/B407511K>

de Causmaecker S, Douglass JS, Fantuzzi A, Nitschke W, Rutherford AW (2019) Energetics of the exchangeable quinone, Q_B , in Photosystem II. *Proc Natl Acad Sci USA* 116: 19458–19463. www.pnas.org/cgi/doi/10.1073/pnas.1910675116

Demeter S, Goussias C, Bern G, Kovács L, Petrouleas V (1993) Participation of the $g = 1.9$ and $g = 1.82$ EPR forms of the semiquinone-iron complex, $Q_A^-Fe^{2+}$ of photosystem II in the generation of the Q and C thermoluminescence bands, respectively. *FEBS* 336: 352–356. [https://doi.org/10.1016/0014-5793\(93\)80836-J](https://doi.org/10.1016/0014-5793(93)80836-J)

Diner BA, Petrouleas V (1987) Light-induced oxidation of the acceptor-side Fe(II) of Photosystem II by exogenous quinones acting through the Q_B binding site. II. Blockage by inhibitors and their effects on the Fe(III) EPR spectra. *Biochim Biophys Acta* 893: 138–148. [https://doi.org/10.1016/0005-2728\(87\)90033-8](https://doi.org/10.1016/0005-2728(87)90033-8)

Ducruet JM (2003) Chlorophyll thermoluminescence of leaf discs: simple instruments and progress in signal interpretation open the way to new ecophysiological indicators. *J Exp Bot* 54: 2419–2430. <https://doi.org/10.1093/jxb/erg268>

Ducruet JM, Vass I (2009) Thermoluminescence: experimental. *Photosynth Res* 201: 195–204. <https://doi.org/10.1007/s11120-009-9436-0>

Forsman JA, Eaton-Rye JJ (2021) The interaction between PsbT and the DE loop of D1 in Photosystem II stabilizes the quinone-iron electron acceptor complex. *Biochemistry* 60: 53–63. <https://doi.org/10.1021/acs.biochem.0c00668>.

Fufezan C, Zhang CX, Krieger-Liszkay A, Rutherford AW (2005) Secondary quinone in photosystem II of *Thermosynechococcus elongatus*: semiquinone-iron EPR signals and temperature dependence of electron transfer. *Biochemistry* 44: 12780–12789. <https://doi.org/10.1021/bi051000k>

Funk C (2000) Functional analysis of the PsbX protein by deletion of the corresponding gene in *Synechocystis* sp. PCC 6803. *Plant Mol Biol* 44: 815–827. <https://doi.org/10.1023/A:1026764728846>

Garcia-Cerdan JG, Sveshnikov D, Dewez D, Jansson S, Funk C, Schroder WP (2009) Antisense inhibition of the PsbX protein affects PSII integrity in the higher plant *Arabidopsis thaliana*. *Plant Cell Physiol* 50: 191–202. <https://doi.org/10.1093/pcp/pcn188>

Holzwarth AR, Müller MG, Reus M, Nowaczyk M, Sander J, Rögner M (2006) Kinetics and mechanism of electron transfer in intact photosystem II and in the isolated reaction center: pheophytin is the primary electron acceptor. *Proc Natl Acad Sci USA* 103: 6895–6900.

<https://doi.org/10.1073/pnas.0505371103>

Huang G, Xiao Y, Pi X, Zhao L, Zhu Q, Wang W, Kuang T, Han G, Sui S-F, Shen J-R (2021) Structural insights into a dimeric Psb27-photosystem II complex from a cyanobacterium *Thermosynechococcus vulcanus*. *Proc Natl Acad Sci USA* 118:

e2018053118. <https://doi.org/10.1073/pnas.2018053118>

Hughes JL, Cox N, Rutherford AW, Krausz E, Lai T-L, Boussac A, Sugiura M (2010) D1 protein variants in Photosystem II from *Thermosynechococcus elongatus* studied by low temperature optical spectroscopy. *Biochim Biophys Acta* 1797: 11–19.

<https://doi.org/10.1016/j.bbabi.2009.07.007>

Inoue-Kashino N, Kashino Y, Takahashi Y (2011) Psb30 is a photosystem II reaction center subunit and is required for optimal growth in high light in *Chlamydomonas reinhardtii*. *J Photochem Photobiol* 104: 220–228.

<https://doi.org/10.1016/j.jphotobiol.2011.01.024>

Ishida N, Sugiura M, Rappaport F, Lai T-L, Rutherford AW, Boussac A (2008) Biosynthetic exchange of bromide for chloride and strontium for calcium in the photosystem II oxygen-evolving enzyme. *J Biol Chem* 283: 13330–13340.

<https://doi.org/10.1074/jbc.M710583200>

Iwai M, Suzuki T, Kamiyama A, Sakurai I, Dohmae N, Inoue Y, Ikeuchi M (2010) The PsbK subunit is required for the stable assembly and stability of other small subunits in the PSII complex in the thermophilic cyanobacterium *Thermosynechococcus elongatus* BP-1. *Plant Cell Physiol* 51: 554–560.

<https://doi.org/10.1093/pcp/pcq020>

Johnson GN, Rutherford AW, Krieger A (1995) A change in the midpoint potential of the quinone QA in Photosystem II associated with photoactivation of oxygen evolution. *Biochim Biophys Acta* 1229: 202–207.

[https://doi.org/10.1016/0005-2728\(95\)00003-2](https://doi.org/10.1016/0005-2728(95)00003-2)

Joliot P, Kok B (1975) Oxygen evolution in photosynthesis, in: Govindjee (Ed.), *Bioenergetics of Photosynthesis*, Academic Press, New York, pp. 387–412.

Kaminskaya O, Shuvalov VA, Renger G (2007) Evidence for a novel quinone-binding site in the photosystem II (PS II) complex that regulates the redox potential of cytochrome b559.

Biochemistry 46: 1091–1105. <https://doi.org/10.1134/S1607672907010048>

- Kashino Y, Lauber WM, Carroll JA, Wang Q, Whitmarsh J, Satoh K, Pakrasi HB (2002) Proteomic analysis of a highly active photosystem II preparation from the cyanobacterium *Synechocystis* sp. PCC 6803 reveals the presence of novel polypeptides. *Biochemistry* 41: 8004-8012. <https://10.1021/bi026012>
- Kashino Y, Takahashi T, Inoue-Kashino N, Ban A, Ikeda Y, Satoh K, Sugiura M (2007) Ycf12 is a core subunit in the photosystem II complex. *Biochim Biophys Acta* 1767: 1269–1275. <https://doi.org/10.1016/j.bbabi.2007.08.008>
- Keren N, Berg A, VanKan PJM, Levanon H, Ohad I (1997) Mechanism of photosystem II photoinactivation and D1 protein degradation at low light: The role of back electron flow. *Proc Natl Acad Sci USA* 94: 1579–1584. <https://doi.org/10.1073/pnas.94.4.1579>.
- Kok B, Forbush B, McGloin M (1970) Cooperation of charges in photosynthetic O₂ evolution—I. A linear four step mechanism. *Photochem Photobiol* 11: 457–475. <https://doi.org/10.1111/j.1751-1097.1970.tb06017.x>
- Komenda J, Sobotka R, Nixon PJ (2012) Assembling and maintaining the Photosystem II complex in chloroplasts and cyanobacteria. *Curr Opin Plant Biol* 15: 245-251; <https://doi.org/10.1016/j.pbi.2012.01.017>
- Krieger A, Rutherford AW, Johnson GN (1995) On the determination of redox midpoint potential of the primary quinone electron acceptor, Q_A, in photosystem II. *Biochim Biophys Acta* 1229:193–201. [https://doi.org/10.1016/0005-2728\(95\)00002-Z](https://doi.org/10.1016/0005-2728(95)00002-Z)
- Lavergne J (1991) Improved UV-visible spectra of the S-transitions in the photosynthetic oxygen-evolving system. *Biochim Biophys Acta* 1060: 175–188. [https://doi.org/10.1016/S0005-2728\(09\)91005-2](https://doi.org/10.1016/S0005-2728(09)91005-2)
- Liu HJ, Chen JW, Huang RYC, Weisz D, Gross ML, Pakrasi HB (2013) Mass Spectrometry-based Footprinting Reveals Structural Dynamics of Loop E of the Chlorophyll-binding Protein CP43 during Photosystem II Assembly in the Cyanobacterium *Synechocystis* 6803. *J Biol Chem* 288: 14212–14220. <https://doi.org/10.1074/jbc.M113.467613>
- Luo H, Jackson SA, Fagerlund RD, Summerfield TC, Eaton-Rye JJ (2014) The importance of the hydrophilic region of PsbL for the plastoquinone electron acceptor complex of Photosystem II. *Biochim Biophys Acta* 1837: 1435–1446. <https://doi.org/10.1016/j.bbabi.2014.02.015>

- Merry SAP, Nixon PJ, Barter LMC, Schilstra MJ, Porter G, Barber J, Durrant JR, Klug D (1998) Modulation of quantum yield of primary radical pair formation in photosystem II by site directed mutagenesis affecting radical cations and anions. *Biochemistry* 37: 17439–17447. <https://doi.org/10.1021/bi980502d>
- Müh F, Zouni A (2005) Extinction coefficients and critical solubilisation concentrations of photosystems I and II from *Thermosynechococcus elongatus*. *Biochim Biophys Acta* 1708: 219–228. <https://doi.org/10.1016/j.bbabi.2005.03.005>
- Müh F, Glöckner C, Hellmich J, Zouni A (2012) Light-induced quinone reduction in photosystem II. *Biochim Biophys Acta* 1817: 44–65. <https://doi.org/10.1016/j.bbabi.2011.05.021>
- Mulo P, Sicora C, Aro E-M (2009) Cyanobacterial psbA gene family: optimization of oxygenic photosynthesis. *Cell Mol Life Sci* 66: 3697–3710. <https://doi.org/10.1007/s00018-009-0103-6>
- Nowaczyk MM, Hebel R, Schlodder E, Meyer HE, Warscheid B, Rogner M (2006) Psb27, a cyanobacterial lipoprotein, is involved in the repair cycle of photosystem II. *Plant Cell* 18: 3121–3131. <https://doi.org/10.1105/tpc.106.042671>
- Nowaczyk MM, Krause K, Mieseler M, Sczibilanski A, Ikeuchi M, Rögner M (2012) Deletion of psbJ leads to accumulation of Psb27–Psb28 photosystem II complexes in *Thermosynechococcus elongatus*. *Biochim Biophys Acta* 1817: 1339–1345. <http://dx.doi.org/10.1016/j.bbabi.2012.02.017>
- Ohad I, Dal Bosco C, Herrmann RG, Meurer J (2004) Photosystem II proteins PsbL and PsbJ regulate electron flow to the plastoquinone pool. *Biochemistry* 43: 2297–2308. <https://doi.org/10.1021/bi0348260>
- Rappaport F, Lavergne J (2009) Thermoluminescence: theory. *Photosynth Res* 101:205–216. <https://doi.org/10.1007/s11120-009-9437-z>
- Regel RE, Ivleva NB, Zer H, Meurer J, Shestakov SV, Herrmann RG, Pakrasi HB, Ohad I (2001) Deregulation of electron flow within Photosystem II in the absence of the PsbJ protein. *J Biol Chem* 276: 41473–41478. <https://doi.org/10.1074/jbc.M102007200>

Romero E, Novoderezhkin VI, van Grondelle R (2017) Quantum design of photosynthesis for bio-inspired solar-energy conversion. *Nature* 543: 355–365.

<https://doi.org/10.1038/nature22012>

Roncel M, Boussac A, Zurita JL, Bottin H, Sugiura M, Kirilovsky D, Ortega J-M (2003) Redox properties of the photosystem II cytochromes b559 and c550 in the cyanobacterium *Thermosynechococcus elongatus*. *J Biol Inorg Chem* 8: 206–216.

<https://doi.org/10.1007/s00775-002-0406-7>

Roose JL, Pakrasi HB (2008) The Psb27 protein facilitates manganese cluster assembly in photosystem II. *J Biol Chem* 283:4044–4050. <https://doi.org/10.1074/jbc.M708960200>

Roose JL, Frankel LK, Mummadisetti MP, Bricker TM (2016) The extrinsic proteins of photosystem II: update. *Planta* 243: 889–908. <https://doi.org/10.1007/s00425-015-2462-6>

Rutherford AW, Crofts AR, Inoue Y (1982) Thermoluminescence as a probe of Photosystem II photochemistry. The origin of the flash-induced glow peaks. *Biochim Biophys Acta* 682: 457–465. [https://doi.org/10.1016/0005-2728\(82\)90061-5](https://doi.org/10.1016/0005-2728(82)90061-5)

Rutherford AW, Zimmermann J-L (1984) A new EPR signal attributed to the primary plastoquinone acceptor in Photosystem II. *Biochim Biophys Acta* 767: 168–175.

[https://doi.org/10.1016/0005-2728\(84\)90092-6](https://doi.org/10.1016/0005-2728(84)90092-6)

Rutherford AW, Zimmermann J-L, Mathis P (1983) The effect of herbicides on components of the PS II reaction centre measured by EPR. *Febs Lett* 165: 156–162.

[https://doi.org/10.1016/0014-5793\(84\)80161-1](https://doi.org/10.1016/0014-5793(84)80161-1)

Rutherford AW, Krieger-Liszka A (2001) Herbicide-induced oxidative stress in photosystem II. *Trends Biochem Sci* 26: 648–653. [https://doi.org/10.1016/S0968-0004\(01\)01953-3](https://doi.org/10.1016/S0968-0004(01)01953-3)

Sedoud A, Cox N, Sugiura M, Lubitz W, Boussac A, Rutherford AW (2011) The semiquinone-iron complex of Photosystem II: EPR signals assigned to the low field edge of the ground state doublet of $Q_A^{\bullet}-Fe^{2+}$ and $Q_B^{\bullet}-Fe^{2+}$. *Biochemistry* 50: 6012–6021.

<https://doi.org/10.1021/bi200313p>

Schatz GH, van Gorkom HJ (1985) Absorbance difference spectra upon charge transfer to secondary donors and acceptors in Photosystem II, *Biochim Biophys Acta* 810: 283–294.

[https://doi.org/10.1016/0005-2728\(85\)90212-9](https://doi.org/10.1016/0005-2728(85)90212-9)

Shen JR (2015) The structure of Photosystem II and the mechanism of water oxidation in photosynthesis. *Annu Rev Plant Biol* 66: 23–48. <https://doi.org/10.1146/annurev-arplant-050312-120129>

Shen J-R, Qian M, Inoue Y, Burnap RL (1998) Functional characterization of *Synechocystis* sp. PCC 6803 Δ psbU and Δ psbV mutants reveals important roles of cytochrome c-550 in cyanobacterial oxygen evolution. *Biochemistry* 37: 1551-1558.
<https://doi.org/10.1021/bi971676i>

Sheridan KJ, Duncan EJ, Eaton-Rye JJ, Summerfield TC (2020) The diversity and distribution of D1 proteins in cyanobacteria. *Photosynth Res* 145: 111–128.
<https://doi.org/10.1007/s11120-020-00762-7>

Shibuya Y, Takahashi R, Okubo T, Suzuki H, Sugiura M, Noguchi T (2010) Hydrogen bond interaction of the pheophytin electron acceptor and its radical anion in Photosystem II as revealed by Fourier Transform Infrared Difference Spectroscopy. *Biochemistry* 49: 493–501.
<https://doi.org/10.1021/bi9018829>

Styring S, Rutherford AW (1987) In the oxygen-evolving complex of photosystem II the S_0 -state is oxidized to the S_1 -state by D^+ (signal-II slow). *Biochemistry* 26: 2401–2405.
<https://doi.org/10.1021/bi00383a001>

Styring S, Rutherford AW (1988) The microwave power saturation of $S_{II\text{slow}}$ varies with the redox state of the oxygen-evolving complex in photosystem II. *Biochemistry* 27: 4915–4923.
<https://doi.org/10.1021/bi00413a049>.

Suga M, Akita F, Hirata K, Ueno G, Murakami H, Nakajima Y, Shimizu T, Yamashita K, Yamamoto M, Ago H, Shen J-R (2015) Native structure of photosystem II at 1.95 angstrom resolution viewed by femtosecond X-ray pulses. *Nature* 517: 99–103.
<https://doi.org/10.1038/nature13991>

Sugiura M, Rappaport F, Brettel K, Noguchi T, Rutherford AW, Boussac A (2004) Site-directed mutagenesis of *Thermosynechococcus elongatus* photosystem II: the O_2 evolving enzyme lacking the redox active tyrosine D. *Biochemistry* 43: 13549–13563.
<https://doi.org/10.1021/bi048732h>

Sugiura M, Boussac A (2014) Some Photosystem II properties depending on the D1 protein variants in *Thermosynechococcus elongatus*. *Biochim Biophys Acta* 1837: 1427–1434.

<https://doi.org/10.1016/j.bbabbio.2013.12.011>

Sugiura M, Inoue Y (1999) Highly purified thermo-stable oxygen evolving Photosystem II core complex from the thermophilic cyanobacterium *Synechococcus elongatus* having His-tagged CP43. *Plant Cell Physiol* 40: 1219–1231.

<https://doi.org/10.1093/oxfordjournals.pcp.a029510>

Sugiura M, Harada S, Manabe T, Hayashi H, Kashino Y, Boussac A (2010a) Psb30 contributes to structurally stabilise the Photosystem II complex in the thermophilic cyanobacterium *Thermosynechococcus elongatus*. *Biochim Biophys Acta* 1797: 1546–1554.

<https://doi.org/10.1016/j.bbabbio.2010.03.020>

Sugiura M, Iwai E, Hayashi H, Boussac A (2010b) Differences in the interactions between the subunits of Photosystem II dependent on D1 protein variants in the thermophilic cyanobacterium *Thermosynechococcus elongatus*. *J Biol Chem* 285: 30008–30018.

<https://doi.org/10.1074/jbc.M110.136945>

Sugiura M, Azami C, Koyama K, Rutherford AW, Rappaport F, Boussac A (2014) Modification of the pheophytin redox potential in *Thermosynechococcus elongatus* Photosystem II with PsbA3 as D1. *Biochim Biophys Acta* 1837: 139–148.

<https://doi.org/10.1016/j.bbabbio.2013.09.009>

[Sugiura M, Taniguchi T, Tango N, Nakamura M, Sellés J, Boussac A \(2020\) Probing the role of arginine 323 of the D1 protein in photosystem II function. *Physiol Plant* 171: 183–199.](https://doi.org/10.1111/ppl.13115)

<https://doi.org/10.1111/ppl.13115>

Suhai T, Dencher NA, Poetsch A, Seelert H (2008) Remarkable stability of the proton translocating F1F0-ATP synthase from the thermophilic cyanobacterium *Thermosynechococcus elongatus* BP-1. *Biochim Biophys Acta* 1778: 1131–1140.

<https://doi.org/10.1016/j.bbammem.2007.12.017>

Takasaka K, Iwai M, Umena Y, Kawakami K, Ohmori Y, Ikeuchi M, Takahashi Y, Kamiya N, Shen JR (2010) Deletion Structural and functional studies on Ycf12 (Psb30) and PsbZ-deletion mutants from a thermophilic cyanobacterium. *Biochim Biophys Acta* 1797: 278–284.

<https://doi.org/10.1016/j.bbabbio.2009.11.001>

Umena Y, Kawakami K, Shen J-R, Kamiya N (2011) Crystal structure of oxygen-evolving Photosystem II at a resolution of 1.9 angstrom. *Nature* 473: 55–60.

<https://doi.org/10.1038/nature09913>

Uto S, Kawakami K, Umena Y, Iwai M, Ikeuchi M, Shen JR, Kamiya N (2017) Mutual relationships between structural and functional changes in a PsbM-deletion mutant of photosystem II. *Faraday Discuss* 198: 107–120. <https://doi.org/10.1039/C6FD00213G>

van Eerden FJ, Melo MN, Frederix PWJM, Periole X, Marrink SJ (2017) Exchange pathways of plastoquinone and plastoquinol in the photosystem II complex. *Nature Comm* 8:15214.

<https://doi.org/10.1038/ncomms15214>

Velthuis BR (1981) Electron-dependent competition between plastoquinone and inhibitors for binding to Photosystem-II. *Feb let* 126: 277–281. [https://doi.org/10.1016/0014-](https://doi.org/10.1016/0014-5793(81)80260-8)

[5793\(81\)80260-8](https://doi.org/10.1016/0014-5793(81)80260-8)

Xiao Y, Huang G, You X, Zhu Q, Wang W, Kuang T, Han G, Sui S-F, Shen J-R (2021) Structural insights into cyanobacterial photosystem II intermediates associated with Psb28 and Tsl0063. *Nature Plants*, [7: 1132–1142](https://doi.org/10.1038/s41477-021-00961-7)~~early access.~~ <https://doi.org/10.1038/s41477-021-00961-7>

Zabret J, Bohn S, Schuller SK, Arnolds O, Möller M, Meier-Credo J, Liauw P, Chan A, Tajkhorshid E, Langer JD, Stoll R, Krieger-Liszkay A, Engel BD, Rudack T, Schuller JM, Nowaczyk MM (2021) Structural insights into photosystem II assembly. *Nature Plants* 7: 524–538. <https://doi.org/10.1038/s41477-021-00895-0>